



Imaging and image-based fluid transport modeling at the pore scale in geological materials: A practical introduction to the current state-of-the-art

Tom Bultreys ^{*}, Wesley De Boever, Veerle Cnudde

UGCT/PProGRESS, Dept. of Geology and Soil Science, Ghent University, Krijgslaan 281 (S8), 9000 Ghent, Belgium



ARTICLE INFO

Article history:

Received 29 November 2015

Received in revised form 27 January 2016

Accepted 1 February 2016

Available online 6 February 2016

Keywords:

Imaging

Image-based fluid transport modeling

Geological materials

Pore scale

ABSTRACT

Fluid flow and mass transport in geological materials are crucial in diverse Earth science applications. To fully understand the behavior of geological materials in this context, the pore scale properties of these materials have to be investigated and related to effective material properties. Imaging techniques are becoming ever more valuable tools to characterize the microstructure (especially in three dimensions), while numerical models to calculate transport properties based on experimental images of the microstructure are quickly maturing. The results of image-based modeling studies depend crucially on both the employed model and the quality of the pore space image on which the model runs. Given the technicality and the cross-disciplinary nature of this matter, this review aims to provide a practical and accessible introduction to both the experimental and numerical state-of-the-art, intended for students and researchers with backgrounds in experimental geo-sciences or computational sciences alike.

© 2016 Elsevier B.V. All rights reserved.

Contents

1. General introduction	94
2. Imaging the microstructure of geological porous media	95
2.1. Introduction and terminology	95
2.1.1. Pixel	95
2.1.2. 3D images	95
2.1.3. Voxel	95
2.1.4. Spatial resolution	95
2.1.5. Microporosity	96
2.2. Optical microscopy	96
2.2.1. Traditional petrographic microscopy	96
2.2.2. Fluorescence light microscopy (FLM)	96
2.3. Scanning electron microscopy (SEM)	97
2.3.1. Introduction	97

Abbreviations: μ , linear X-ray attenuation coefficient; μ XRF, micro-X-ray fluorescence spectroscopy; 2D, two-dimensional; 3D, three-dimensional; A, cross-sectional surface area; BGK, Bhatnagar–Gross–Cook approximation; BIB-SEM, broad ion beam scanning electron microscopy; BSE, backscattered electrons; CDI, coherent diffractive imaging; CFD, computational fluid dynamics; CT, computed tomography; DOHT, distance-ordered homotopic thinning; D-PNM, dual pore network model; EDS or EDX, energy-dispersive (X-ray) spectroscopy; EMP, electron-microprobe; ESRF, European Synchrotron Radiation Facility (France); eV, electron volt; FE-SEM, field-emission scanning electron microscopy; FIB, focussed ion beam; FIB-nt, focussed ion beam nanotomography; FLM, fluorescence light microscopy; G, shape factor; g_{ij} , conductivity from pore i to pore j; I, intensity; I_0 , incident intensity; IFPEN, Institut Français du pétrole et des énergies nouvelles; keV, kilo electron volt; LB, lattice-Boltzmann; LG, lattice-gas; L_{ij} , distance between pores i and j; Micro-CT, micro-computed tomography; MIP, mercury intrusion porosimetry; MLA, mineral liberation analyzer; MRI, magnetic resonance imaging; MTF, modulation transfer function; P, perimeter length; P_c , capillary pressure; pc-micro-CT, phase contrast micro-CT; PEEK, polyether ether ketone (a type of polymer); P_i , pressure in pore i; Pixel, picture element; PNM, pore network model; PSD, pore size distribution; PSI, Paul Scherrer Institute (Switzerland); QEMSCAN, Quantitative Evaluation of Minerals by SCANning electron microscopy; q_{ij} , flux from pore i to pore j; r, radius; SAXS, small-angle X-ray scattering; SE, secondary electrons; SEI, secondary electron imaging; SEM, scanning electron microscopy; SPH, smoothed particle hydrodynamics; TOMCAT, the beamline for TOnographic Microscopy and Coherent rAdiology experimentTs at the Paul Scherrer Institute; Voxel, volume Element; XRD, X-ray diffraction; XRF, X-ray fluorescence spectroscopy; Z, atomic number; θ , contact angle; σ , interfacial tension.

* Corresponding author.

E-mail addresses: Tom.Bultreys@UGent.be, tombultreys@hotmail.com (T. Bultreys), deboever.w@gmail.com (W. De Boever), Veerle.Cnudde@ugent.be (V. Cnudde).

2.3.2. Applications	98
2.4. Focused ion beam nanotomography (FIB-nt)	98
2.4.1. Introduction	98
2.4.2. Applications	99
2.5. X-ray (micro-)computed tomography (CT)	99
2.5.1. Introduction	99
2.5.2. Monitoring structural dynamic processes	100
2.5.3. Phase contrast micro-tomography	101
2.6. Ptychographic tomography	102
2.7. Dealing with (3D) images	103
2.7.1. Introduction	103
2.7.2. Geometrical and topological pore characterization	103
2.7.3. Skeleton extraction and analysis	103
2.7.4. Data fusion	104
3. Direct pore scale modeling	105
3.1. Introduction	105
3.2. Lattice Boltzmann	105
3.2.1. Method	105
3.2.2. Applications	106
3.3. Traditional computational fluid dynamics	107
3.3.1. Method	107
3.3.2. Applications	108
3.4. Smoothed particle, semi-implicit-particle and dissipative hydrodynamics	108
3.5. Direct hydrodynamics	109
3.6. Molecular dynamics and Monte Carlo methods	109
4. Pore scale modeling with pore network models	109
4.1. Introduction	109
4.2. Image based network extraction	111
4.2.1. Topology-central methods	111
4.2.2. Morphology-central methods	112
4.2.3. Other methods	113
4.3. Transport simulations based on pore network models	113
4.3.1. Quasi-static multi-phase flow modeling	113
4.3.2. Dynamic multi-phase flow modeling	114
4.3.3. Solute/colloid transport and reactive flow modeling	115
4.3.4. Other applications	116
4.4. Comparison of network extraction methods	116
4.4.1. Overview of comparative studies	116
4.4.2. Robustness of network extraction	116
4.5. Multi-scale pore network modeling	117
5. Summary and conclusion	118
6. Outlook	120
Acknowledgments	120
References	120

1. General introduction

Fluid flow and mass transport in geological porous media (e.g. rocks, sediments, soils) are crucial aspects of several important geological applications, e.g. hydrology, petroleum engineering, CO₂-sequestration, sub-surface storage of nuclear waste, geothermal energy generation and building stone performance. To reduce uncertainties related to these systems and to increase their efficiency, accurate predictions of their behavior over time have to be made. This is typically done by running large-scale numerical models (on the order of meters to kilometers), which use constitutive equations to describe the behavior of the geological materials in question. They therefore require the input of effective material properties such as porosity, permeability, and dispersivity, which are characteristic of the geological materials in which the processes take place. These materials are composed of minerals on the one hand and pores or fissures/cracks on the other hand. Properties of the pores and minerals, such as geometry, size, surface area, connectivity and distribution have a strong effect on the material's behavior. The internal microstructure, the chemical composition, and the macroscopic material properties are indeed strongly and directly related to each other. Therefore, understanding why and how the macroscopic features of the materials vary over space and time requires the

examination of the material's microstructure. Given the complexity and the heterogeneity of many of these natural porous media, such a deep understanding is crucial, as it is often impossible to acquire and test all the relevant samples at all the relevant conditions (e.g. in the case of kilometer-sized geological reservoirs). Experimental measurements of transport properties in this context are often difficult, expensive and time-consuming, making models at the scale of the material's microstructure (typically termed "pore scale") an attractive tool to supplement direct measurements, to enhance the understanding of a material's behavior, and therefore to help interpolate and extrapolate effective material properties.

The different transport processes to be modeled in this context can be classified as single-component or multi-component flows (i.e. multiple chemical species may be mixed in the same fluid phase); single-phase and multi-phase flows (i.e. multiple immiscible or partially miscible fluids may be present) and non-reactive or reactive flows (i.e. fluids in the pore space may react with each other or with the solid minerals). In nature, these processes often take place simultaneously and may be strongly coupled. The behavior may be driven by several forces, including gravity, capillarity, thermal forces, entropy and applied hydraulic pressure. While the processes and driving forces may differ between different porous media applications (which are not limited to geological

applications) many of the concepts and techniques to study pore scale transport behavior are readily carried over from one application to another. This review will treat broadly applicable experimental and numerical techniques to study how this behavior is linked to the properties of porous geological materials, without going into detail on the physics and chemistry behind it. Of course, any pore scale modeling study requires a good understanding of the fundamental physical and chemical processes at play for the specific application of interest, for which we refer to standard works on flow and transport in porous media, e.g. Bear (1975), Dullien (1992) and Sahimi (2011).

To build a realistic pore scale model, a first requisite is of course to perform a suitable characterization of the microstructural properties of the material. Several destructive and non-destructive characterization techniques exist to obtain chemical and structural information of the porous material at different resolutions, going from the molecular scale to the field scale. In this review, we will discuss the applicable imaging techniques, as these techniques offer local information on the pore structure, which is necessary if one wants to reliably model pore scale properties. Besides a description of the (pore) structure, a full characterization of a geological material includes an examination of the mineralogical composition. However, since this review deals with pore characterization methods which can be used as input for pore-scale modeling, the often used chemical characterization techniques for geomaterials, such as XRD, μ XRF, and EDX, will not be discussed. We will rather focus on techniques to gather 2D and 3D information on the internal pore structure of rocks and other geomaterials (Section 2). The quality of the obtained data is of the greatest importance to build accurate pore-scale transport models. For each of the described techniques, strengths and limitations will be discussed.

A first approach is often optical mineralogy (Section 2.2), which provides information in 2D. This is often used to identify and study the composing minerals, structures and textures. However, the resolution is limited to approximately 0.23 μm (in the most advanced microscopes) (Heintzmann and Ficz, 2006). To obtain higher resolutions and better contrast between pore and material phases, scanning electron microscopy is frequently applied (Section 2.3). Yet, accurate modeling requires taking into account the three-dimensional nature of the microstructure. To obtain such 3D images at high resolutions, focused ion beam nanotomography was developed (Section 2.4). X-ray microtomography provides lower resolutions than focused ion beam nanotomography, but is non-destructive, more versatile with regards to the size of the imaged sample and widely accessible (Section 2.5). Other X-ray imaging techniques we describe are phase contrast imaging (Section 2.5.3) and ptychographic imaging (which allows to obtain very high resolution images non-destructively in 3D on very small samples, Section 2.6). In Section 2.7, we discuss how the obtained images can be processed and analyzed, to serve either as input information or validation for pore scale transport models. Although many other imaging methods exist to characterize geological materials, currently these methods often lack the resolution needed to image the complex structure of these materials at the pore scale. Two important methods in this category are magnetic resonance imaging (MRI) and neutron tomography and radiography. MRI is mainly used for the visualization of fluids in rocks, and can reach resolutions of around 100 μm (Lakshmanan et al., 2015; Peth et al., 2010). Neutron imaging is also mainly used for the visualization of liquids (generally water) in porous materials, and can reach resolutions down to 30 μm . Other downsides next to the rather limited spatial resolution are the long measuring times for full tomograms and the fact that analyzed samples become radioactive (Cnudde et al., 2008; Derluyn et al., 2013; Dewanckele et al., 2014). As the application of these methods to build and validate pore scale transport models has been limited, they will not be further discussed in this review.

To simulate fluid flow behavior or other dynamic processes on the obtained images, transport equations have to be solved with the complex boundary conditions of the rock's microstructure taken into

account. Sections 3 and 4 will treat the main methods which have been developed to perform pore scale modeling of single- and multi-phase transport phenomena based on experimentally obtained images of a rock's pore space. Rather than giving an in-depth technical description, we present the working principles and explore the strengths and weaknesses of these algorithms through reviewing their applications. We elucidate the treatment and the use of pore scale images in these modeling applications and devote particular attention to complex pore geometries and heterogeneity, present in many natural porous media.

A first class of algorithms runs directly on 3D images (segmented into pore voxels and solid voxels) of the pore space and will be described in Section 3. These methods include lattice-Boltzmann, classical computational fluid dynamics (CFD), particle-based hydrodynamics and direct hydrodynamics (Sections 3.2–3.5). Out of these methods, we focus on lattice-Boltzmann and classical CFD methods, because they have been applied to realistic 3D pore geometries most widely. A second class of algorithms, usually called the pore network modeling (PNM) approach, first simplifies the pore space geometry while trying to retain the characteristics which are essential to the rock's transport properties. Since these models are to date the most successful at simulating multi-phase flow, we discuss them in detail in Section 4. We review network extraction (Section 4.2), network simulations (Section 4.3) and studies which compare different algorithms (Section 4.4). Finally, multi-scale pore network models are treated.

Currently, modeling and validation of transport processes on the microscale is possible, but it is essential that this information is also upscaled to larger sample sizes than those originally examined and modeled. For a review of these upscaling methods we refer to Farmer (2002).

2. Imaging the microstructure of geological porous media

2.1. Introduction and terminology

In the following paragraphs, definitions of some frequently used parameters and terms are given.

2.1.1. Pixel

A pixel is one raster element from an image. A pixel consists out of one single color or gray value, and represents a particular distance in the image. Pixels are usually squares, so they have the same dimensions in x and y, called the pixel size.

2.1.2. 3D images

A stack of 2D images, representing a 3D volume. These 3D datasets have a certain pixel size in x and y directions, and an additional spacing between the images in z direction. It is important to know that this spacing between images in z direction is not always the same as the pixel size.

2.1.3. Voxel

One element in a 3D image is called a voxel, or volume element, which could be described as a 3D pixel. Voxels are usually cuboids with a square base (the pixel size of the 2D images). The height of the cuboid is the z-spacing between the images.

2.1.4. Spatial resolution

One of the most important properties of imaging techniques is the spatial resolution which can be obtained with them. This spatial resolution (or resolving power) is defined as the smallest distance between two features in a sample, for which these features are seen as separate objects. Readers should be aware that pixel/voxel size is often confused with spatial resolution. The latter is a measure for the resolving power of an imaging system based on the modulation transfer function (MTF) of the complete imaging system, expressed in line pairs per distance unit.

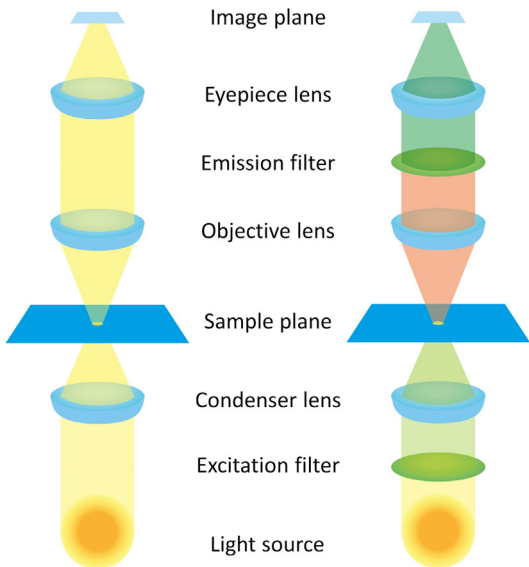


Fig. 1. Schematic representation of the principle of traditional optical microscopy (left) and fluorescence light microscopy (right). Light travels from the light source through a condenser lens and hits the sample plane. An objective lens and eyepiece lens enable magnification. In fluorescence mode, an excitation and emission filter enable detection of the correct wavelengths for fluorescence imaging.

Due to the complexity of the MTF, the term resolution is commonly used to denote the reconstructed voxel size. It must be noted that the term resolution can also denote the number of pixels or voxels in an image (Cnudde and Boone, 2013).

2.1.5. Microporosity

Several definitions for the term 'microporosity' exist, including the approach by Sharkey and McCartney (1981), stating that all pores smaller than 2 nm are considered micropores, and pores larger than 50 nm are called macropores.

When dealing with geological samples, however, even 50 nm pores are very small, and impossible to characterize using most imaging techniques. Therefore, in this review we use a practical definition of microporosity, stating that macropores are the pores larger than 1 μm , while micropores are those with a diameter below 1 μm .

2.2. Optical microscopy

2.2.1. Traditional petrographic microscopy

The most widespread and 'standard' method for the determination of the porosity and visualization of the pore space of geological material is thin section analysis using an optical microscope (Fig. 1). The main advantage of this technique is that it is fast, cheap and widely accessible. Analysis of standard geological thin sections (thickness = 30 μm) under a petrographic microscope (Fig. 2, left and center) provides valuable

information about both the mineralogical composition and texture and structure of rocks and soils. High-end light microscopes are only limited in resolution to about half the wavelength of visible light (± 390 –700 nm), known as the diffraction barrier. This means that at best, resolutions of about 0.23 μm can be achieved (Gustafsson, 2000; Heintzmann and Ficz, 2006). Petrographic microscopy can be used to analyze the porosity of geological materials, since pores appear transparent (white) in planar polarized light and black under cross-polarized light (Andriani and Walsh, 2002; Ingham, 2013). Since this may have overlap with certain opaque (e.g. pyrite) or isotropic minerals present (e.g.: fluorite, garnet), embedding samples with a blue colored dye before thin section manufacturing, can help analysis quite a bit (Zhang et al., 2009).

2.2.2. Fluorescence light microscopy (FLM)

Fluorescence light microscopy (FLM) can be used for more exact characterization of the pore space, since porosity and other components of geological samples can be hard to distinguish from each other using classical optical microscopy, both in planar and cross-polarized light (Nishiyama and Kusuda, 1994; Wajima et al., 2000) (Fig. 2, left and center). In FLM, samples are embedded with a fluorescent resin after putting the samples under vacuum in order to remove all air outside the pores; when excited with light of correct wavelength, this fluorescent dye emits characteristic light, which provides a very clear contrast between material (black) and porosity (bright) (Ammouche et al., 2001; Sousa et al., 2005) (Fig. 2, right). This makes the technique very useful for the study of pores and (micro)cracks in rocks and concrete (Bisschop and van Mier, 2002; Jacobsen et al., 1995; S. Li et al., 2014b; Matějček et al., 2006; Poulikakos and Partl, 2010) and for the examination of the porosity in very low-porosity materials (Cnudde et al., 2013; Malaga-Starzec et al., 2006; Rivas et al., 2003). Furthermore, the sharp contrast between solid and void, makes the use of automated image analysis techniques to determine porosity of samples much more straight-forward (Soroushian et al., 2003). The technique requires a careful sample preparation, since an improper preparation can lead to false conclusions, e.g. over- or underestimation of porosity or crack density when the fluorescent dye is mixed inhomogeneously with the epoxy resin (Bisschop and van Mier, 2002; Soroushian et al., 2003).

Zones of intermediate fluorescence intensity are an indication of pores with a size that is smaller than the resolving power of the microscope. The intensity of these zones depends on the degree of microporosity, where brighter zones are more porous than darker ones. This way, porosity that is invisible in traditional transmitted light microscopy can be observed (Leith et al., 1996). However, this technique is not adequate to thoroughly characterize the pore shape, connectivity and other properties of microporous materials, especially since it is a 2D analysis technique (Anselmetti et al., 1998). Nevertheless, FLM has been widely accepted in concrete research, where fluorescence intensity is used to determine the water/cement ratio of concrete, which stands in direct relationship with the capillary porosity of the concrete paste (Gran, 1995; Neville, 2003).

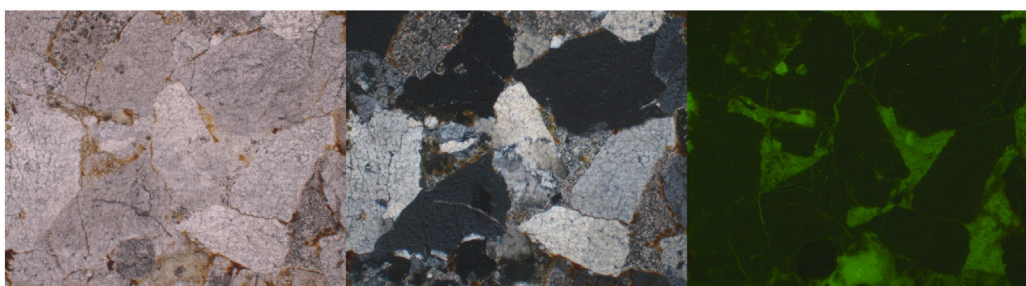


Fig. 2. Example of a thin section (Baumberger sandstone) under traditional petrographic microscopy using parallel polarized light (left), cross-polarized light (center) and fluorescence light microscopy (right).

The combination of a fluorescent dye and structured illumination microscopy can boost the resolution of optical microscopy up to a factor two (Gustafsson, 2000). More recent algorithms, which combine over 100 images into one single reconstructed plane can even go down to 50 nm resolution (Heintzmann and Ficz, 2006; Rego et al., 2012), however, this technique is very time-consuming and not yet used on geological samples.

2.3. Scanning electron microscopy (SEM)

2.3.1. Introduction

2D imaging at higher resolutions than optical microscopy, going down to several nanometers, can be obtained using scanning electron microscopy (SEM). With SEM, high-resolution images of both the minerals and the pore space in 2D can be obtained. SEM machines equipped with an energy-dispersive X-ray spectroscopy (EDX) unit can provide chemical information and, with correct calibrations and software, can even perform automated mineralogy (Hoal et al., 2009; Sutherland, 2007; Zhang et al., 2015). SEM is a close relative of the electron microprobe (EMP), but is designed primarily for imaging rather than chemical analysis. Images are produced by scanning the sample with the electron beam while displaying the signal from an electron detector on a television screen or computer monitor. By choosing the appropriate detection mode, either topographic or compositional contrast (based on the mean atomic number) can be obtained. Since EMP instruments have electron-imaging capabilities, used primarily for locating points for chemical analysis, the functions of the EMP and the SEM overlap considerably.

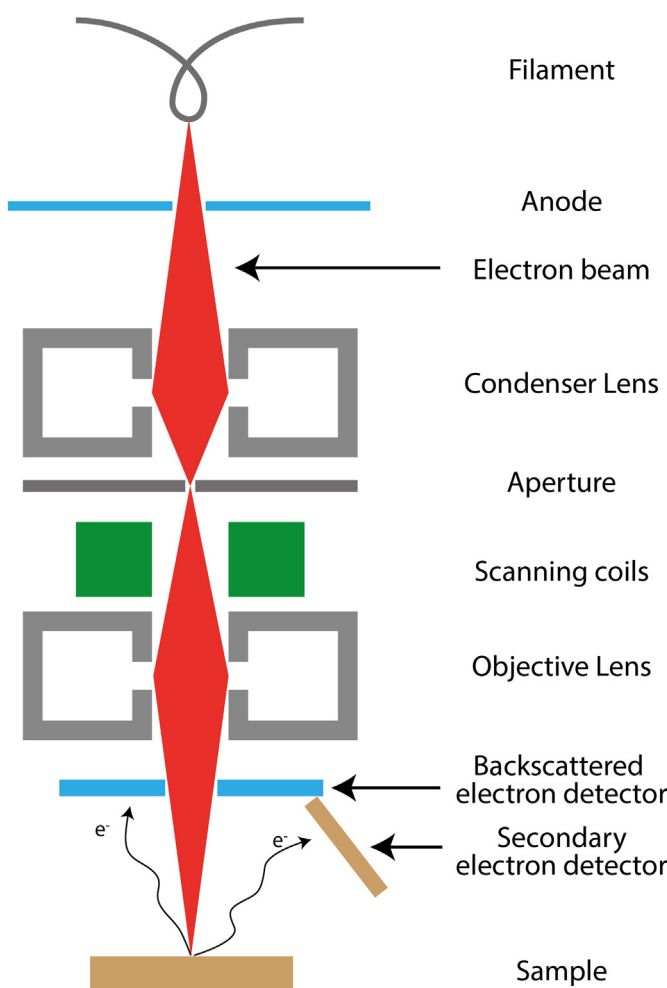


Fig. 3. Schematic representation of a SEM.

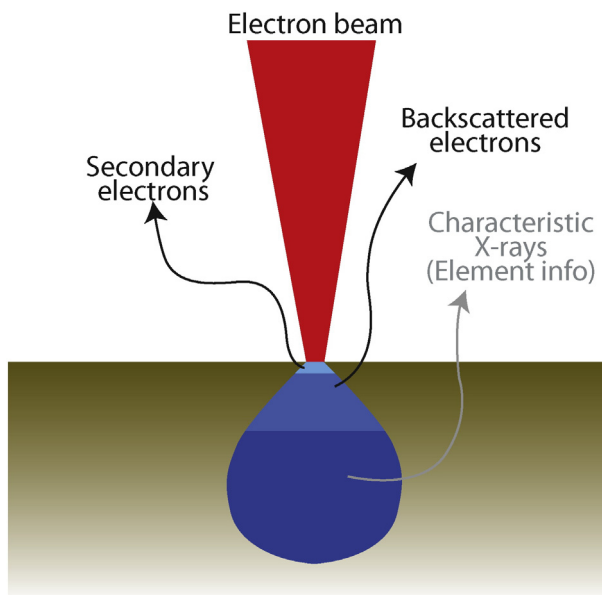


Fig. 4. Electron beam-specimen interactions. Secondary electrons originate from a region close to the sample surface (± 5 nm), backscattered electrons originate up to 500 nm deep, and characteristic X-rays can originate about 2 μ m below the sample surface.

The SEM is optimized for imaging, with chemical analysis often as an extra, whereas in the EMP the priorities are reversed and various additional features that facilitate chemical analysis are incorporated. The advantages of the SEM as an imaging instrument make it an invaluable tool in many branches of geology, including paleontology (e.g. SEM is ideally suited to study fossil morphology, especially that of micro-fossils), sedimentology (e.g. data on fabric and porosity can be generated as well as images of individual grains and intergrowths), mineralogy (to study crystal morphology on a micro-scale), etc.

In SEM, a high-energy electron beam scans the surface of the analyzed samples (Fig. 3). These electrons interact with the atoms of the sample, producing signals that contain information about the sample's topography and composition (Reed, 2005). One important disadvantage for SEM on geological materials is the fact that the samples often need some prior treatment. Most geological samples, being electrical insulators, require a conductive coating to prevent charging under electron bombardment unless this is avoided by using an "environmental" or "low-vacuum" SEM (Robinson and Nickel, 1979). The preferred coating element for X-ray analysis is carbon, because it has a minimal effect on the X-ray spectrum (Reed, 2005; Welton, 1984). However, for SEM imaging, owing to its low secondary-electron yield, this is not ideal. For this purpose a metal such as gold is preferable, but this is less suitable for X-ray analysis and backscattered electron (BSE) imaging.

The types of signals produced by an SEM include secondary electrons (SE), back-scattered electrons (BSE) and characteristic X-rays (Fig. 4). SE are produced when an incident electron excites an electron in the sample. This excited electron moves towards the surface of the sample, where it can escape the sample, and reaches the detector. Secondary electrons can only escape the sample if they are formed within 5 nm of the sample surface, and typically have very low energies (up to 50 eV). Due to their very small production volume, resolution of secondary electron images (SEI) is very high, and is effectively the same as the electron beam size, which is normally below 10 nm.

SEMs equipped with a Field Emission electron gun (FE-SEM) can even reach beam sizes of about 1 nm. Another effect of this very small interaction volume is that SE are very sensitive to sample topography, making SE images very useful to study this property of a material (Reed, 2005), as they provide an intuitive 3D-like look (Fig. 5). The high resolution of SE images makes them very suited for analysis of microstructures and (micro)porosity in various fields of geosciences

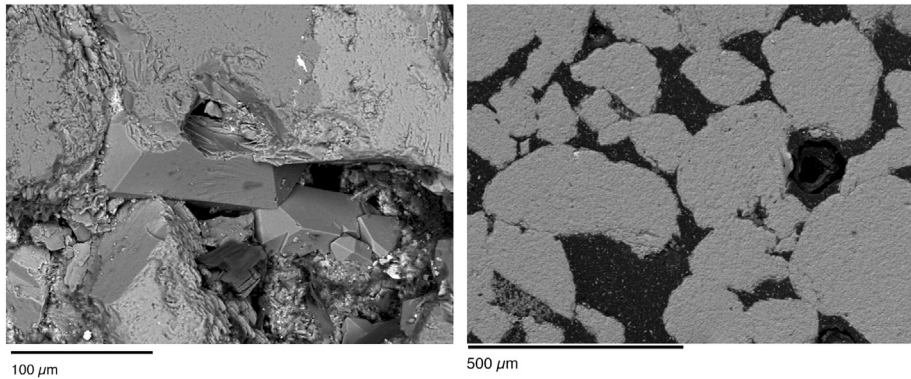


Fig. 5. Left: BSE image of unpolished Vosges sandstone, showing primary quartz grains and secondary prismatic quartz crystals. The high working distance creates a 3D impression in the picture. Right: BSE image of a polished, resin embedded Bentheim sandstone sample. This type of image is ideal for 2D porosity determination. From De Boever et al. (2015b).

(Huang et al., 2013; Jiao et al., 2014) and soil science (Marcelino et al., 2007; Prakongkep et al., 2010), as well as in concrete research (Ammouche et al., 2001; Bisschop and van Mier, 2002).

Backscattered electrons (BSE) are electrons that originate from the beam, but reflect from the sample by elastic scattering, meaning there is no significant energy loss. Most BSE have slightly lower energy than that of the incident electron beam (1 to 30 keV), but energies as low as ± 50 eV are possible for backscattered electrons scattering deep inside the sample. Since the fraction of beam electrons that is backscattered strongly depends on the average atomic number of the sample (higher Z causes more backscattering, due to higher charge of atomic nuclei), BSE images provide information about a sample's composition (Fig. 5).

BSE images of polished sections of geological materials are a very useful tool for analysis of composition and porosity, since pores appear black and heavy elements bright in these images. Spatial resolution in BSE images is considerably lower than in SE images, due to the larger interaction volume (Fig. 5). Best spatial resolution is therefore reached by using a low accelerating voltage (Reed, 2005).

Characteristic X-rays, which are emitted when the electron beam removes an inner shell electron from the sample, causing a higher energy electron to fill the shell and release energy, are used to identify the composition and to measure the abundance of elements in the sample and are thus not used to study porosity. These characteristic X-rays can be studied with energy-dispersive X-ray spectroscopy (EDS or EDX), an analytical technique used for the elemental analysis or chemical characterization of a sample. This technique is one of the variants of X-ray fluorescence spectroscopy, which relies on the investigation of a sample through interactions between electromagnetic radiation and matter, analyzing X-rays emitted by the matter in response to being hit with charged particles. Its characterization capabilities are due to the fundamental principle that each element has a unique atomic structure allowing X-rays, that are characteristic of an element's atomic structure, to be uniquely identified from one another.

2.3.2. Applications

SEM is widely accessible, and therefore a very frequently used technique in geology, starting very soon after the first commercial machines became available in the 1960s. Earliest applications of the method were the characterization of natural stones and minerals. SEM was used as a tool to study pore systems (Timur et al., 1971) and the morphology of limestone as early as 1971 (Margolis and Rex, 1971). A good review of the use of BSE images to distinguish different mineral phases has been made by Lloyd in (1987). Besides that, SEM was used for the investigation of important geological processes, such as diagenesis and weathering. Longman and Mench (1978) used the technique to study the diagenesis of cretaceous limestone, while others used it to study different types of very fine-grained clay minerals, formed by the weathering of feldspars

(Keller, 1978). In the 1980s, automated procedures were developed to characterize stone microstructure automatically, laying the foundations of current image analysis procedures (Krohn and Thompson, 1986). Later, SEMs were used in reservoir geology, for the investigation of nano-porous cap rocks, tight shales (Katsube and Williamson, 1994) and clay minerals (Hillier, 1994). In recent years, research and imaging towards microporous limestones and fine-grained clay stones are the main applications of SEM in geological research (Marszałek et al., 2014; Mavris et al., 2012; Vázquez et al., 2013; Vazquez-Calvo et al., 2007). Using automated EDS analysis algorithms such as Qemscan and MLA, automatic mineralogy of rock samples can be performed (Hoal et al., 2009; Meyer et al., 2013; Sutherland, 2007; Zhang et al., 2015).

2.4. Focused ion beam nanotomography (FIB-nt)

2.4.1. Introduction

Over the last decades, dual-beam systems, combining a focused ion beam (FIB) and an electron beam became commercially available. These systems are mainly used for the preparation of small samples, e.g. for transmission electron microscopy (Wirth, 2009) or X-ray nanotomography (Lombardo et al., 2012), but can also be used to perform a destructive type of nanotomography. Focused Ion Beam nanotomography (FIB-nt) combines an electron beam and a FIB

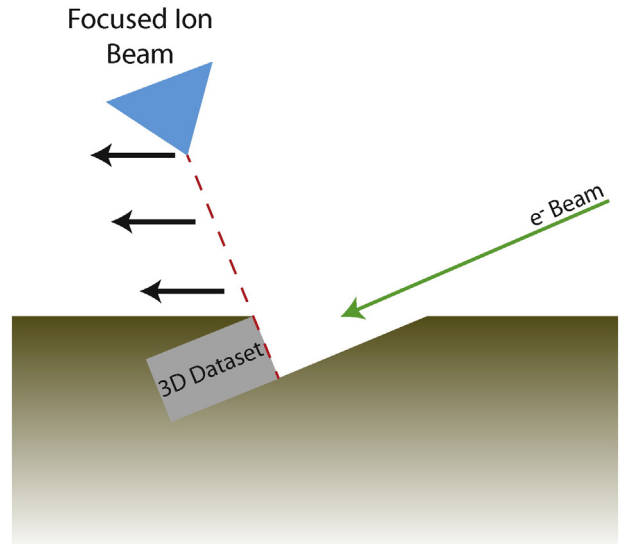


Fig. 6. Schematic representation of FIB nanotomography. A focused ion beam sections the material, and images are taken using the electron beam. After each image, the FIB moves in the direction of the black arrows, and a new section is made.

(Bera et al., 2011; Holzer et al., 2004), to obtain the high resolutions of SEM images in three dimensions. In this technique, serial sectioning of samples using a FIB is performed, while taking a SEM image after each section (Fig. 6). This series of images results in a 3D dataset of high resolution SEM images with a certain z-spacing. Due to the limitations of the FIB, the best achievable z-spacing is about 10 nm (Möbus and Inkson, 2007).

Acquisition of FIB-nt datasets is time consuming (between 4 and 12 h, depending on the analyzed volume) and the analyzed volume is very small (less than 10 µm in x and y directions, and usually less than 2 µm in z direction). This implies that FIB-nt can only be used for the 3D analysis of very small regions of interest with very high detail. The destructive nature of the technique implies that dynamic processes cannot be followed on the same area of a sample, and that, especially for important samples, great care has to be taken during image acquisition.

The technique was first presented at the end of the 1990s (Cheng, 1998; Dunn and Hull, 1999), but Holzer et al. (2004) and Wu et al. (2003) were among the first to demonstrate the technique on (non-geological) porous materials. Ever since, a lot of analysis has been performed on various geological materials.

2.4.2. Applications

FIB-nt allows the analysis of microstructures, porosity and its inter-connectivity at micrometer to nanometer scale. Therefore, the technique represents a further step in the 3D analysis of rocks, complementing techniques such as X-ray tomography (described below). For these reasons, FIB-nt has great potential in porosity and permeability analysis, and most recent (geological) applications concern claystones and shales, to predict and improve production of natural gas from these tight rock types (Bera et al., 2011; Jiao et al., 2014; Sok et al., 2010) and to understand sealing behavior of the cap rock (Heath et al., 2011). This research is gaining importance, as traditional reservoirs are becoming depleted, and these new tight gas reservoirs are poorly understood. Other applications in the field of shale hydrocarbon reservoirs are the study of porosity in the organic matter of shales, at different thermal maturities (Curtis et al., 2012). Note that this organic matter porosity can only be analyzed through the combined use of ion beam milling and SEM, since sample surface relief obtained by mechanical polishing tends to be higher than the diameter of most shale pores (Loucks et al., 2009). Characterization of low-permeability stones or sediments is also of importance to study the potential of deposits for radioactive disposal systems. Examples of these deposits include the Swiss Opalinus clay (Keller et al., 2011) or the Belgian Boom Clay formation (Desbois et al., 2009). Modern Cryo-FIB-SEM systems can study materials in different stages of fluid saturation, by studying samples in frozen condition, at –150 °C (Lubelli et al., 2013).

Recent applications made the technique a complementary tool to some of the most traditional geological analysis methods, as Wirth and Morales (2012) demonstrated. They analyzed different samples of shale, which were sputtered with the FIB directly from standard petrographic thin sections. Sectioning normal to the thin section surface revealed a number of details that could not be observed through the optical microscope, such as the distribution of clay minerals coating the other grains of the material. Kelly et al. (2015) employed the method for the extraction of 3D rock models of shales, and raised the question on what can be considered as the REV for such tight, low-porosity materials. Furthermore, they incorporated BIB-SEM in their research, to provide high-resolution 2D images, over a much larger area than traditional FIB-nt datasets. In BIB-SEM, a broad ion beam is used to polish samples down to a topography of less than 5 nm, enabling imaging at resolutions of around 10 nm (Desbois et al., 2009; Hemes et al., 2015; Klaver et al., 2012), over an area of around 100 × 100 µm². These properties place BIB-SEM as a complementary technique between traditional SEM analysis on polished thin sections, and 3D FIB-nt.

Outside of the geo-sciences, FIB-nt has been used in a large variety of application fields dealing with micro- to nanoporous media. It gave novel insights in the 3D microstructure of batteries, where permeability

is of great importance for charging and discharging (Hutzenlaub et al., 2012; Joos et al., 2011). Gostovic et al. (2011) used FIB-nt to create a 3D dataset, which was then segmented into pores and solid, to serve as input for pore network extraction, giving information about connectivity and permeability of the pore system. In life sciences, FIB-nt is mainly used to study the microstructure of bones and teeth. Earl et al. (2010) could visualize and analyze the 3D shape of tubular pores inside human teeth. Giannuzzi et al. (2007) observed so-called osseointegration in dental implants, which meant that new bone forms into the porous wall of the implant, causing a mechanical locking mechanism at the bone/implant interface. In the study of Giannuzzi et al. (2007), FIB-nt proved to be a far more precise tool than traditional SEM microscopy, which did not provide much information on the exact nature of this interface. In concrete research, FIB-nt provided new insights about morphology of pores and phases inside microporous cement pastes (Munch et al., 2006; Trtik et al., 2011). Many other applications can be found in Möbus and Inkson (2007).

2.5. X-ray (micro-)computed tomography (CT)

2.5.1. Introduction

X-ray computed tomography (X-ray CT) provides 3D structural information of geomaterials at (sub-)micron to millimeter scale. This makes the technique exceptionally suited for multi-scale characterization of these materials. The method is based on the attenuation of X-rays when they travel through material, expressed by the Lambert-Beer law. This law is presented in Eq. (1); transmitted X-ray intensity I depends on the incident intensity I_0 and the linear attenuation coefficient $\mu(s)$ along the raypath s . Since X-ray attenuation depends on both atomic number and density, direct information on the elemental or chemical composition of the sample is not easily obtained using X-ray CT.

$$I = I_0 e^{-\int \mu(s) ds} \quad (1)$$

Lambert-Beer law for the attenuation of X-rays.

An X-ray CT setup consists of an X-ray source and detector, which rotate around the sample in medical CT setups, but are generally stationary with a rotating sample in typical laboratory micro-CT setups (Fig. 7). The sample is positioned between the source and detector, resulting in a radiograph recorded at the detector. Sample thickness, composition and density determine the intensity of the X-rays reaching the detector. Over an angular reach of 360 (or 180) degrees, several hundreds to thousands of radiographs are recorded, and using reconstruction algorithms (Vlassenbroeck et al., 2007), these data are transformed into a 3D volume. This volume is a 3D distribution of the linear attenuation coefficient, represented by gray values, often stored as a stack of virtual 2D slices. The resolution of high-quality laboratory X-ray setups is currently limited to around 0.5 µm for traditional micro-CT setups, but can reach 50–100 nm for systems using scintillators and magnification optics (Feser et al., 2008; Gelb et al., 2009). Traditional laboratory setups can acquire high-quality images within a time frame of minutes to hours, while synchrotron setups can do the same with second to minute time resolution due to the higher X-ray flux provided by synchrotron beam lines.

For a detailed review devoted to high-resolution X-ray tomography, we refer to Cnudde and Boone (2013), which provide a comprehensive summary of the history, technique and geoscientific applications of micro-CT before 2013. Other, excellent reviews on this topic have been written by Ketcham and Carlson (2001), in which the early days of micro-CT as a geoscience tool are reviewed, and by Wildenschild and Sheppard (2013), who focus more on micro-CT as a tool for hydrology and hydrocarbon reservoir research. In this work, we focus on dynamic micro-CT imaging, as this specific application has seen rapid

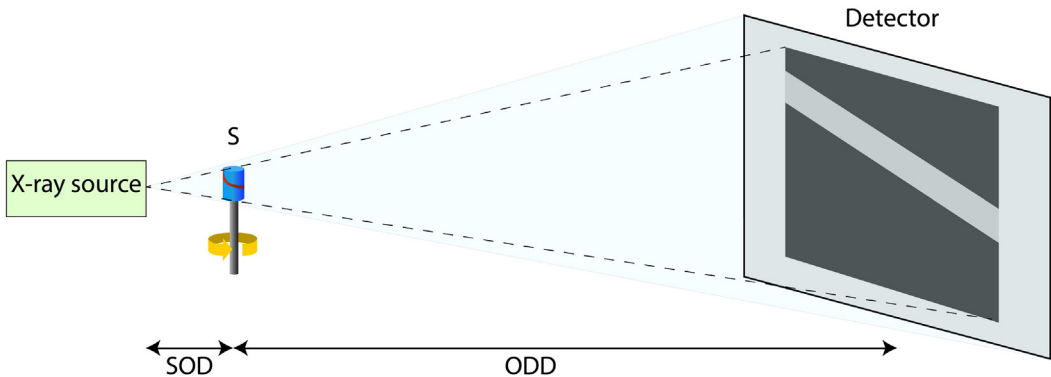


Fig. 7. Schematic representation of a typical laboratory micro-CT setup, equipped with an X-ray tube, using a cone-beam configuration. A sample (S) is positioned between the X-ray source and detector. X-rays interact with the specimen, and a 2D projection (radiograph) is recorded by the detector. By combining information of 100 s of radiographs acquired over 360°, a 3D volume can be reconstructed.

evolution since 2013. Furthermore, it is an excellent tool to validate pore scale transport models.

2.5.2. Monitoring structural dynamic processes

The non-destructive character of micro-CT allows the monitoring of dynamic processes inside porous media by imaging the sample at multiple points in time. However, in order to perform quantitative analysis, the 3D images that are taken at different moments have to be perfectly aligned with each other (Wildenschild and Sheppard, 2013). Therefore, these experiments are most convenient when the sample does not have to be removed from the micro-CT setup in between different imaging steps. This type of analysis has rapidly developed over recent years, but first experiments date back to the end of the previous century (Coles et al., 1998). A lot of effort is therefore being put into the development of special sample containers (Buffiere et al., 2010) that allow to run controlled processes on the scanner setup without strongly degrading the image quality. Key considerations here are the size and shape of the container, which ideally is cylindrical with a small diameter (typically on the order of one to a few centimeters), and the material

from which it is made, which should be X-ray transparent and mechanically and chemically robust (e.g. aluminum, carbon, PEEK, beryllium).

The monitoring of dynamic (chemical) transport processes can either be done by using time-lapse CT or by continuous imaging. While the former is well suited for slow running processes that only require imaging at set time intervals, the latter continuously follows the evolution of a sample with a high time resolution (on the order of seconds), enabling (pseudo) real-time visualization of the processes happening in its structure. Many different processes in geosciences can be studied this way, including fluid flow in porous media (Berg et al., 2013), compression of materials (Terzi et al., 2009; Voide et al., 2009) or chemical processes like corrosion of metals (Knight et al., 2010), carbonation processes (Boone et al., 2013) and dissolution (Menke et al., 2015) (Fig. 8).

Time-lapse CT has been performed both at synchrotron beam lines and using laboratory setups, as the real challenge in this case is the exact alignment of images taken at different time intervals. In cases where the sample does not have to be removed from the setups, this step is considerably simplified. Recent examples of time-lapse CT at synchrotron facilities in geosciences are heating experiments, e.g. to follow the evolution of shales (Panahi et al., 2013), multi-phase fluid transport experiments (Herring et al., 2015, 2014; Madonna et al., 2013) and reactive transport (Menke et al., 2014). Similar multi-phase flow studies have recently been performed with laboratory-based micro-CT scanners as well (Aghaei and Piri, 2015; Andrew et al., 2014, 2013; Georgiadis et al., 2013; Pak et al., 2015). Laboratory-set ups are also suitable to studying the evolution of limestone pore systems upon weathering (De Kock et al., 2015; Dewanckele et al., 2013, 2012), investigating salt transport and crystallization inside pore systems (Derluyn et al., 2014, 2013; Ott et al., 2014; Rad et al., 2015) and following dissolution and precipitation processes in building and reservoir materials (Boone et al., 2014; Noiriel, 2015).

Continuous, truly dynamic experiments have seen a rapid rise at synchrotron facilities over the last years. This evolution was possible due to the development of fast read-out detector technology and fast computer memory, permitting to make use of the high X-ray flux at these facilities to allow very short image acquisition times. These short acquisition times are a necessity to capture fast-occurring processes in geological materials without motion blurring artifacts. Pistone et al. (2015) performed experiments at the TOMCAT beam line of the Paul Scherrer Institute (PSI) in Switzerland, to follow the evolution of melting magma over time. Therefore, both high temperature, high spatial resolution and a temporal resolution of around 8 s were required. Experiments at the same beam line provided information on single Haines-jump events in multi-phase flow experiments in sandstones (Armstrong et al., 2014b; Berg et al., 2013; Youssef et al., 2013), on trapped non-wetting phase remobilization (Armstrong et al., 2014a) and on ganglion dynamics during two-phase flow (Rücker et al., 2015). A specially developed flow cell, powered by slip-rings at the

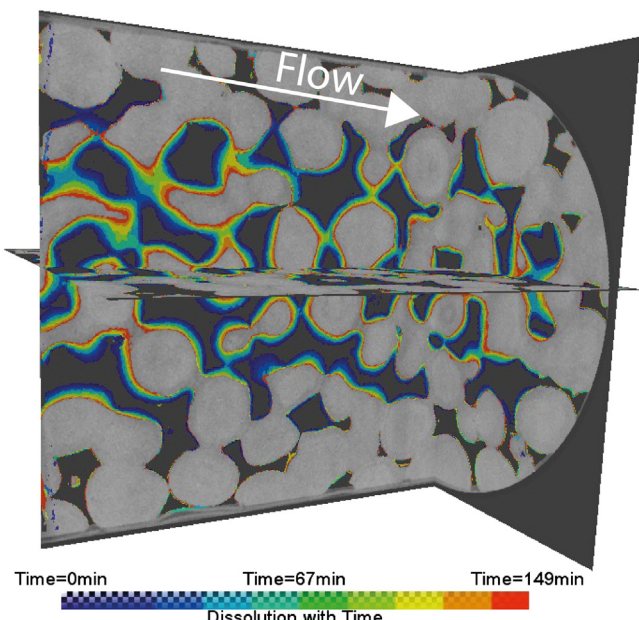


Fig. 8. An experiment from Menke et al. (2015) performed with a laboratory-based micro-CT scanner visualized dissolution in a Ketton carbonate rock core during injection of CO₂-saturated brine. An image with a voxel size of 3.8 μm was captured every 15 min over the course of 2.5 h.

Figure reprinted with permission from Menke et al. (2015).

TOMCAT sample stage, allowed for continuous acquisition of images (Armstrong et al., 2014b). By using this method, one tomographic reconstruction can be started at any given radiograph. This can either provide information on changes faster than the time resolution, or can be used to start reconstructions only at interesting time intervals. Similar experiments have been performed at the Diamond Light Source (Andrew et al., 2015; Fanis et al., 2013). The latest developments at synchrotron imaging beam lines have led to even sub-second acquisition speeds.

Recent developments at laboratory setups have attempted to bring synchrotron-like continuous dynamic imaging capabilities to a much more accessible laboratory environment. A detailed overview of the challenges and the progress made in fast laboratory-based micro-CT can be found in Bultreys et al. (2015a). Important emerging hardware technologies are fast X-ray detectors which are efficient at the higher X-ray energies used in the lab, and new high-flux X-ray sources with liquid metal jet anodes. Furthermore, gantry-based system is being developed to allow continuous imaging of samples which are attached to tubing or sensor wiring (Dierick et al., 2014). On the software front, iterative reconstruction techniques are being developed (Batenburg and Sijbers, 2011; Brabant et al., 2014; Kazantsev et al., 2015). In addition to having superior noise characteristics, these methods allow the incorporation of prior information on the pore space geometry and the physical processes which take place, thereby severely improving the image quality of fast, flux-limited scans (Myers et al., 2014, 2011a; Sheppard et al., 2014). Aside from reconstruction techniques, specialized image analysis methods are important, in order to extract information from low signal-to-noise ratio datasets (Bultreys et al., 2015a; Maire and Withers, 2014; Mendrik et al., 2015). By using scan speeds down to 12 s, dynamic two-phase flow processes (including capillary water uptake) have been imaged (Bultreys et al., 2015b; De Kock et al., 2013; Myers et al., 2011b) (Fig. 9) and solute transport has been monitored at the pore scale (Boone et al., 2015; Koestel and Larsbo, 2014) (Fig. 10).

2.5.3. Phase contrast micro-tomography

Micromotography that is based on X-ray phase contrast (pc-micro-CT) is mainly performed at synchrotron radiation facilities, and provides an X-ray technique that is useful for imaging of low-contrast specimens. It is an ideal technique for the investigation of samples that consist out of light chemical elements, such as organic tissues (Beckmann et al., 1997), or for samples where the attenuation contrast is very low. In attenuation contrast micro-CT, it can be problematic to distinguish organic material inside stone, since the X-ray attenuation coefficient of light elements is very low. The X-ray phase contrast effect is caused by local alterations of the X-ray refractive index, causing phase changes of the X-ray wave as it passes through the sample. This 'refraction of X-rays' causes an edge-enhancing effect which is considered an artifact in "normal" (attenuation contrast) CT, and can hinder correct segmentation of datasets (Cnudde and Boone, 2013). However, it can also be very

favorable for visualization, exposing very small structural details, even if the difference in absorption is very small or the features are very thin (Beckmann et al., 1999, 1997; Bronnikov, 2002). This effect is mainly useful at synchrotron facilities, since it is well pronounced due to the high coherence of synchrotron radiation. At laboratory setups, the effect mainly arises at very high resolutions and with weakly attenuating samples (Cnudde and Boone, 2013). The amount of edge enhancement depends on sample-detector distance, X-ray energy, detector resolution, and of course the phase properties of the sample itself (Tafforeau et al., 2006).

Lak et al. (2008) and Tafforeau et al. (2006) show a great application of pc-micro-CT in geosciences, by using the technique to study fossils. Although fossils usually do not consist of light elements, the chemical alterations in the fossilization process (all bones, tissues and other features are converted to 'stone'), make it very hard to distinguish between different phases in attenuation contrast. An example of this kind of study is pc-micro-CT of fossil teeth, which shows no absorption contrast, due to diagenesis (all of the structures are fossilized with the same mineral composition). Pc-micro-CT was used to measure enamel thickness and distribution, an important feature for paleoanthropologists (Smith et al., 2010; Tafforeau et al., 2006).

On the edge between life sciences and geosciences, pc-micro-CT and phase contrast radiographies are used to study fossils in amber. Especially when the amber fragments are completely opaque and the organisms (flowers, insects, spiders, etc.) are invisible in attenuation tomography, pc-micro-CT is a technique with unprecedented potential (Tafforeau et al., 2006) even leading to the discovery of new species (Henderickx et al., 2012, 2006).

Evidently, medicine and life sciences were among the early adopters of phase contrast radiographies and tomography. In this field, phase contrast imaging was one of the biggest innovations in X-ray imaging since the invention of computed tomography (Lewis, 2004), although the technique is not a mainstream and commercialized procedure yet. Early applications included the detection and visualization of cancer lesions at the university of Tsukuba in Japan (Takeda et al., 2000, 1995). Recently, pc-micro-CT has been used for the *in vivo* scanning of a fly. So-called time-resolved tomography was used, to see the actual muscle movement of this fly, while operating her wings (Walker et al., 2014).

An advancement in pc-micro-CT is holotomography or quantitative phase micromotography. Holotomography enables imaging at good quality of materials with even smaller differences in attenuation coefficients. This way, slight variations in soft tissues or other organic matter can be imaged even better than using pc-micro-CT. The method was pioneered by Cloetens and co-workers at the ESRF synchrotron in the late 1990s (Cloetens et al., 1999). The main difference between holotomography and pc-micro-CT is that holotomography uses the phase shift information acquired at different sample-detector distances for the production of phase maps (Heethof and Cloetens, 2008). Holotomography in geosciences is especially valuable in paleontology, where distinction can be made between fossilized soft

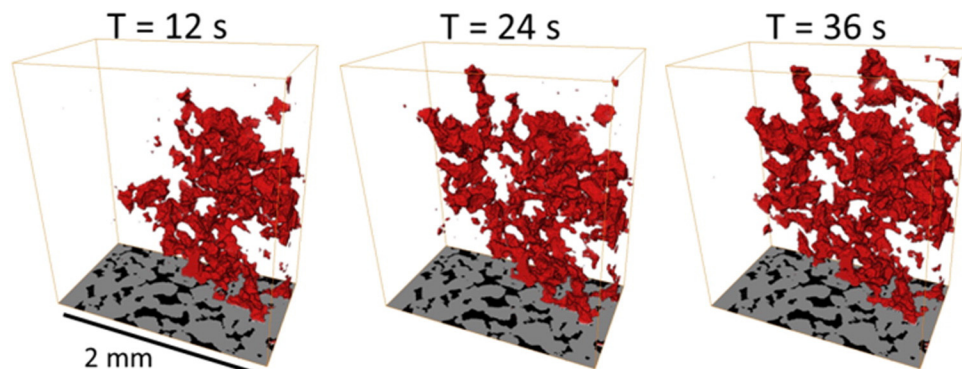


Fig. 9. Three consecutive timesteps from a drainage experiment (Bultreys et al., 2015b) performed with a laboratory-based micro-CT scanner, showing oil (in red) displacing brine (not visualized) in a sandstone sample. Each scan took 12 s to complete at a voxel size of 15 μm , allowing to study Haines jumps during the displacement.

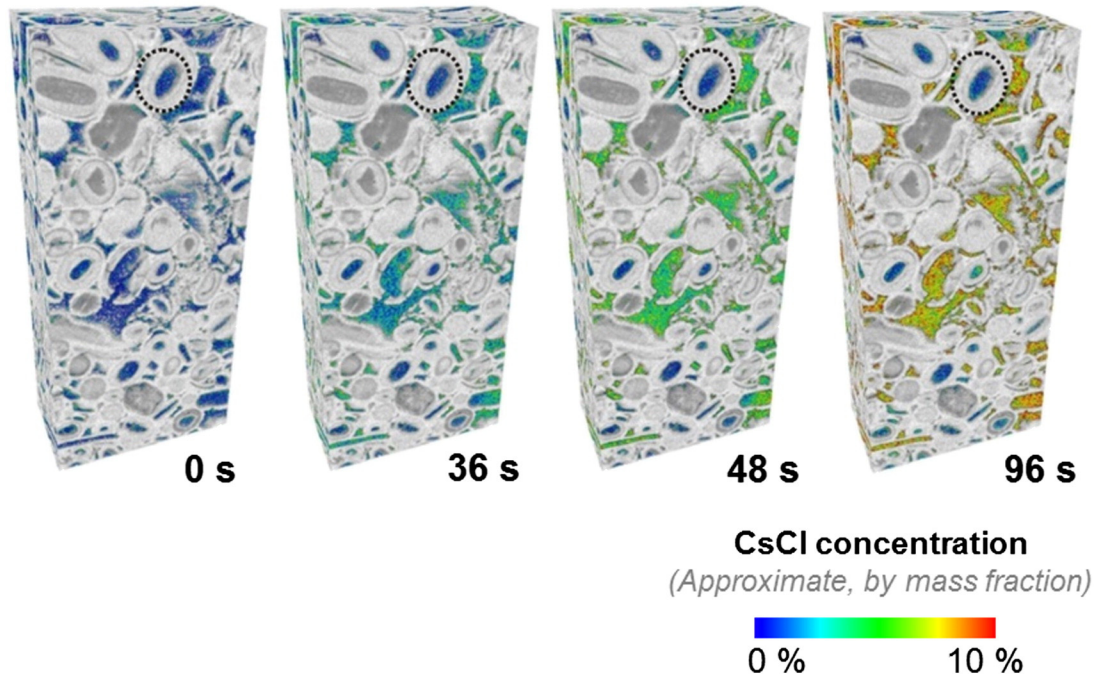


Fig. 10. Four selected timesteps from a solute transport experiment, where a CsCl brine was pumped into a water-saturated carbonate rock sample. Each scan took 12 s to complete at a voxel size of 15 μm . The time series shows how the solute spreads in the carbonate according to preferential flow paths, with relevance to reactive transport and spreading of pollutants.

tissues, e.g. to reconstruct the brain of a fossilized fish (Pradel et al., 2009).

2.6. Ptychographic tomography

Recently, ptychographic X-ray computed tomography, based on small-angle X-ray scattering (SAXS) at synchrotron facilities provides the possibility to gather 3D structural information at nanometer scale (30–60 nm) resolution, be it on very small (30–300 μm) samples (Diaz et al., 2012; Dierolf et al., 2010). The basic principle of this technique is coherent diffractive imaging (CDI), where a monochromatic X-ray beam usually hits a pinhole to create a pencil beam, to obtain a localized illumination (a few microns wide) on the sample. In some cases, focusing optics are used to acquire a small, coherent X-ray spot. Unlike in scanning transmission X-ray microscopy, where only the X-ray intensity is taken into account, the detector measures diffraction patterns of the beam going through the sample in the far field (Nugent, 2010; Thibault et al., 2008). The entire sample is scanned, measuring

diffraction patterns on a large number of locations on the sample. X-ray ptychography enables resolutions of (better than) 10 nm (Schropp et al., 2012). In ptychographic X-ray CT, this whole procedure is repeated for different angles over 180° (usually 1° intervals), so that a three-dimensional volume can be reconstructed (Fig. 11). The first demonstration of this technique was reported by Dierolf et al. in 2010, where a 30 μm bone sample was analyzed with a 65 nm³ voxel size, but resolutions up to 16 nm in 3D have been realized (Holler et al., 2014). Since 2010, experiments have been carried out in various field, for different kinds of porous and non-porous materials, including concrete (Tritik et al., 2013), textiles (Esmaeili et al., 2013), carbon fibers (Diaz et al., 2014), coatings (Chen et al., 2013), solar cells (Dam et al., 2015), etc. Recently, ptychographic tomography has been used to study the composition and structure of clay minerals, extracted from different sandstones, at resolutions down to 45 nm (De Boever et al., 2015a). Using this method, they were able to visualize small structural changes upon changing relative humidity and identify different mineral phases within individual clusters of clay-sized particles.

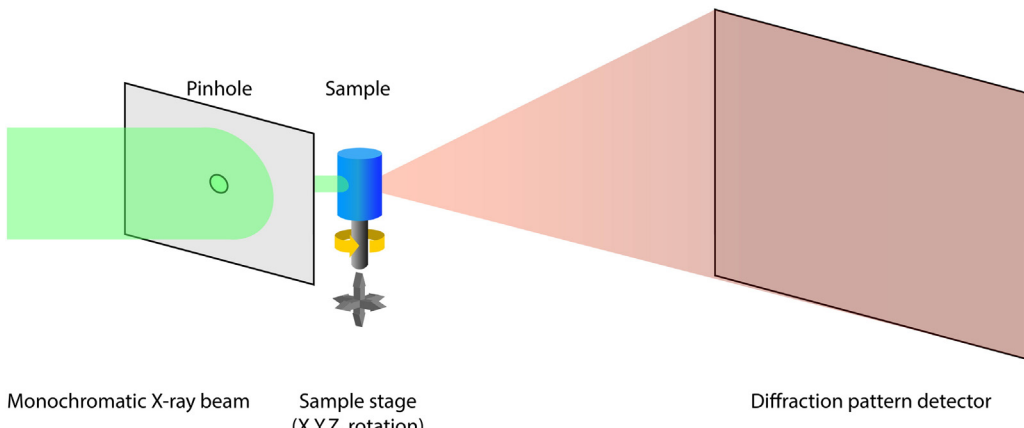


Fig. 11. Schematic setup for ptychographic tomography. A monochromatic X-ray beam hits a pinhole or focusing optics (optional, this is usually not done for larger samples), and the resulting beam interacts with the sample. The diffraction pattern is measured by the detector. This procedure is repeated for many spots in the samples X,Z plane, before rotating it over a small angle and repeating the entire procedure.

2.7. Dealing with (3D) images

2.7.1. Introduction

For quantitative analysis of 2D images and 3D datasets, data should be analyzed using dedicated software. For 2D image analysis, there is a huge amount of software available, ranging from very good open source tools to well-known commercial packages such as Adobe Photoshop®. Although the market for 3D analysis software is much younger, more and more excellent tools are becoming available. At the moment, some of the best software packages include Avizo (www.avizo.com), VGStudioMAX (www.volumegraphics.com), MAVI (www.itwm.franhofer.de), Pore3D (Brun et al., 2010), 3DMA-Rock (Lindquist and Venkatarangan, 1999), Morpho + (now known as Octopus Analysis, distributed by www.insidematters.eu; Brabant et al., 2011; Vlassenbroeck et al., 2007) and Fiji (open source, www.fiji.sc; Schindelin et al., 2012). In the following, we describe some of the key image analysis methods described in the literature, with an emphasis on 3D analysis (although many of the measures are directly applicable to 2D images as well).

2.7.2. Geometrical and topological pore characterization

A first class of measures is based on the statistics of a gray value image (usually the output of an experimental pore characterization method using 3D digital imaging techniques like X-ray CT or FIB-nt), notably the variogram (2-point correlation function) and first or second derivatives of the gray values (gradient function and hessian matrix). The former measure is typically used to assess a sample's heterogeneity and representative volume size, while the latter is often employed to assess its isotropy (Schladitz, 2011). However, when measurements are performed directly on gray value images, image noise and sharpness can be an issue. Furthermore, small bright spots (resulting for example from highly attenuating minerals) can result in difficult measurements and interpretations (Wildenschild and Sheppard, 2013). Other measures demand the partition of voxels into material phases, instead of working on gray values. We will assume that the provided image quality is high and that image artifacts related to the used technique are reduced as much as possible by selecting the correct hardware and software setup, the best acquisition and reconstruction parameters and possibly by performing image processing after the data acquisition (including binary operations like opening and closing, and methods like watershed separation) (Bovik et al., 2001; Russ, 1999). Then, the next step in the analysis process is image segmentation.

During segmentation each voxel in the 3D region of interest is assigned a label according to the material it is assumed to belong to. Because segmentation is typically the first step in the processing, it plays a crucial role in errors and uncertainties related to pore characterization from experimental methods. The easiest method to segment an image consists of using a single threshold: all values within a certain grayscale interval are assigned to a certain material phase. Although many automated methods for threshold selection are available (Huang and Wang, 1995; Otsu, 1979; Ridler and Calvard, 1978) this step is very often performed manually, and is therefore user-dependent. Dual thresholding (often also referred to as hysteresis thresholding) uses two intervals; voxels with a gray value in the first interval are classified as a certain material phase, while voxels in the second interval are only considered to belong to this phase if they are connected to voxels from the first interval. This approach reduces the sensitivity to residual image noise. Obviously, manual adjustment of thresholds to produce a result that is considered to be correct based on visual inspection by a human operator has to be reduced as much as possible. User-dependency is one of the major drawbacks of image-based analysis methods, since it implies that results on the same data can vary between different users and research institutions. Automated threshold methods are a vital part of the solution to this problem, but the diversity of applications, image types and image artifacts makes this a very challenging task.

Another problem with the previously discussed thresholding techniques, is that every voxel in the image is treated the same, i.e. no local information is taken into account when deciding to which phase a certain voxel belongs. This poses problems when not all voxels of a certain material phase fall in the same gray value range, for example due to differences in illumination over the sample. Furthermore, the use of local information is a powerful way to reduce misclassification due to statistical noise. It can help to segment phases with low contrast by including edge information, and it often reduces user dependency (many of these methods ask user input to pin down the phase of voxels which are easy to segment, and then automatically segment the "difficult" parts of the image). Several of these segmentation methods exist, but a detailed description of all image segmentation methods would justify a review on its own.

All segmentation methods (automatic methods in particular) make some assumptions about the nature of the image, and in order to choose the proper algorithm, it is important to know as much as possible about the nature of the image, how it was acquired, and what kinds of structure are present in it (Russ, 1999). A comprehensive survey of many techniques is available in Sezgin and Sankur (2004), while the review by Iassonov et al. (2009) compares advanced segmentation methods for X-ray micro-CT scans of porous materials in particular. As can be seen in these review articles, many automatic segmentation methods have been devised, but in practice segmentation typically still requires user intervention, resulting in subjectivity. Segmentation is often a bottle neck in the image analysis process, in particular for images with low contrast-to-noise ratio or which contain certain artifacts. After segmentation, voxels that are erroneously classified as foreground voxels due to noise can sometimes be removed by applying several binary operations like eroding, dilating, opening, closing, and hole filling (Soille, 1999). However, when attention has been paid towards the production of high quality images with good contrast and an experienced user is controlling the 3D analysis software, excellent data can be obtained, giving valuable information about the material's structure.

Once an experimental structural representation has been obtained and segmented, it is possible to assess geometrical properties of a pore space (Brabant et al., 2011). The previously mentioned statistical measurements can be performed on segmented images and are then easier to interpret (Arns et al., 2005; Blair et al., 1996; Torquato, 2002; Wildenschild and Sheppard, 2013). The homogeneity of the medium can also be checked by measuring partial porosity, local porosity and local percolation. Other important measures are porosity, percolating porosity and (specific) pore surface area (possibly divided into pore surface in contact with certain minerals). Topologic descriptors (e.g. Betti numbers and related the Euler characteristic) can provide information about global pore connectivity (Arns et al., 2001), and further topology characterization can be performed by extracting a skeleton from the segmented image.

By calculating the Euclidean distance map (in which every local maximum is a unique point that represents one specific feature) on the segmented image and performing a watershed transformation, the pore space can be divided into individual pores, separated at the pore throats (Brabant et al., 2011; Vincent and Soille, 1991). Separation of a pore space into individual pores is also an important problem in pore network extraction methods, which will be discussed in Section 4. Once this pore separation has been performed, pore shape can be quantified by determining individual pore volume, surface area, form factor (to characterize roughness) and the diameter of the largest inscribed and smallest circumscribed sphere. More advanced methods use ellipse fitting or spherical harmonics to describe pore shape (Wildenschild and Sheppard, 2013).

2.7.3. Skeleton extraction and analysis

A skeleton can serve to quantify pore space topology by means of measures such as shortest path determination through the pore space,

network tortuosity, coordination number, and off-diagonal network complexity (Wildenschild and Sheppard, 2013). Skeleton representations can also be used to detect individual pores and throats in pore network models. Ideally, such a skeleton should lie centrally in the pore space ("medialness") and preserve the pore space topology (Cornea et al., 2007). Furthermore, the skeleton should be thin (i.e. only one voxel wide except where larger thickness is needed to represent the topology correctly). Many skeletonization methods, such as grassfire algorithms, satisfy one or two of these requirements but not all three. Homothopic thinning algorithms on the other hand, try to meet all three demands by performing a thinning scheme where voxels are only removed if the topology of the remaining space is not changed, i.e. is homotopically equivalent. This method is therefore currently by far the most popular. Nonetheless, skeleton extraction is notoriously sensitive to noise in the segmented source image, and many pre- and post-processing methods have been devised to obtain cleaner skeletons (Plougonven and Bernard, 2011; Sheppard et al., 2005).

2.7.4. Data fusion

Although most of the pore characterization techniques mentioned above are mature methods for pore space characterization, data interpretation is still not straightforward. Each technique has its own strengths and limitations regarding resolution, reproducibility, dimensionality, cost, etc. The main challenges for the user lie in making correct assumptions and intelligent combinations between different techniques.

A first hurdle is that information in a 2D cross-section is not directly transferable to a 3D environment. This problem can be solved by using stereology, which bridges the gap between 2D planes and 3D information, by means of statistics and empirical formulas.

Another tool is 2D to 3D registration, in which a 2D image is aligned to its corresponding plane in the 3D volume of the same sample. This tool provides additional high-resolution 2D information directly on 3D datasets. This might be necessary when for example the spatial resolution or chemical information obtained from a CT volume is not sufficient. Since such additional information often comes from techniques that are not capable of imaging a 3D volume (SEM, EDS, etc.) merging 3D data such as CT data with 2D high resolution and/or chemical information from these techniques has become a key operation. Different methods exist for this purpose; a first method is manual alignment of the 2D data with the 3D volume. Since this is both labor-intensive and inaccurate, this is usually not the best option. Landmark based

registration is a more precise way to align data acquired with different techniques onto each other. In this method, corresponding points (called landmarks) are identified on both the 2D and 3D images (Fig. 12). Transformation algorithms then calculate the transformation to fit both landmark groups together, as well as the interpolation needed for the interlaying points (Bookstein, 1986).

A final class of methods for 2D to 3D registration consists of fully automated algorithms. Although such algorithms have been developed (Latham et al., 2008), they are not yet commercially available. These registration algorithms face the difficulty of solving a transformation problem with 7 degrees of freedom: 3 translational, 3 rotational and 1 isotropic scaling. The algorithm designed by Latham et al. (2008) uses a multi-resolution search strategy, where an exhaustive low-resolution search determines an initial small set of transformation parameters. The objective is that these initial parameters bring the image already in a 'global minimum' of deviation with reference to the target volume, and are used as starting values for an optimization method, looking for the local minimum. These values can be used to transform the 2D image to the target volume (Sok et al., 2010). As mentioned before, successful alignment of SEM images to CT volumes can provide additional structural information, due to the higher spatial resolution of these SEM images. This way, details about the microstructure can be linked to zones with specific gray values, corresponding to 'microporous' regions in the CT volume.

2D-to-3D registration can also be used to provide additional information about sample composition. Aligning backscattered SEM images and elemental mappings, acquired with EDS, provide an insight in the 3D distribution of certain elements, thus certain mineral phases throughout the sample. Fig. 13 shows the orientation of an iron-rich layer inside a sample of Vosges sandstone. A cuboid sample of this sandstone was scanned using micro-CT, and SEM mosaic images and EDS mappings were performed on all sides of the sample. An iron-rich layer is visible in the EDS mappings (Fig. 13, right). Since iron was only present in low quantities in the cement, contrast in the CT images was insufficient to threshold this layer. However, alignment of the EDS mappings provides 'pseudo-3D' information.

Besides 2D-to-3D registration, aligning different volumes with each other is also an important procedure in 3D analysis. 3D-to-3D registration can be useful for multi-scale (multi-resolution) imaging, as well as for time-lapse imaging and analysis. In the first case, different volumes with different voxel sizes are fused with each other, to link high-resolution data of small volumes to bigger volumes with lower spatial resolution. In the latter case, image registration is used to be

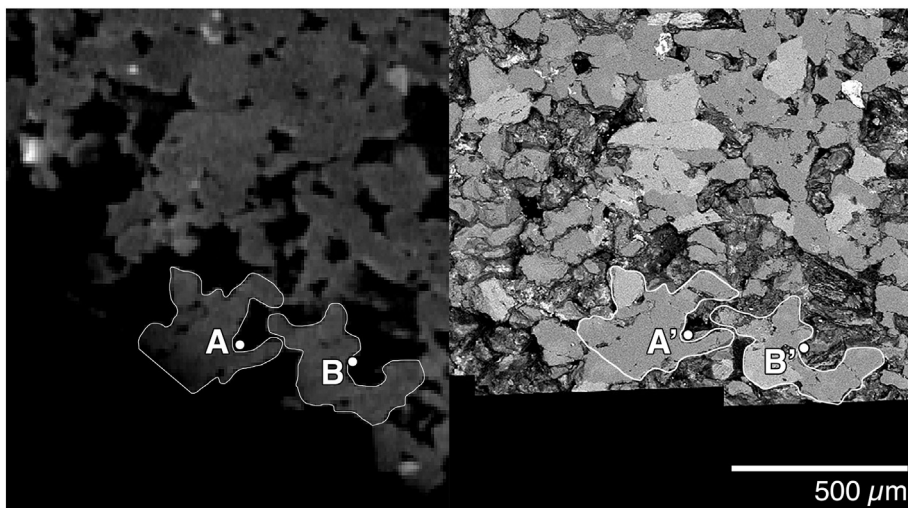


Fig. 12. Landmark selection for registration of a 2D SEM image (right) to a 3D CT volume (left). White lines indicate corresponding areas in a CT slice and an SEM image. The white dots indicate possible points for landmark placement (A, A' and B, B').
Reprinted with permission from De Boever et al. (2015b).

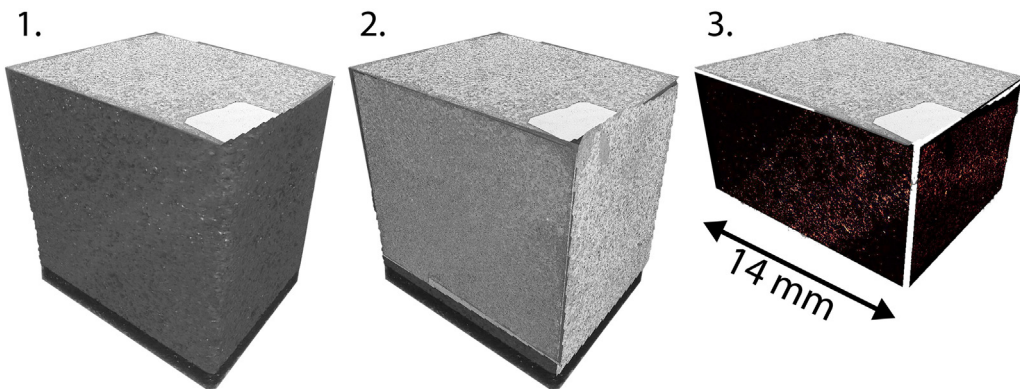


Fig. 13. Registration of 2D images to a 3D volume. Left: CT volume with SEM image registered to the top surface; middle: SEM images registered to all sides of the volume; right: aligned EDS mappings for iron show the orientation of an iron-rich layer in the sample. Registration was done using landmark registration. Reprinted with permission from De Boever et al. (2015b).

able to follow dynamic processes with voxel-size precision. Much work has been done recently to improve both forms of data fusion, and just as in 2D-to-3D registration, registration can be performed completely manually (Dewantkele et al., 2012), which is often a time-consuming and operator-dependent analysis step. Another option to perform registration is landmark-based alignment of datasets. Ideally, registration is fully automatic, but as in 2D-to-3D registration, not many of these algorithms exist, and none are freely available (Latham et al., 2008; Sok et al., 2010).

3. Direct pore scale modeling

3.1. Introduction

Direct pore scale flow modeling methods attempt to solve the Navier–Stokes equations (or in some cases a simplification of it) on the complex boundary conditions provided by a 3D representation of the pore space. While simulating single-phase fluid flow is fairly straightforward in principle, the complex geometries of pore spaces and fracture networks can result in practical difficulties (Meakin and Tartakovsky, 2009). Nevertheless, direct methods are currently the standard method of choice to calculate single phase flow and transport (Blunt et al., 2013). However, multi-phase flows add a number of difficulties. Since many geological multi-phase flow problems are slow, capillary dominated flows, tracking the interfaces of the fluids is paramount, as the curvature of the interfaces controls the capillary pressure (Blunt et al., 2013). This brings forth significant numerical challenges, as the fluid–fluid interfaces undergo intricate motions related to the complex boundary conditions posed by the porous medium (e.g. interfaces coalescing). Furthermore, the finite resolution of the computational grid or mesh makes it difficult to simulate small-scale processes such as wetting film flow in crevices, which is important to represent the wetting phase connectivity correctly, as well as to simulate instabilities of oil-filled pores during imbibition. The aforementioned complications add to the computationally demanding nature of direct methods, making it difficult to perform simulations on representative volumes, particularly in heterogeneous rocks. Therefore, the amount of studies performed on experimentally determined pore space geometries of “real” geological porous media (rather than simple model systems such as glass bead packs) is still relatively limited, compared to the large body of literature on the development of numerical algorithms to perform these simulations.

Several classes of methods can be distinguished based on the numerical scheme they employ and on the way the geometry of the pore space is treated. An overview of the most important ideas behind these methods will be presented in this section, along with their applications in Earth science fields.

3.2. Lattice Boltzmann

3.2.1. Method

Among the most popular methods for pore-scale flow simulation is the lattice-Boltzmann (LB) method. These methods have evolved from lattice-gas (LG) models (cellular automata), which are more intuitive to understand. In LG models, space is discretized by introducing a regular lattice, on which fluid particles can move with discretized velocities (Higuera et al., 1989; Sukop and Thorne, 2006). At each time step, these particles propagate (i.e. “jump”) to a neighboring lattice point, depending on their velocity and initial position, and collide with each other, in such a way that momentum is conserved. This can be seen as a discretization of the behavior of an ideal gas. To simulate the presence of multiple phases or components, particles can be given a label (or “color”) according to the phase or component they belong to, after which the collision rules are adapted to model interactions between the different phases or components (Rothman and Zaleski, 1994). To simulate immiscible phases, particles of each phase collide such that they are directed as much as possible towards other particles with the same label, resulting in phase separation. To simulate reactive flow, particles are created or destroyed when particles collide with each other or with solid walls. However, lattice-gas models suffer from noisy statistics and Galilean invariance, which can be overcome by using lattice-Boltzmann methods. Here, the moving particles on the

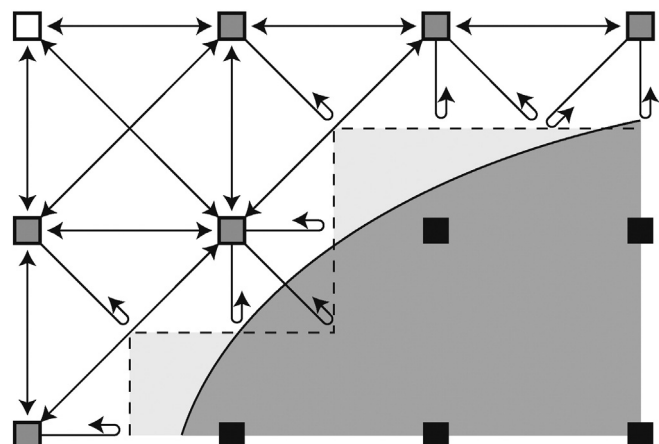


Fig. 14. Fluid solid boundary handling in lattice-Boltzmann methods. Solid is shown in dark gray, pore space in white. Black nodes are in the solid phase, gray nodes are in the pore space but are neighboring solid space, and white nodes are in the pore spaces. Reprinted with permission from Llewellyn, 2010. At each time step, particles can be redistributed according to the arrows between the nodes.

lattice are replaced by “packets” of moving particles, i.e. particle velocity distributions (Meakin and Tartakovsky, 2009). Today, lattice-Boltzmann (LB) methods have almost completely replaced lattice-gas models for flow simulations in geological materials.

The LB method solves a discretized Boltzmann equation of fluid-particle distributions that move and interact on a regular lattice with very few degrees of freedom (Ramstad et al., 2010). This means that at each node on a regular lattice, a particle distribution for each possible particle velocity vector is defined. The number of these vectors is limited by only allowing particles to move to a neighboring node in one time step. During each time step of the simulation, packets of particles are propagated according to their velocities, and the velocity populations are relaxed by a collision step (mimicking molecular collisions) (Meakin and Tartakovsky, 2009). The simplest, most popular collision rule is the single-relaxation time Bhatnagar–Gross–Krook (BGK) approximation, however, correctly modeling viscosity effects requires the use of two-relaxation time models (Talon et al., 2012). It can be shown that the Navier–Stokes equations can be recovered from the lattice-Boltzmann scheme in the incompressible limit (Thijssen, 2007). Typically, the lattice is just the voxel grid of the 3D image obtained from for example a micro-CT scan. Consequently, no complicated meshing procedures have to be performed. Solid boundaries are typically handled with a simple bounce-back condition, meaning a packet of particles which hit a solid wall node at a certain time step are “bounced back” to the node in the pore space where they came from (see Fig. 14, Llewellyn, 2010). Sukop and Thorne (2006) provide an in-depth introduction into this numerical technique, aimed at geoscientists and engineers.

The LB method is noted for its relatively simple implementation and its suitability for parallelization (e.g. McClure et al., 2014). Furthermore, it has a natural extensibility to represent multi-phase flow by tracking multiple types of interacting particles, each type representing a fluid phase, thereby removing the need to track interfaces explicitly (Geiger et al., 2012; Kuzmin and Mohamad, 2010; Shan and Chen, 1993). When simulating multi-phase flows, there are different methods of taking the fluid–fluid interactions into account: most notably color gradient models (Gunstensen et al., 1991), free energy models (Swift et al., 1996) and Shan–Chen (also-called pseudo-potential) models (Shan and Chen, 1993). For detailed descriptions of how these models work, we refer to the original sources or more in-depth reviews on lattice-Boltzmann modeling.

One of the main disadvantages of the method is its computational inefficiency, even with a massively parallel implementation. The run time scales approximately inversely with the real flow rate, making it difficult to accurately capture capillary-controlled flow on representative images (Blunt et al., 2013). Other important limitations are that the numerical stability of the method is problematic in the situation of multiphase flows with large density and viscosity ratios, which is the case in for example water–gas systems (Meakin and Tartakovsky, 2009), and the fact that in multi-phase flows, linking the model's interaction forces to the modeled physical processes is not trivial (Ferrari and Lunati, 2013).

3.2.2. Applications

3.2.2.1. Single-phase flow. Over the last 20 years, LB algorithms have been used extensively to study porosity–permeability relations on 3D images of rocks and sediments, obtained from stochastic or process-based reconstruction (Keehm, 2004; Wu et al., 2006), FIB-nt images (Yoon and Dewers, 2013), and most notably micro-CT imaging (Andrä et al., 2013; Fredrich et al., 2006; Jin et al., 2004; Khan et al., 2012; Manwart et al., 2002; Shah et al., 2015). Parallel implementations allow to investigate the link between the microstructure and the single-phase flow field in volumes of more than 1000^3 voxels, allowing to achieve representative elementary volume at sufficient voxel resolution in many rock types. Most studies investigate laminar flow as this is usually the

case of interest in geological problems, but LB models can also be used to study high-Reynolds number flows (Chukwudozie et al., 2012).

Despite these successes, simulations in heterogeneous materials with very broad pore size distributions (e.g. many carbonates) remain challenging. To tackle this problem, so-called “gray” LB models are being developed (Kang et al., 2002; R. Li et al., 2014a; Yehya et al., 2015; Zhu and Ma, 2013). In these multi-scale models, nodes which contain sub-resolution microporosity (e.g. clay or micrite) only partially bounce back the arriving fluid packets. Microporous domains in the image are therefore treated as permeable regions and contribute to the flow in the sample. While this is certainly an interesting approach, further validation is needed, and some theoretical issues have been brought forth recently (Ginzburg, 2014).

Another challenge which has recently received a lot of attention is the simulation of flow fields in tight, often fractured materials, including shale, chalk and coal (Kelly et al., 2015). Not only do Klinkenberg effects have to be taken into account when the pore or fracture sizes are on the order of the mean free path of the fluid molecules (Chen et al., 2015), but reliably segmenting thin fractures with sufficient detail on representative samples may cause problems (Ma et al., 2010). Simulations on fracture networks with fracture openings which are only a few lattice nodes wide result in significant uncertainties on permeability (Welch et al., 2015).

3.2.2.2. Solute and reactive transport. To investigate the influence of pore structure on dispersion, the transport of dilute tracers can be modeled by simulating the flow field of a carrier fluid on one lattice, and propagating each tracer on a separate lattice according to the flow field determined from the carrier fluid (Stockman, 2006). A number of such studies exist on 2D samples and single fractures (Jiménez-Hornero et al., 2005), while recent studies have also tackled 3D images extracted from micro-CT scans (Boek et al., 2014; J. Yang et al., 2013b). Promising LB models have also been developed to simulate reactive transport (Huber et al., 2014; Kang et al., 2010; Patel et al., 2014a, 2014b; Sullivan et al., 2005) by adding source and sink terms to represent the chemical reactions. However, most applications of these methods have remained limited to simulations in very simplified 2D porous geometries. Very recently, such models have been applied to study the coupling between dissolution and precipitation in 3D images based on micro-CT scans of geological media (Gao et al., 2015; Jiang et al., 2014). In this context, it is interesting to couple micro-CT scans with chemical information obtained with other imaging methods like QEMSCAN, EDS or XRF (Gao et al., 2015; Landrot et al., 2012; Peters, 2009). A comprehensive review on the use of lattice-Boltzmann for pore scale reactive transport modeling can be found in (Yoon et al., 2015).

3.2.2.3. Multi-phase flow. The three main models (color gradient, Shan–Chen and free energy) are compared in (Yang and Boek, 2013). The authors conclude that the (Oxford) free energy and color gradient models seem appropriate to simulate the flow of binary fluids with high viscosity contrast with high numerical stability, while the Shan–Chen (pseudo-potential) model is capable of simulating high density ratio fluids (e.g. brine–gas) but provides lower numerical stability and wide interfaces for immiscible systems. Despite the computational challenges, the LB method has been used for a number of studies concerning multi-phase simulations on realistic, 3D pore structures; be it usually on rather homogeneous rock types and rather small rock volumes (see Table 1) (Boek and Venturoli, 2010; De Prisco et al., 2012; Ferréol and Rothman, 1995; Harting et al., 2005; Hazlett et al., 1998; Landry et al., 2014a, 2014b; Pan et al., 2004; Porter et al., 2009; Ramstad et al., 2010, 2012; Schaap et al., 2007; Sukop et al., 2008). As an example of the benefit of applying direct modeling, Jiang et al. (2014) show how LB can elucidate the influence of the interfacial tension on relative permeability in a sandstone: three different zones of interfacial tension values were found, each showing distinct characteristics in terms of

Table 1

Selection of studies presenting two-phase LB simulations on realistic 3D pore geometries.

Publication	Study subject	Sample	Algorithm	Grid size
Ferréol and Rothman (1995)	Qualitative study	Fontainebleau	Color gradient	64 ³
Hazlett et al. (1998)	Influence of wetting on displacement dynamics and relative permeability	Berea	Color gradient	128 ³
Pan et al. (2004)	Hysteretic capillary pressure, REV	Digital sphere pack	Shan-Chen	512 ³
Harting et al. (2005)	Fluid distributions in drainage and imbibition compared to MRI	Bentheim	Shan-Chen	512 ³
Schaap et al. (2007)	Capillary pressure compared to experiment for air-water and air-soltrol	Glass beads	Shan-Chen	405 × 405 × 100
Sukop et al. (2008)	Equilibrium distributions compared to micro-CT experiments	Sandpack	Shan-Chen	
Porter et al. (2009)	Hysteresis in capillary pressure and wetting/non-wetting interfacial area, compared to experiment	Glass beads	Shan-Chen	207 × 207 × 166
Ramstad et al. (2010)	Steady and unsteady state relative permeability	Bentheim (micro-CT & PBM)	Color gradient	256 ³
Boek and Venturi (2010)	Relative permeability	Bentheim	Shan-Chen	128 ³
De Prisco et al. (2012)	Relative permeability	Middle eastern Carbonate	Phase field	500 ³
Ramstad et al. (2012)	Steady and unsteady state relative permeability	Bentheim and Berea	Color gradient	256 ³
Landry et al. (2014a)	Fluid–fluid and fluid–solid interfacial areas, relperms, influence of wetting	Bead pack	Shan-Chen	100 ³
Landry et al. (2014b)	Fracture–matrix fluid transfer, compared to 4D microCT	Fractured sintered glass	Shan-Chen	200 × 200 × 300
Mohnke et al. (2014)	Simulate NMR relaxometry experiments and two-phase flow	Sandpack	Color gradient	200 × 200 × 240
Jiang et al. (2014)	Influence of interfacial tension on fluid flow characteristics	Berea	Color gradient	320 ³
Jiang and Tsuji (2015)	Impact of interfacial tension on trapped cluster size	Berea	Color gradient	400 × 400 × 400

breakthrough time, displacement patterns, equilibrium invading fluid saturation and mean flow velocity.

Some fairly mature open-source lattice-Boltzmann libraries which have been used for porous media applications are Palabos (Parmigiani et al., 2011) and Taxila (Coon et al., 2013) (see for example Fig. 15). Lattice Boltzmann methods to simulate multi-phase, high-density-contrast flows in porous materials have been developed as well (Liu et al., 2014, 2013).

3.3. Traditional computational fluid dynamics

3.3.1. Method

A second class of methods are the traditional mesh-based CFD (computational fluid dynamics) approaches, such as finite difference, finite volume and finite element methods. These are probably the most popular methods to be used in natural porous media applications after lattice-Boltzmann. Unlike the latter, these schemes follow a top-down approach by discretizing the Stokes or Navier–Stokes equations on a (structured or unstructured) mesh (Icardi et al., 2014). The finite volume method is used most frequently, because it is naturally volume conserving. In this method, a local mass and momentum balance is written for each cell in the mesh (the “control volume”). These balances, which are obtained by integrating the mass and momentum balance equations (i.e. the Navier–Stokes or Stokes equations) over the control volume, are then written in terms of fluxes through the boundaries of the control volume: fluid and momentum flowing out of a cell boundary have to arrive in the neighboring cell (Eymard et al., 2000). By also discretizing time in small time-steps, the partial differential equations which govern the fluid transport are approximated as a set of algebraic equations, which can be solved numerically (Raeini, 2013). For the working principles of finite element and finite difference methods, we

refer to Thijssen (2007) and other standard works. Traditional CFD methods are numerically efficient and can simulate fluid flow with very large density and viscosity ratios (Meakin and Tartakovsky, 2009). While most porous media problems concern laminar flow, CFD methods can be applied to study non-Darcy flow at high flow rates as well (Muljadi et al., 2015).

Some of the difficulties encountered specifically for multiphase flow in porous and fractured media are the tracking of fluid interfaces, the implementation of a contact line/contact angle model and the increase of computational times and numerical instability for slow flow rates (Blunt et al., 2013; Meakin and Tartakovsky, 2009; Renardy and Renardy, 2002). Several strategies have been developed to deal with the problem of tracking the fluid interfaces during multi-phase flow. In the moving mesh methods, both fluids are meshed separately. Therefore, this method has the advantage of providing a sharp interface. Difficulties are the need to remesh often, making this method computationally inefficient, and dealing with topological changes of the interfaces (Raeini, 2013). The level-set method, on the other hand, uses an indicator function that is positive in regions occupied by one phase and negative in regions occupied by the other. The indicator function is advected with the flow. The effect of surface tension can be included as a body force (based on the curvature of the indicator function at zero), working only in the vicinity of the interface (continuous surface tension force model). The sharp interface is then replaced by a smeared out function over this region. This method handles topological changes well, but often violates mass conservation (Meakin and Tartakovsky, 2009; Prodanović and Bryant, 2006). Particle level set methods use particles with different labels inserted on opposite sides of the interface to track it, resulting in improved mass conservation.

One of the most promising interface tracking methods is the volume of fluid method (Ferrari and Lunati, 2013). Here, a “fuzzy” approach to

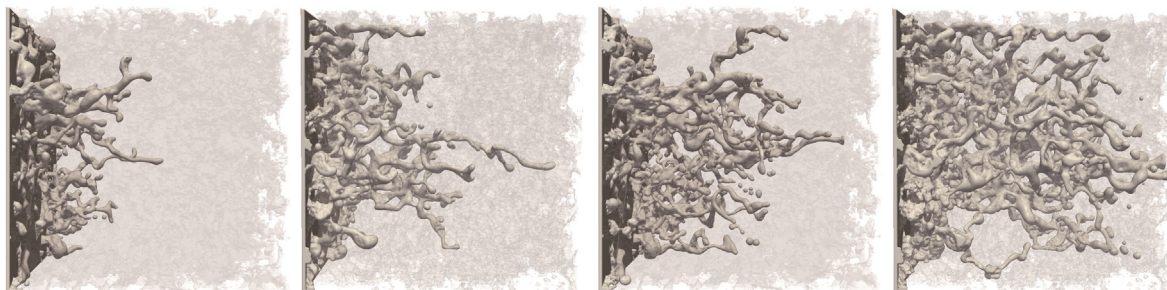


Fig. 15. Four snapshots of the non-wetting fluid intruding in a Berea sandstone during drainage, simulated with a color gradient lattice-Boltzmann model. Figure reprinted with permission from Jiang et al. (2014).

the presence of multiple immiscible fluids is followed, by tracking the volume fraction of each phase in each mesh cell (i.e. some cells can formally be thought to contain a mixture of the two fluids, meaning the interface need not be sharp). The interface can then be reconstructed from the gradient of this volume fraction. The effects of surface tension are expressed in terms of a body force that acts near the cells where the gradient of the volume fraction is non-zero (Raeini, 2013).

3.3.2. Applications

3.3.2.1. Single-phase flow. Like lattice-Boltzmann methods, classical CFD methods have been used extensively to solve single phase flow on direct, experimental 3D images of real rocks: e.g. with finite volume (Peng et al., 2014; Zhang et al., 2012) and finite element methods (Mostaghimi et al., 2013). Similarly, stochastically generated 3D pore spaces have been investigated (Hyman et al., 2012). In Veselý et al. (2015), flow and diffusion calculations on stochastically reconstructed porous geometries are compared to those on micro-CT scans of the same porous medium, illustrating both the sensitivity of the micro-CT based simulations on the image processing (filtering and segmentation), and the intrinsic difficulty of stochastically reconstructing realistic pore geometries, even in relatively homogeneous media.

A comparison of single-phase flow calculations with a finite volume and 2 finite difference schemes can be found in Siena et al. (2015). The authors note that despite significant differences in implementation and complexity between the three tested methods, consistent results were obtained. In Manwart et al. (2002), single-phase lattice-Boltzmann and finite-difference permeability simulations are compared. They note that while both methods delivered acceptable results, there were also differences, mainly caused by numerical concerns in the lattice-Boltzmann algorithm. A recent comparison between a finite volume, a lattice-Boltzmann, a smoothed-particle hydrodynamics and a pore network model was presented in Yang et al. (2015). Although all models gave broadly similar results, there were some differences believed to originate mainly from differences in meshing and grid resolutions. It should be noted that in general, drawing broad conclusions from model inter-comparison studies is complicated due to the variable capabilities of codes, the differences between individual implementations of similar algorithms and the difficulty of obtaining ground truth data to compare results with. To obtain such ground truth data, the flow field can be measured locally in the pore space by MRI measurements (X. Yang et al., 2013a).

When solving single-phase flow in very heterogeneous samples with unresolved porosity features, the flexibility and generality of the classical CFD methods pays off. Two different multi-scale methods have been developed in this context (Ligaarden et al., 2010). These methods are comparable to gray lattice-Boltzmann methods in set-up, but seem to have a more firm theoretical basis. The first method is the Darcy–Stokes method, which solves Stokes flow in the larger pores and Darcy flow through regions which contain unresolved porosity and are therefore considered permeable, e.g. Arbogast and Gomez (2009) and Scheibe et al. (2015). Coupling the Stokes and Darcy regions in the volume requires a complex treatment of the boundaries. The second approach is to solve the Stokes–Brinkman equation: the flow in both Stokes and Darcy regions is then described with this single equation with variable parameters (Krotkiewski et al., 2011; Popov et al., 2009; Yang et al., 2014), eliminating the need for complicated boundary treatment.

Workflows have also been developed to calculate single-phase flow on fractures extracted from micro-CT measurements, with or without interaction with a porous matrix around the fracture (Crandall et al., 2010; Huber et al., 2012). A finite element method specially adapted to deal with single-phase flow in coal and other tight samples with very small fractures was used by Ramandi et al. (2015). The method works with voxel-based local conductivities measured from the Euclidean distance map.

3.3.2.2. Solute and reactive transport. Classical CFD methods have been used to simulate solute transport on 3D images, either by moving particles along streamlines based on the computed advective flow field (Bijeljic et al., 2013a, 2013b; Mostaghimi et al., 2012; Pereira Nunes et al., 2015) or by solving the Navier–Stokes and advection–diffusion equations (Zaretskiy et al., 2010). Generally, particle-based methods are preferred to calculate transport of chemical species, as these methods are free of numerical dispersion (Mehmani and Balhoff, 2015). Such methods can be used to study for example the effect of pore space homogeneity on local velocity distributions and molecular displacement probabilities (Bijeljic et al., 2013b), showing that heterogeneous pore spaces produce non-Fickian behavior due to a persistently immobile solute concentration long after injection. The solute transport concepts have been further adapted to simulate reactive transport (Alhashmi et al., 2015; Molins et al., 2014; Siena et al., 2014; Trebotich et al., 2014).

3.3.2.3. Multi-phase flow. Only few applications of classical CFD methods to multi-phase flow on three-dimensional pore space images of geomaterials can be found in literature. Raeini et al. (2015, 2014) perform two-phase flow simulations on segmented 3D micro-CT images of Berea sandstone (Fig. 16) and a sandpack to investigate capillary trapping (on maximally 400^3 voxels), while Arrufat et al. (2014) show relative permeability simulations on micro-CT images of Clashach sandstone and two carbonates (with maximally 432^3 voxels). Piller et al. (2014) present relative permeability simulations on a 200^3 synchrotron-micro-CT scan of a sandstone (200^3 voxels). All of these examples employ the volume-of-fluid method. Applications of multi-phase finite volume simulations on 2D images can be found in e.g. Ferrari and Lunati (2013) and Huang et al. (2005).

It should be noted that direct numerical models such as Cardenas (2008) and Raeini et al. (2013) can provide highly-detailed sub-pore information, which can then be incorporated in less detailed, numerically more efficient simulations (e.g. pore network simulations).

3.4. Smoothed particle, semi-implicit-particle and dissipative hydrodynamics

An alternative to lattice Boltzmann and CFD methods are the smoothed particle hydrodynamics (SPH) methods (Bandara et al., 2013; Berry et al., 2004; Sivanesapillai et al., 2015; Tartakovsky and Meakin, 2006; Tartakovsky and Panchenko, 2015; Tartakovsky et al., 2009). Closely related are the moving particle semi-implicit (Ovaysi and Piri, 2011; Ovaysi et al., 2014) and dissipative (Español and Warren, 2007; Pan and Tartakovsky, 2013) particle hydrodynamics. These are mesh-free Lagrangian particle based methods, which share with lattice Boltzmann simulations the advantages of being able to deal with complex boundary conditions relatively easily, and of not requiring explicit interface tracking or contact angle models. In addition, the SPH model allows unsaturated (liquid/gas) flows with large viscosity and density ratios to be simulated (water and air with a viscosity ratio on the order of 100 and a density ratio on the order of 1000, for example). Another advantage of the SPH approach is its simple physical interpretation, since the Navier–Stokes equations are reduced to a system of ordinary differential equations with the form of Newton's Second Law of motion for each particle. This simplicity allows a variety of physical and chemical effects to be incorporated into SPH models with relatively little code-development effort through pairwise molecular type interactions (Tartakovsky and Meakin, 2006). The method is however computationally demanding compared to other methods described here, and it is therefore an attractive method to study multi-phase flow in complex geometries and in the case of large interface movements, but on smaller volumes than the previously described methods (which typically run on images of 200^3 to 300^3 voxels) (Raeini, 2013).

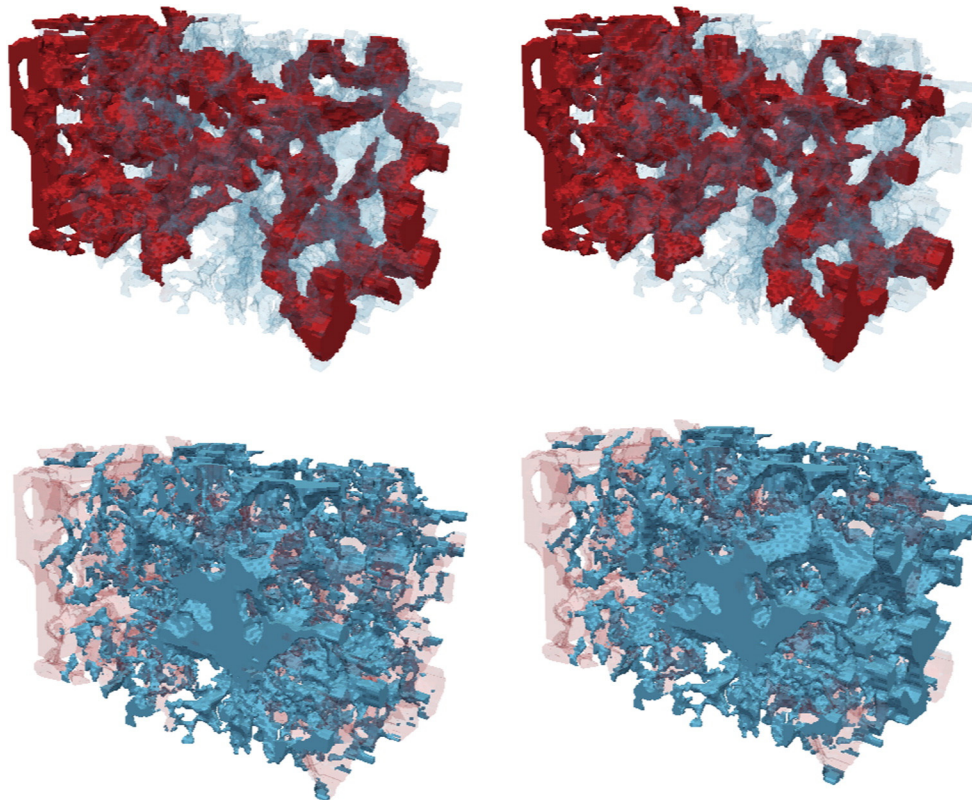


Fig. 16. 3D rendering of the wetting phase (top, red) and the non-wetting phase (bottom, blue) at the end of primary drainage simulations on a micro-CT image of Berea sandstone, for a high capillary number (10^{-5}) on the left and lower capillary number (2.5×10^{-6}) on the right. These simulations were performed with a finite-volume method. Figure from Raeini (2013).

3.5. Direct hydrodynamics

Since the late 2000s, researchers at Schlumberger Moscow and Shell have been jointly developing a novel direct pore-scale modeling method called “direct hydrodynamics” (Koroteev et al., 2013). This method is based on the density functional method for multi-phase compositional hydrodynamics (Demianov et al., 2011). It employs a diffuse description of the fluid interfaces, in combination with continuum fluid mechanics and thermodynamic principles (mass, momentum and energy balance). The method is capable of simulating a broad range of physical phenomena, including multiphase flows with phase transitions and mobile solid phase, different types of fluid–rock and fluid–fluid interactions (e.g. wettability and adsorption), and various types of fluid rheology. Thanks to the diffuse interface approach and a massively parallel GPU implementation, the method seems to be fairly efficient. Some results are shown in Figs. 17 and 18. A downside of this method is that to our knowledge, only one, proprietary implementation of this fairly young method exists.

3.6. Molecular dynamics and Monte Carlo methods

For completeness, we mention that molecular dynamics and Monte Carlo methods can be used to simulate molecular transport. Molecular dynamics methods can be useful to investigate very small scale phenomena, such as the behavior of very thin fluid films on solid surfaces and fluid–fluid contact line dynamics (Meakin and Tartakovsky, 2009). Monte Carlo methods have been used to simulate the behavior of non-ideal gas particles. In practice, these methods are not used to simulate flow in representative pore spaces of geological materials, because they are designed to work on a much smaller and more detailed scale. Therefore, we will not discuss them further. However, findings from these very detailed models can potentially

be inputted to models better suited to deal with pore spaces on the micrometer-scale.

4. Pore scale modeling with pore network models

As discussed in the previous section, while advances are being made, the modeling of multi-phase transport properties directly on pore space images remains a challenging task. Specifically, the computational demands limit these simulations in most applications to small images of rather homogeneous rocks with narrow pore size distributions (typical applications are glass bead packings, sand packs and well-sorted, “simple” sandstones, e.g. Bentheim, Berea and Fontainebleau sandstone). In the future, direct pore scale modeling methods are expected to become more broadly applicable, but to date, pore network models (PNM) have been the most successful models for practical applications of pore scale simulations of two- and three-phase flow in the geological field (Blunt, 2001; Blunt et al., 2013). These models will be presented in this section.

4.1. Introduction

Pore network models represent a complex pore space by a network of pore bodies and pore throats (the narrow constrictions which link pores together) with idealized geometries (Blunt, 2001) (Fig. 19). The first study using this idea was performed by Fatt (1956), who used a regular lattice of tubes with random radii to simulate transport through a porous medium. This model was seen to match experimental properties of porous media much better than the previously adopted bundle-of-capillary-tubes model, and has since served as a standard approach to think about transport in porous media. In later work, pore size distributions were used as constraints to regular lattices of pore bodies and throats, while some throats were removed ad random to match coordination number distributions (the distribution of the amount of neighbors each pore has). However, it is very difficult to generate a

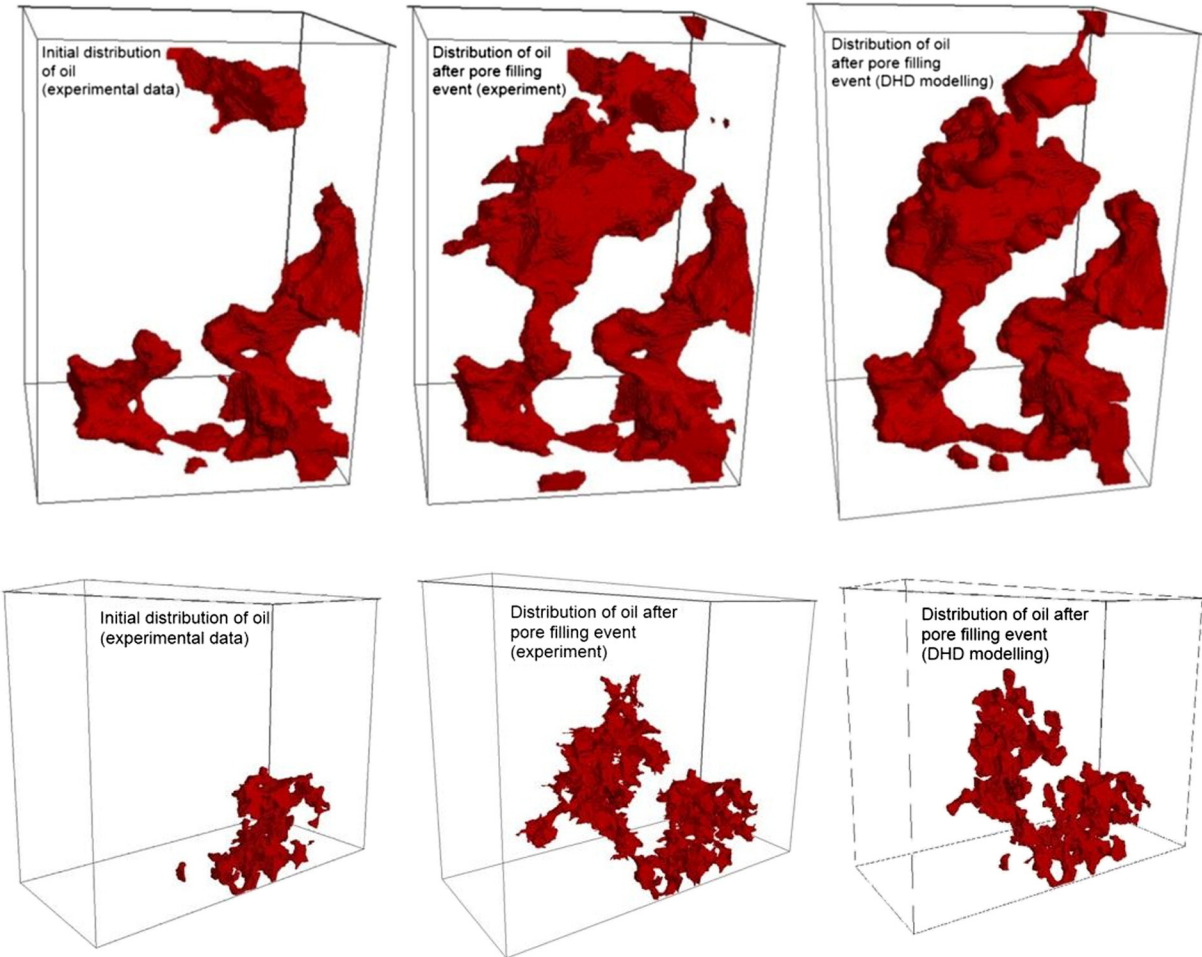


Fig. 17. Comparison between experimental micro-CT data of pore filling during drainage in a Berea sandstone in the middle (Berg et al., 2013) and direct hydrodynamic simulations on the right. Oil is visualized in red, water and rock grains are not visualized. Numerical modeling of the pore filling event used initial oil distributions from micro-CT (on the left) as starting condition.

Figure from Koroteev et al. (2013).

lattice-based network model in such a way that the spatial correlations of, and between, the properties of the network elements (e.g. throat and pore radii, connectivity) honor reality. Furthermore, networks based on regular lattices often have difficulties with representing the topology of complex porous media adequately. Replicating the real topology is crucial (Vogel and Roth, 2001), and it has been shown that simply matching an average coordination number is insufficient to replicate realistic drainage (Arns et al., 2004) and imbibition (Mahmud et al., 2007) behavior. In conclusion, both the topology and the correlations greatly

affect transport behavior, meaning it is often difficult to simulate realistic rock behavior on lattice-based network models (Sok et al., 2002). While such models may prove tremendously useful if these issues are taken into account (Jerauld and Salter, 1990; Raoof and Hassanizadeh, 2010), image-based network models are currently gaining in popularity.

Since the 1990s, much effort has been put into extracting network models directly from 3D image-based representations of pore spaces by using image analysis techniques (Fig. 20), in contrast to using

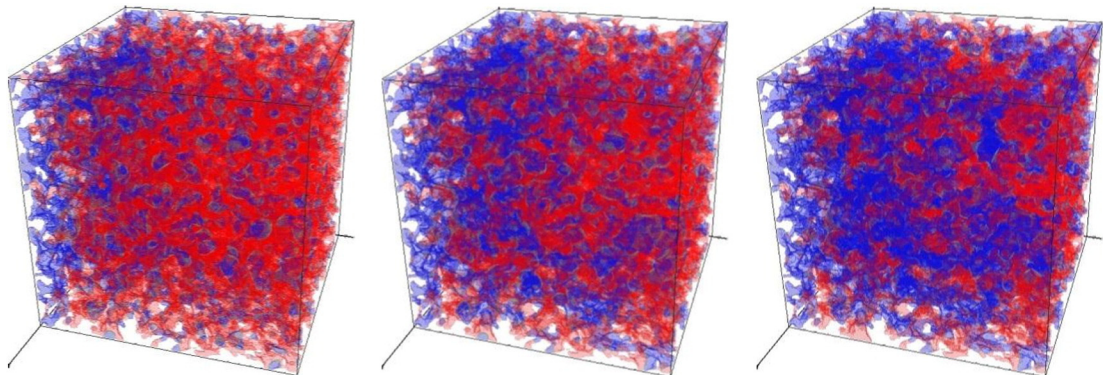


Fig. 18. Direct hydrodynamics simulation of oil recovery by waterflooding in a sandstone. Water is blue, oil is red.
Figure from Koroteev et al. (2013).

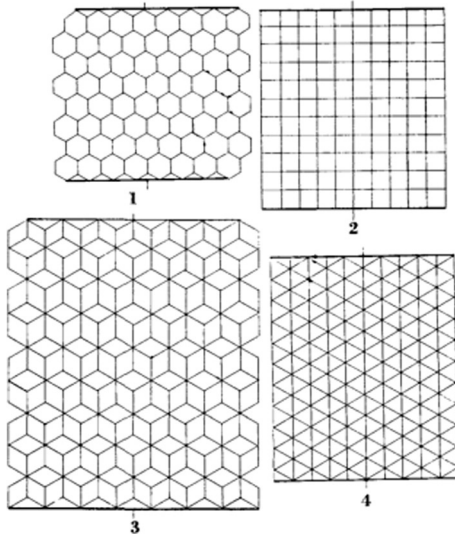


Fig. 19. Two-dimensional, lattice-based networks originally investigated by Fatt in 1956 (figure from Fatt, 1956). Compare this to the contemporary 3D image-based networks in Fig. 20.

stochastically generated lattice-based networks constrained by experimental data. In addition to circumventing the problem of characterizing all the correlations in the porous medium by basing the network on local measurements of pore space geometry, these methods typically also attempt to capture the real topology of the pore space (Lindquist et al., 1996).

The idea of extracting networks from pore space images merits the question “what is a pore”? A pore space is continuous, and therefore splitting it up into discrete network elements will require some arbitrary decisions (Hunt et al., 2014). The assumption is that a rock’s pore space can be treated as if it consists out of a number of pores, separated by constrictions. One would expect this assumption to at least be valid for a granular medium, where the grains are typically convex objects, meaning the pores will be concave, yet even in this case arbitrary decisions have to be made as to where a pore ends and a constriction begins. It is therefore clear that PNM are a non-unique representation of a pore space (Arns et al., 2007), and any PNM extraction method is built on certain assumptions which might hold only for the media or the physical processes one wants to investigate with the resulting networks. This complicates comparison of different network algorithms.

Despite these theoretical objections, image-based PNMs have greatly helped to increase the understanding of geological porous media’s multi-phase flow behavior (Blunt, 2001). In addition to providing insight into the collective behavior of a complex system of pores, which each adhere to certain well-defined (usually relatively simple) rules, pore network models have been shown to be able to actually predict constitutive relations (e.g. capillary pressure and relative permeability curves) in individual rocks (Øren et al., 1998; Valvatne and Blunt, 2004). This allows calculating transport properties (e.g. relative permeability) on small rock samples, which may be important when cored material is scarcely available. Furthermore, rock properties such as wettability can easily be varied to investigate the sensitivities involved. As a rock’s wettability in reservoir conditions is often difficult to restore in lab samples, this analysis can be very useful.

In the following, we will first treat the different image-based PNM extraction algorithms in Section 4.2; we will provide an oversight of how the resulting network models can be used to simulate transport properties in Section 4.3, and we will address the influence of the PNM extraction on the simulated transport properties by reviewing comparative studies in Section 4.4. In Section 4.5, PNM methods specifically developed for multi-scale problems will be discussed.

4.2. Image based network extraction

Network extraction consists out of two parts: splitting up the pore space representation into discrete elements and subsequently measuring the geometric properties of each network element; properties that will be used in the flow modeling. Usually, these include the inscribed radius (or alternatively a hydraulic radius), the length, the volume and some sort of shape-describing parameter for each network element.

Several ways of classifying PNM extraction exist, however, since the central idea is to simplify a pore space by capturing its topology and the relevant traits of its geometry, we will classify the methods into two classes: methods which split up the pore space in a topology-central way and methods which do this in a morphology-central way (Wildenschild and Sheppard, 2013). Many methods to split the pore space have been developed, often with common characteristics. We discuss the main ideas behind these methods.

4.2.1. Topology-central methods

One of the first image-based PNM extraction algorithms was a topology-central method developed by Brent Lindquist and co-workers (Lindquist and Venkatarangan, 1999; Lindquist et al., 1996). They used

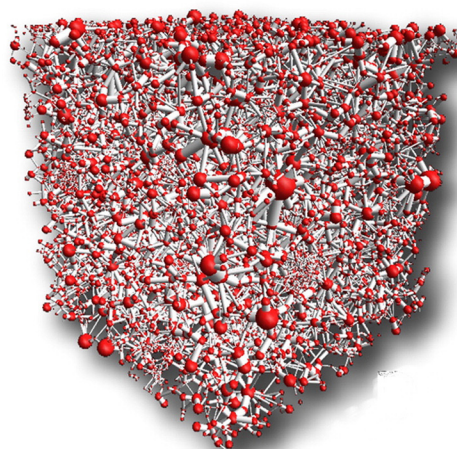
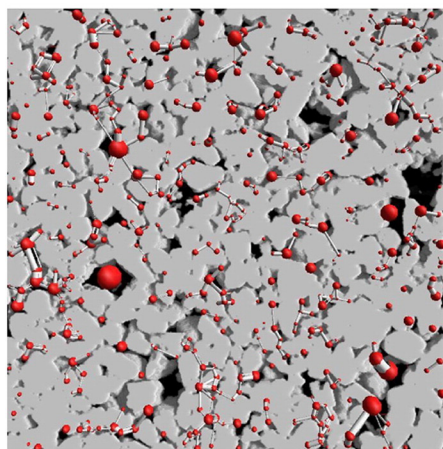


Fig. 20. Pore network models extracted from a micro-CT scan of a Bentheim sandstone, on the left a front view of a part of a 3D network, shown on top of a rendering of the micro-CT scan it was extracted from. Note that some of the pores in the PNM are not visualized, for clarity. On the right, a full PNM is rendered separately. Networks were rendered with FEI’s ECORE software.

the concept of a medial axis, a representation of the pore space by a central skeleton, an approach that is still popular today (Fig. 21). First, a medial axis extraction is performed (see Section 2.7.3), after which the branching points in the skeleton are considered to be the centers of pore bodies. Most methods use a distance-ordered homotopic thinning (DOHT) algorithm (Pudney, 1998) to find the medial axis, as this algorithm delivers homotopically equivalent skeletons which lie central in the pore space. In the original Lindquist algorithm, the throats were then found by dilating the branches of the medial axis to find the throat perimeter where the contact points of the solid space and the dilations of the medial axis form a closed loop first. Other authors follow a different approach to the throat-identification problem and to determine the parameters of individual network elements (Al-Raoush and Willson, 2005; Arns et al., 2007; Jiang et al., 2007; Youssef et al., 2007). Usually, the medial axis is used as an embedded search structure to find the throat locations in the form of the narrowest sections transversal to it (Lindquist, 2002) (see Fig. 21), although (Sheppard et al., 2006) use a watershed transform seeded by the pore centers to split up the pore space.

One of the most important problems when constructing pore network models from medial axis representations extracted from experimental pore space images, is the sensitivity of the medial axis to small defects in the pore space surface. This will lead to an over-identification of pores, as there will be spurious branches in the medial axis when image noise leads to misidentification of pore and solid voxels. Attempts to reduce these problems often propose advanced pre-and post-processing (Plougonven and Bernard, 2011; Sheppard et al., 2005) to reduce noise in the input image and to merge spurious pores a-posteriori (Fig. 22).

It should be noted here that differences in for example the identified number of pores do not necessarily have large effects on the simulated properties, as long as the topology and the geometry (i.e. the widest and narrowest passages in the pore space) are well captured (Thompson et al., 2005). Therefore, a more fundamental problem with this type of network extraction is that the junctions in the network, which are identified as pore bodies, do not necessarily coincide with geometrical pore bodies (i.e. points where the pore space is wider) (Arns et al., 2007). This is problematic as slow drainage and imbibition in porous media are to a large degree geometrically dominated phenomena. The advantage of using a medial axis, on the other hand, is its direct relationship to the topology of the original image.

4.2.2. Morphology-central methods

One of the first morphology-based pore network extraction methods was developed by Zhao et al. (1994), who used multi-orientation scanning through a digital reconstruction of a rock sample to identify constrictions. In their view, measurements on parameters like pore size and coordination number can only be reliable when the constrictions separating pores are identified first, since these actually define the individual pores (compare this to the identification of pores as branching points of a medial axis in topological methods). However, using their

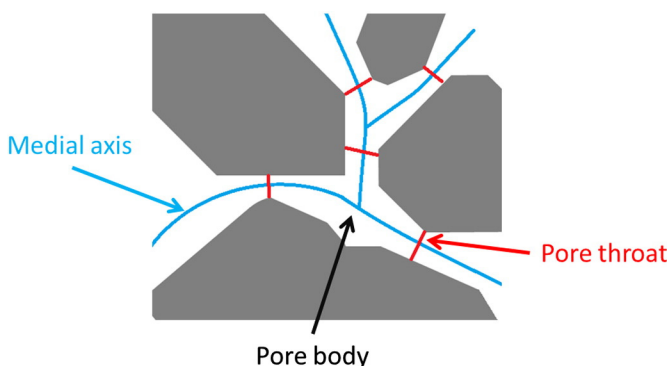


Fig. 21. A pore space, its medial axis, and its throats identified by using a medial axis.

approach of a discrete number of scanning orientations, some throats may be missed and some may be misidentified. Later on, other researchers like Baldwin et al. (1996) and Liang et al. (2000) improved on this approach by identifying minima in the hydraulic radius of pore space channels, the former by a thinning approach, the latter by scanning the planes perpendicular to the pore space skeleton, after which these plains define the separate pores in the image.

A second type of morphology-based network extraction methods, which is however somewhat related to the medial axis method, is the grain-based method (Bakke and Øren, 1997). While more sophisticated methods have been developed since, this is still considered to be somewhat of a benchmark (Wildenschild and Sheppard, 2013). First, the individual solid grains in the rock are identified, after which these grains are dilated until there is no pore space left. Places where three grains touch then form a skeleton, while points where four or more grains touch are nodes in the network. The grain-identification step is heavily influenced by the rock's morphology, hence the classification of the method as morphology-central.

In this work, the authors employ a rotating vector method to scan the surfaces perpendicular to the skeleton line, in order to find the narrowest constrictions between pores (Fig. 23) (Bakke and Øren, 1997). A similar vector scanning method is used to find the volume and the inscribed sphere radius in the pores. Furthermore, a pore shape factor is determined (see further) which describes the surface roughness of the network elements. The authors used their method on process-based reconstructions of sedimentary rocks, meaning they had all the information on individual grains in their input image. The process-based method utilizes petrographical information obtained from two-dimensional thin sections to stochastically model the results of sedimentary rock forming processes (sedimentation, compaction, and diagenesis) (Øren and Bakke, 2002). However, when one employs this method to a segmented micro-CT scan, grain identification can be a bottle neck, as noise in the image will commonly lead to oversegmentation of grains. Also, it is not clear if this grain-based method holds any validity when trying to extract networks from non-granular porous media (e.g. certain carbonate rocks like travertine). A similar grain-based method was developed by Thompson et al. (2005). It first identifies seeds for pore center identification by triangulating the set of grain center points. Then, these seed points are used to find local maxima of the distance map by using a watershed algorithm. These local maxima define pore centers. Afterwards, all voxels in the image are assigned to pores or grains by using a restricted burn algorithm (for more details we refer to Thompson et al., 2005). This process should be less dependent

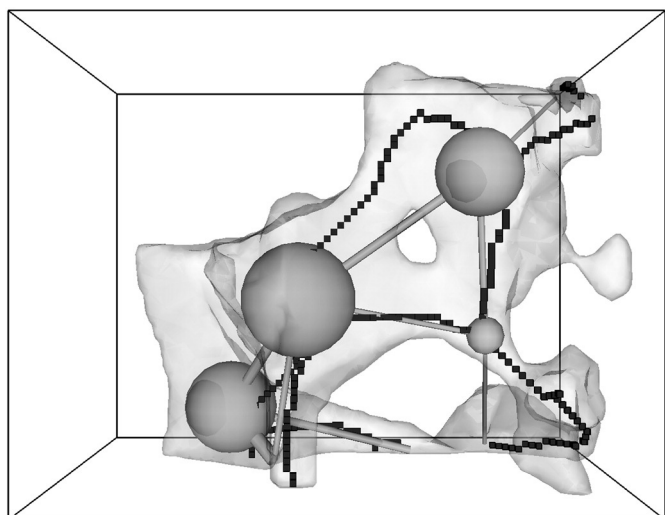


Fig. 22. A medial axis and the pore network extracted with it, illustrating a case in which the geometry and the topology of the pore space are hard to express as a network. Figure from Sheppard et al. (2005).

on defects in the grain identification; however, this method could use further validation.

A third very well-known morphology-based method starts from the extraction of so-called “maximal balls” (Silin and Patzek, 2006). These are the largest inscribed spheres centered on each voxel of the image that just touch the grain or the boundary. Then, the spheres which are fully included in other spheres are removed. The set of maximal balls describes the pore space without redundancy.

The maximal balls are clustered into families according to their size and the size of the maximal balls they overlap with (Fig. 24). Locally, the largest maximal balls (i.e. the “ancestor” of a family of maximal balls) identify pores. The smallest balls which belong to more than one family and therefore connect the pores identified by these families, are throats (Al-Kharusi and Blunt, 2007; Dong and Blunt, 2009). The advantage of this method is that it attempts to explicitly identify wide passages in the pore space as pores and narrow passages as throats. However, while the larger pores are identified well, the method seems to find a cascade of smaller and smaller network elements down to the image resolution (Blunt et al., 2013).

Finally, the pore space can also be decomposed by performing a watershed algorithm on the distance map calculated from the segmented pore space image (see also Section 2.7.2). The throats are then found as surfaces which separate the pores from each other (Rabbani et al., 2014; Wildenschild and Sheppard, 2013). Watershed algorithms have been implemented in many commercial and open source software packages, e.g. Octopus Analysis, Avizo, Fiji, and ITK.

4.2.3. Other methods

Aside from the previously discussed methods, some lesser known network extraction methods are based on genetic algorithms (Nejad Ebrahimi et al., 2013) or on single-phase flow fields calculated with computational fluid dynamics (Dong et al., 2008). To accurately represent film flow in network models (see further), some algorithms incorporate more complex pore and throat shapes in the geometrical characterization of network elements (Joekar-Niasar et al., 2010a; Ryazanov et al., 2009). Other advanced geometry-determination algorithms take into account the converging/diverging nature of throats (Bauer et al., 2011), or calculate network elements' fluid conductances by running lattice Boltzmann or CFD algorithms on the subvolumes defined by each separate network element (Sholokhova et al., 2009).

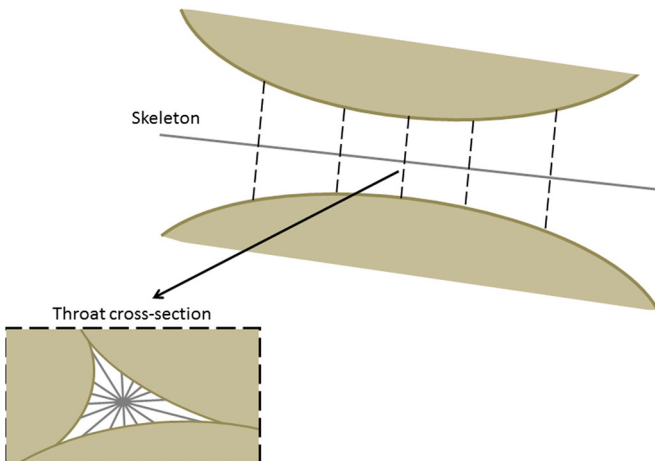


Fig. 23. Schematic depiction of the geometrical analysis of pore throats in Bakke and Øren (1997). On the top, the skeleton line and the sections transversal to it are shown. On the bottom, the scanning vectors used to determine throat radius and volume in such a section are drawn.

Figure inspired by Bakke and Øren (1997).

4.3. Transport simulations based on pore network models

4.3.1. Quasi-static multi-phase flow modeling

During pore network extraction, the pore space is split up into simple geometrical units (pores and throats, which from a conceptual point of view can be seen as spheres and cylinders), which locally capture features important to the process one is investigating. For multi-phase flow studies, local constrictions and dilations of the pore space, as well as surface roughness, are usually captured. For slow flows (low capillary numbers), the sequence of fluid invasion in network elements during drainage and imbibition is often modeled by an invasion-percolation algorithm. For this situation, capillary forces dominate and determine which parts of the pore space can be filled with an invading fluid at a certain pressure difference imposed on the fluids. If the porous medium is wetted by the defending fluid (drainage), the constrictions limit which part of the pore space can be filled. On the other hand, if the medium is wetted by the invading fluid (imbibition), the dilations in the pore space determine which parts of the pore space can be invaded. In a cylindrical network element, Young–Laplace's law can be used to relate the radius r of the inscribed sphere to the capillary pressure (P_c), which needs to be overcome for it to be invaded:

$$P_c = 2\sigma \cos\theta/r \quad (2)$$

Young–Laplace equation for capillary pressure with σ the interfacial tension, r the radius of the inscribed sphere of the network element, and θ the contact angle.

At the beginning of the displacement process, consider one face of the network to be connected to a reservoir of the invading fluid, while the other is connected to a reservoir of the defending fluid. Invasion-percolation describes the displacement process at constant flow rate (Wilkinson and Willemsen, 1983), leading to the dynamic rule of advancing the interface at the point of least resistance: during drainage the widest network element available for invasion is filled, while during imbibition the narrowest element available is invaded (Fig. 25).

A network element is available for invasion when it neighbors an element already filled with the invading fluid, and when the defending fluid present in the element has an “escape path” to the outlet face. When the defending fluid in an element is not connected to the outlet face, it is considered to be trapped in that element. Advancing the interface at the point of least resistance as opposed to advancing all interfaces up to a certain threshold invasion pressure (mimicking constant pressure flow) is important when trapping is taken into account, because invasion percolation defines a unique time sequence of events, which in turn determines whether or not a given portion of the defending fluid becomes trapped. Modeling the invasion as a discrete series of events is consistent with experimental observations of drainage and imbibition in porous media (Lenormand et al., 1983). The invasion percolation algorithm was pioneered by Wilkinson and Willemsen (1983).

Over the years, sophisticated invasion percolation based PNM approaches have been developed (Blunt et al., 2002; Øren et al., 1998; Patzek, 2001; Valvatne and Blunt, 2004). Many of these methods take into account the existence of water films in crevices. Usually, this is done by assigning triangular or square cross sections to the network elements, which retain wetting fluid in their corners (Fig. 26). Often, the exact shape of the cross section is determined from the shape factor G of the part of the pore space which is represented by the element in the network:

$$G = A/P^2 \quad (3)$$

Shape factor, with A as the cross-sectional surface area and P the corresponding perimeter length of this cross-section (Patzek and Silin, 2001).

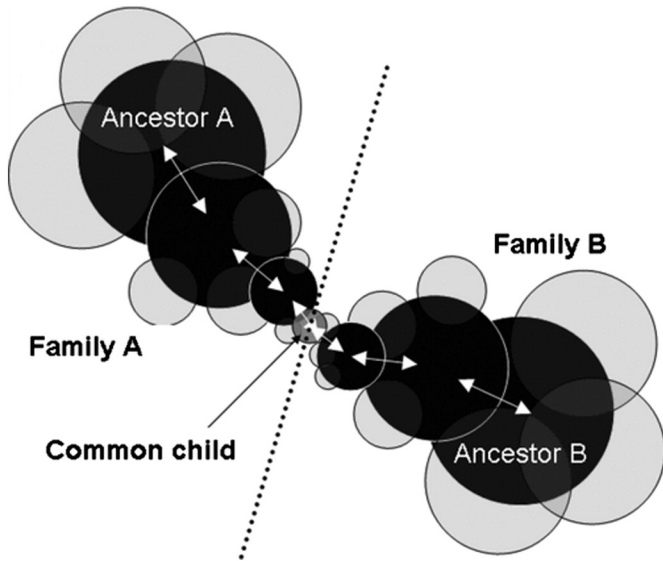


Fig. 24. The clustering of overlapping maximal balls into families, resulting into two pores (centered on ancestors A and B) and a throat between them (at the location of the common child of the two families) (Dong and Blunt, 2009). The white arrows indicate the pore-throat chain.

Figure from Dong and Blunt (2009).

The reasoning is that one does not need to include the exact pore space roughness or wall shape, but that the ratio of the cross-sectional surface areas occupied by film and by bulk fluid should be maintained in the model. This way, one can better approximate the water connectivity in the model, as well as include instabilities when swelling water films touch each other during imbibition (so-called snap-off events), an effect which has been shown important to non-wetting phase trapping (Iglauer et al., 2012; Lenormand et al., 1983). The pressure needed to overcome the capillary force in triangular and square prisms can be calculated semi-analytically (Ma et al., 1996; Mason and Morrow, 1991).

Intrinsic wettability of network elements is assigned a-priori, and is usually drawn from a user-defined range of values. Many network simulators use this value in the receding/advancing contact angle model by Morrow (1975). There is currently no workflow which succeeds in assigning local wettability properties on a rigorous, experimental basis. The best approach available is usually to adapt the range of contact angles to reproduce global wettability measurements (e.g. Amott wettability). Network models are however very useful to study the dependence and sensitivity of flow parameters on that range, and on wettability modification after drainage. In many models, pores which have been in contact with oil can change their wettability from water to oil-wet, mimicking asphaltene precipitation (Fig. 26).

More complex pore shapes than triangular and square prisms have been devised to better approximate the film flow behavior. For example, Ryazanov et al. (2009) used n-cornered star shapes, based on shape factors and dimensionless hydraulic radii. Furthermore, in their model, corner film existence is based on a rigorous thermodynamic criterion (rather than on a geometric criterion as is usually the case). Joekar-Niasar et al. (2010b) investigate the effect of cross sectional shapes by comparing a set of regular and irregular hyperbolic polygons for the pore throats and prolate spheroids for the pore bodies (see Fig. 27). They show that the choice of cross-sectional shapes has a significant effect on entry capillary pressure and saturation in crevices.

During the displacement process, saturations and permeabilities of both (or, in the case of three-phase flow, three (Piri and Blunt, 2005)) phases can be calculated in separate runs. To calculate the flow rates, network elements which are completely filled with one fluid are considered to be completely closed off for flow of another fluid. Mass conservation is then imposed in every pore. If a conductivity is assigned to

each pore-to-pore connection, this results in a linear system which can be solved for the pressures P_i in each pore i (Eq. (4)), thereby also yielding the flow rate through each pore.

$$\sum_j q_{ij} = 0, \text{ for every } i$$

$$q_{ij} = \frac{g_{ij}}{L_{ij}} (P_j - P_i) \quad (4)$$

Linear system to solve the pressures (and equivalently the flow rates) in each pore, with q_{ij} the flux from pore i to pore j , g_{ij} the conductivity from pore i to pore j , and L_{ij} the length of the connection from pore i to pore j .

The pore-to-pore conductivities are usually based on the inscribed sphere radius or on an equivalent hydraulic radius for the throat connecting the two pores, which can be related to its length and shape factor (Patzek and Silin, 2001). For example, for a cylindrical network element Poiseuille's law can be used. The permeability of the network can be calculated by finding the flow rates through the pores in a surface perpendicular to the flow injection. A similar calculation can yield the electrical flux through the network, to calculate its electrical resistivity. This way, absolute and relative permeability curves can be calculated, as well as formation factors and resistivity index curves. These properties are relatively easily calculated (definitely when compared to the much more computationally intensive direct simulation methods), which is ultimately an effect of splitting up the pore space into simple elementary building blocks (pores and pore throats) of which the hydraulic or electric resistivity can be calculated (semi-)analytically. Note that the calculation of the fluid arrangement is decoupled from the computation of the flow rates of the separate fluids through the part of the pore space which they occupy. This comes down to neglecting the viscous pressure drop during the displacement, an assumption which is only approximately valid when capillary forces dominate over viscous forces (i.e. for low capillary numbers) (Valvatne and Blunt, 2004).

As stated in the introduction of this section, quasi-static network modeling is extremely useful to study how the wettability and pore characteristics influence the multi-phase flow behavior in rocks. For example, Gharbi and Blunt (2012) use this approach to explain that optimal waterflood efficiency during oil recovery in carbonates is seen in mixed-wet samples with poor connectivities. This behavior was found to be different for sandstones, where network modeling explained why neutrally-wet conditions are optimal (Øren et al., 1998; Valvatne and Blunt, 2004). Quasi-static models can also help to investigate theoretical properties of two-phase flow behavior, e.g. their application suggests that taking into account the specific interfacial area reduces capillary pressure hysteresis (Joekar-Niasar et al., 2010b) and shows that capillary trapping models should take the topology of the fluid phases into account (Joekar-Niasar et al., 2013).

4.3.2. Dynamic multi-phase flow modeling

Over the last few years, a number of models have been developed to take the previously mentioned viscous effects (e.g. viscous pressure drop) into account (Hammond and Unsal, 2012; Idowu and Blunt, 2010; Joekar-Niasar et al., 2010b; Nguyen et al., 2006). These models are usually called "dynamic pore network models", and unlike static pore network models, they can be used to investigate flow rate-dependency of relative permeability curves (caused by for example displacement rate-induced inhibition of snap-off) or the remobilization of trapped fluid globules. For example, Hammond and Unsal (2012) investigated the effects of surfactant on the displacement pattern during waterflooding in a dynamic network model, and find that the resulting decrease in interfacial tension reduces residual oil saturation by flushing out the large trapped oil clusters, whereas the wettability change simultaneously caused by the surfactant tends to act in the opposite direction. A comprehensive review on dynamic pore network models can be found in Joekar-Niasar and Hassanizadeh (2012).

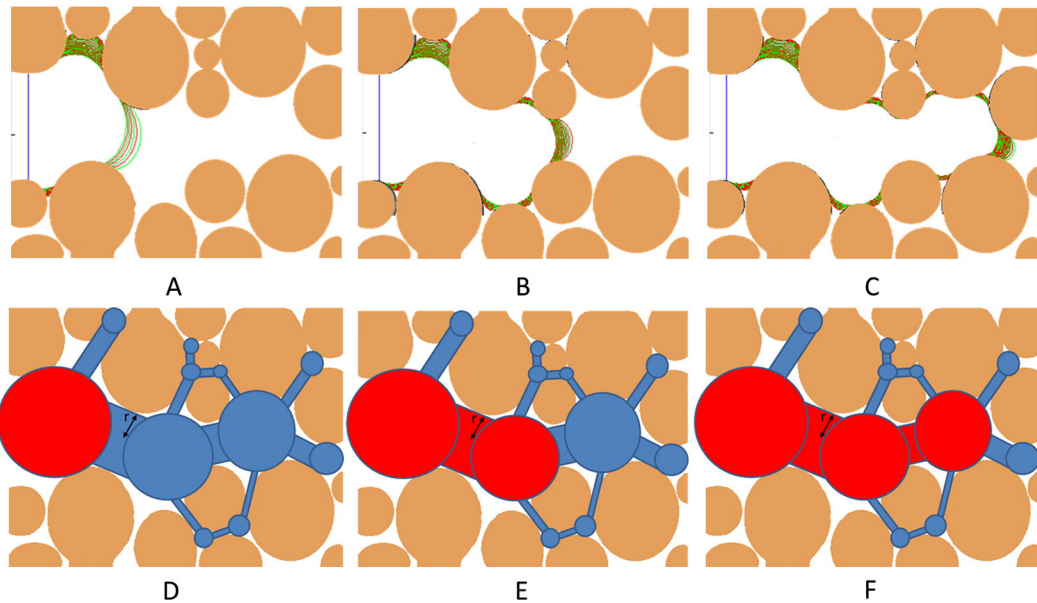


Fig. 25. From A to C: evolving interfaces during drainage, modeled using a level-set method (Prodanović and Bryant, 2006). From D to E: corresponding consecutive steps in a drainage process modeled with invasion percolation in a pore network model. Oil-filled network elements are shown in red, water-filled network elements in blue. The prevailing capillary pressure can be calculated at each step by applying the Young-Laplace equation to the radius of the throat invaded last. Pore space and interface images are adapted from Prodanović (2008).

4.3.3. Solute/colloid transport and reactive flow modeling

Network descriptions can also be used to simulate reactive transport in porous media. In many respects these methods can be seen as an extension on the multi-phase flow network simulations described before, where colloid or solute transport is taken into account. Similar to the multi-phase flow case, mass balance equations for all the chemical species are set up in each network element, taking into account advection, diffusion and reaction (Raouf et al., 2013). Note that this way, multi-phase, multi-component systems can be analyzed. The models allow us to calculate for example the mean effective reaction rate, velocity and dispersivity, as well as solute breakthrough curves. An interesting application is the simulation of dissolution or precipitation of the porous medium. After each time step, the medium's pore space is altered, changing for example porosity, permeability and specific surface area, and thereby influencing how the reaction will take place in the next time step. This way, the evolution of a porous medium can be followed

through time. For example, Raouf et al. (2012) use reactive pore network modeling to explain why multiple regions with distinctly different porosities develop in cement when it is exposed to a CO₂-bearing solution, e.g. in wellbore cement during CO₂ sequestration. They show how these zones result in a decrease in average permeability of the cement in the direction parallel to the CO₂-gradient, suggesting a sealing behavior, which was confirmed by experiments.

Reactive pore network models have been used in a variety of applications, to simulate for example dissolution of organic liquids (Held and Celia, 2001; Zhou et al., 2000), mineral precipitation and dissolution during CO₂ sequestration (Algire et al., 2012; Kang et al., 2009; Kim et al., 2011; Varloteaux et al., 2013), biomass growth (Dupin et al., 2001; Gharasoo et al., 2012; Kim and Fogler, 2000; Rosenzweig et al., 2013; Suchomel et al., 1998), solute dispersivity (Vasilyev et al., 2012), adsorption (Acharya et al., 2005; Köhne et al., 2011; Li et al., 2006; Raouf et al., 2010), particle capture and release (Ochi and Vernoux,

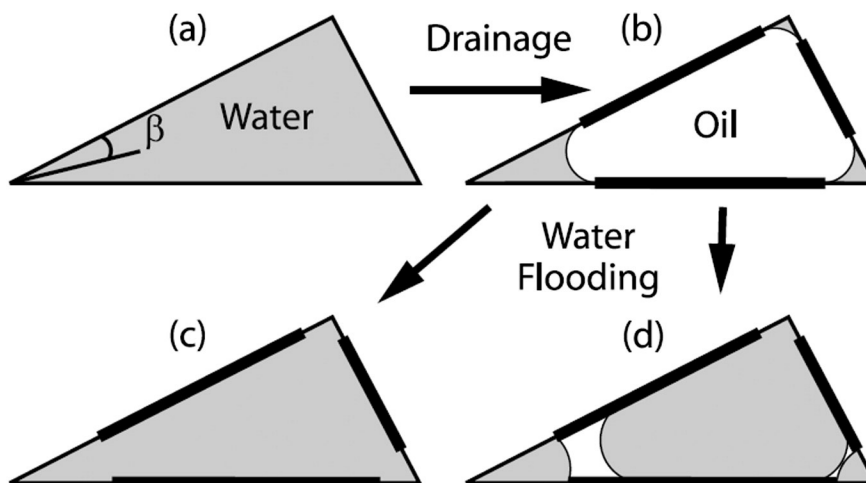


Fig. 26. Different filling states of an initially water-wet pore with a triangular cross-section (Valvatne and Blunt, 2004), showing water films after drainage (b). After imbibition, oil films can arise if the wettability of the pore is altered by being in contact with oil (d). If this is not the case, oil films cannot exist (c). Figure from Valvatne and Blunt (2004).

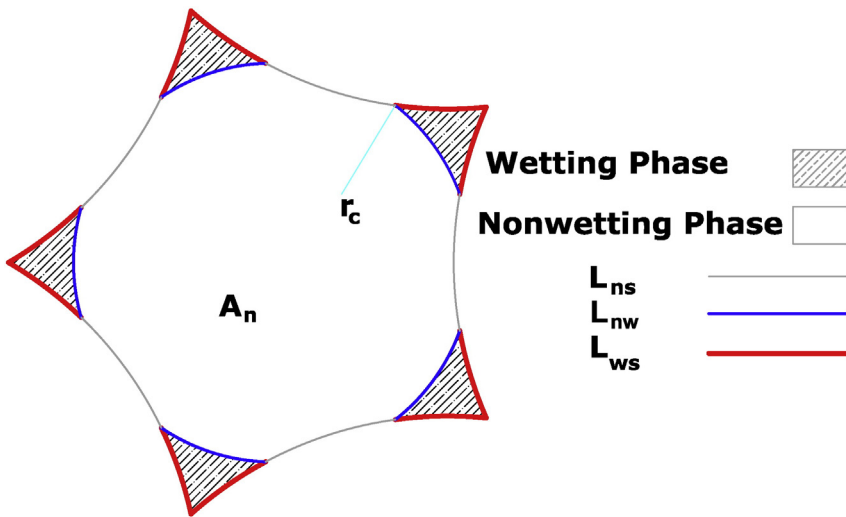


Fig. 27. Regular hyperbolic polygonal pore cross-section used by Joekar-Niasar et al. (2010b), showing the wetting films after drainage. The curvature of the non-wetting/wetting interface is denoted by r_c . Figure reprinted with permission from Joekar-Niasar et al. (2010b).

1999), asphalt precipitation (Sahimi et al., 2000) and deposition and dissolution in diatomite (Bhat and Kovsek, 2013).

4.3.4. Other applications

Further applications are drying in porous media (Freitas and Prat, 2000; Yiotis et al., 2006) and the simulation of viscous flows in granular materials where the forces exerted by the fluid on the grains (whether or not deformable) are of particular importance (Chareyre et al., 2012). PNM can also be used as static characterization tool, for example to investigate the influence of connectivity numbers or constriction ratio (the ratio of a pore's radius to one of its connecting throats' radius) (Tanino and Blunt, 2012; Vogel and Roth, 2001).

4.4. Comparison of network extraction methods

Given the multitude of network extraction algorithms available, it is important to compare the influence of the PNM extraction on the resulting simulations. While a number of such studies have been published (Al-Raoush et al., 2003; Dong and Blunt, 2009; Dong et al., 2008; Idowu et al., 2012, 2014; Ngom et al., 2011), the non-uniqueness of the network extraction and the possible dependence on the specifics of the investigated medium (e.g. consolidated or unconsolidated, granular or non-granular) make it difficult to predict a-priori which method is best suited to a given problem. Furthermore, comparison of the different methods is complicated by the fact that algorithms and datasets are often not publically available to other researchers. Initiatives such as the Pore Scale Benchmark Project (porescalebenchmark.pbworks.com) or the Digital Rocks Portal (Prodanovic et al., 2015) attempt to alleviate these difficulties. In the following, some broad conclusions are drawn from the literature; however, in many cases there is no short or easy answer to the question which network extraction algorithm would be the best choice for a given problem.

4.4.1. Overview of comparative studies

An overview of comparative studies in the literature can be found in Table 2. We can discern between studies where the skeleton extraction is done using different methods, but where the geometrical characterization of pore bodies and throats is maintained (Bhattad et al., 2011; Dong et al., 2008; Idowu et al., 2012, 2014), and studies which compare completely different methods (Al-Raoush et al., 2003; Caubit et al., 2008). In other work, three methods are compared, two of which use

the same skeleton, but a different geometric partitioning (Bondino et al., 2012; Idowu et al., 2013).

Wildenschild and Sheppard (2013) report that network simulations are less sensitive to the initial pore space partitioning, and more to how the geometrical properties are assigned to each pore body and throat. This statement indeed coincides with the results from the network comparison articles: when geometrical characterization is maintained, the methods are reported to produce somewhat different absolute single-phase transport properties, but similar multi-phase properties (these properties are usually expressed relative to absolute properties, and trends were seen to be reproduced by the different methods). Even though static network properties (e.g. number of pores) varied greatly between the methods, the spread on predicted transport results was reported to be reasonable, and a good agreement with experimental and grid simulated data was reported by Idowu et al. (2013). Some side notes are:

- The medial axis method may fail when there is a high level of noise (Dong et al., 2008; Idowu et al., 2012), as it tends to identify more isolated and “dead-end” pores.
- The maximal ball method seems to be good at capturing the larger pores, but is troubled by finding too many small throats which are not necessarily real hydraulic constrictions (Dong and Blunt, 2009).
- The grain-based method may give discrepancies in non-granular media (Dong et al., 2008).
- The networks tend to be worse at predicting electrical resistivity, as it depend more strongly on the small pores (Caubit et al., 2008; Dong and Blunt, 2009; Dong et al., 2008). The PNM methods have more problems to capture these, probably due to finite resolution of the input images.

4.4.2. Robustness of network extraction

A general conclusion from pore network comparison studies is that multi-phase properties are consistent, if the initial partitioning preserves the topology well (Idowu et al., 2012). This is thought to be a result of the balancing of several competing properties (Bhattad et al., 2011). For example, when a flow channel is divided into more pores, one would expect it to have a higher resistance to flow, as there are more “resistors in series” in that channel. However, this effect will be counterbalanced by the shorter length of each pore, resulting in a lower resistance per pore. Bhattad et al. (2011) conclude that the modeling algorithms are doing their job by counter-balancing variations in network

structure by pore-geometry based modeling, therefore mitigating the non-uniqueness of PNM extraction. Caubit et al. (2008), who compare two completely different workflows performed on the same rocks, also find a relatively good match of the results. However, the difficulty in capturing the amount of microporosity and the presence of small-scale heterogeneity in the rock samples may cause differences in results, exacerbating the non-uniqueness problem of PNM methods.

Despite these reports, using pore network models as a truly predictive tool (without the use of other experimental results as input) has shown to be difficult in a number of studies (Bondino et al., 2012; Sorbie and Skauge, 2011). The former report large variations in water and oil relative permeability when using different extraction methods on the same sandstone, including even counter-intuitive trends for some methods. Idowu et al. (2013) investigated these counter-intuitive trends, and show that they are a consequence of how volume is assigned to pore throats, providing a good example of the sensitivity of network models to the applied geometric characterization. Bondino et al. (2012) note that applying two different networks on the same image has much larger consequences than applying the same algorithm on two different images, while using different simulators had a much milder effect than using different network extractions. They conclude that the prediction of multi-phase flow properties using digital rock physics is currently in general not possible. They state that pore network modeling, which is the most established digital rock physics technique, can produce results which are difficult to interpret due to the high number of parameters involved in the workflow, that the representation of the rock is still a weak point, and that a strict characterization of wettability is currently not possible in these methods (wettability is considered as a sort of tuning parameter, see also Section 4.3.1). Sorbie and Skauge (2011) also note the high number of parameters in any network modeling workflow, and state that true predictive modeling is therefore currently impossible with this approach. However, they propose a number of very useful applications of network models, including explanation, interpolation and extrapolation of experimentally observed two- and three-phase flow trends and properties. Network models are also very useful if they are “anchored” to some experimental data which is relatively easy to obtain, such as porosity, permeability and capillary pressure curves (Ravlo and Arland, 2014). It is to be noted that Caubit et al. (2008) report that when these parameters are well matched, the relative permeability curves (which are significantly more difficult to measure) could be considered as reliable.

4.5. Multi-scale pore network modeling

As mentioned before, one of the most severe problems in pore-scale modeling of geological materials is dealing with the multiple spatial scales inherent to the pore structure of many natural rocks. This means that often, not all pores are captured in one single imaging experiment, due to finite resolution and sample volume of these experiments. However, the presence of multiple pore scales in rocks can severely influence a rock's transport properties, an effect which is notably important in carbonates and tight-gas sandstones (Mehmani and Prodanović, 2014).

Even if one finds a way to merge data from multiple experiments, taking all relevant pore sizes into account in simulations remain hard, as the necessary resolution of such a model is dictated by the smallest pores of importance, while the minimal size of the model is dictated by the representative elementary volume of the medium. The discrepancy between these scales, which often amounts to several orders of magnitude, poses computational problems. Since PNM describe individual network elements with infinite resolution (i.e. pores of indiscriminate size can be described without loss of detail) and because they are very computationally efficient, PNM are currently probably the most suitable technique for multi-scale simulations of this kind. In this section, we will give an overview of PNM specially developed to deal with multi-scale simulations. These models, presented schematically in Fig. 28, are often referred to as dual pore network models (D-PNM). In this section, “micropores” are defined ad-hoc as pores smaller than the resolution of the imaging experiment performed to characterize the largest pores (“macropores”) in the sample under investigation. Typically, in geological applications using micro-CT, micropores are pores with sizes smaller than approximately 1 μm.

Jiang et al. (2013) propose a workflow to join PNM extracted from images at different resolutions. A PNM of indiscriminate volume representative of the microporosity is stochastically created based on a small network extracted from high-resolution imaging data (Jiang et al., 2011), thereby circumventing the resolution-size trade-off of the experimental technique used to image the micropore space. A PNM of the macropores is then merged with the microporosity network by characterizing the cross-scale connection structure between the two networks. Theoretically, networks of more than two scales can be fused using this methodology. However, a disadvantage of this method is that the number of network elements can quickly become

Table 2

Overview of comparative studies on network extraction methods. The software in which the algorithms are implemented is reported between brackets.

Publication	Methods compared	Samples used for comparison
Al-Raoush et al. (2003)	- Medial axis (3DMA) - Modified Delaunay Tesselation (own)	- Computer-generated regular and random sphere packings
Dong et al. (2008)	- Medial axis: DOHT (Avizo) - Maximal ball (own) - Flow velocity-based (Lithicon) - Grain-recognition based (Lithicon)	- Computer-generated regular sphere packing - Computer-generated sandstone (process-based approach, Fontainebleau) - Micro-CTs of poorly sorted channel sandstone, vuggy replacement dolostone and Mt. Gambier limestone - Micro-CT of Berea, Bentheim and Fontainebleau sandstone - Micro-CT of 4 sandstones from the Statfjord field
Idowu et al. (2012) and Idowu et al. (2014)	- Medial axis: pore-based thinning (Fiji) - Medial axis: DOHT (Avizo) - Grain-recognition based (Lithicon)	- Clashach sandstone
Bondino et al. (2012)	- Voronoi-based (origin unreported) - 2 watershed-transform based methods w/different throat lengths (origin unreported)	- Computer generated sphere packings and 1 computer-generated sandstone - 1 micro-CT of sandpack - 10 micro-CTs of sandstones - 2 micro-CTs of carbonates - Micro-CTs of soil aggregates and soil management systems
Dong and Blunt (2009)	- Maximal ball (own) - Grain-recognition based (Lithicon)	- 6 artificial and outcrop rocks - 6 unconsolidated and consolidated reservoir rocks - Micro-CT images of glass spheres packing, sand pack and cylinder pack
Ngom et al. (2011)	- Medial axis (3DMA) - Delaunay tessellation (own)	- Same as (Bondino et al., 2012) (Clashach)
Caubit et al. (2008)	- Medial axis (ANU)	
Bhattad et al. (2011)	- Grain-recognition based (Lithicon) - Delaunay-tessellation based (Thompson et al., 2005) - 3 different maximal-ball based (own)	
Idowu et al. (2013)	- Same as (Bondino et al., 2012)	

computationally prohibitive since each individual micropore is taken into account separately. A similar approach is followed by Mehmani and Prodanović (2014) and Prodanović et al. (2014). They use a less strict approach to generate the microporosity, but investigate the influence microporosity has on transport properties in general terms. Therefore, they pay attention to the location of microporosity with respect to the macropore space, by taking into account information on its genesis.

Acknowledging the computational difficulties of treating microporosity as a network of individual micropores, researchers at Institut Français du Pétrol et des Energies Nouvelles (IFPEN) have developed an approach where the macropores are treated with a PNM approach, while micropores are treated as blocks of continuous porous medium, characterized by for example a porosity, a permeability and a capillary pressure curve (Bauer et al., 2012, 2011; Bekri et al., 2005; Moctezuma et al., 2003; Youssef et al., 2008). Their model has evolved to an image-based D-PNM approach in which a certain percentage of the throats in the macropore network is assigned a block of microporosity in parallel. The approach is very successful for certain kinds of rocks in which micro-and macroporosity indeed conduct in parallel, however, when this is not the case, the method is expected to run into problems.

In order to allow microporosity to act both in parallel as in series to the macropore network, (Bultreys et al., 2015c) use a similar approach of treating the microporosity as a continuous porous medium. Pores in the macropore PNM which touch the same microporous region are connected by so-called “micro-links”, a third type of network elements which carry the upscaled properties of the microporous region they represent (Fig. 29). In this model, the connectivity and the conductivity added by microporosity are derived from local micro-CT information. Macropores are allowed to be drained as a consequence of their connection with microporosity, permitting simulations where the macropore network alone does not percolate. Despite showing to be a promising method of simulating two-phase flow in multi-scale porous rocks, issues which remain to be addressed are the assessment of the microporosity's transport properties (e.g. permeability, porosity), the rather oversimplified transport model for the microporosity, and a remaining user-defined parameter related to the microporous connectivity.

5. Summary and conclusion

In this review, some of the most commonly used pore characterization methods were discussed, going from older, well-known methods such as optical microscopy to novel, young methods like ptychographic tomography. None of these methods are without flaws, and every method has its own strong features.

As an adequate visualization and characterization over multiple scales is needed to understand the full complexity and connectivity of pore networks, a combination of methods will usually be a necessity (Fig. 30). Sub-micron-scale structures can be analyzed on representative samples using well-known geological characterization methods like SEM and optical microscopy. For the study of these features in

three dimensions, one can use FIB-nt, a very promising method that is developing fast and becoming more and more accessible to the scientific and industrial community. However, the destructive nature of the technique is disadvantageous if dynamic processes need to be visualized. Ptychographic tomography at synchrotron facilities overcomes this problem, but has the shortcoming of being limited to these facilities, making this technique less available. For both of these techniques, analysis time is long and costly, and samples are very small, which is a major issue in geological specimens. Non-visual techniques such as MIP and N₂ adsorption can provide valuable additional information. Both methods can be used to study the pore size distribution of a particular sample, helping the selection of an appropriate image-based technique, or validating the results that were obtained using one of these techniques.

Micro-computed tomography is currently perhaps the most universal, mature and accurate porosity characterization method, especially when the most important part of the pore network is situated above the 1-μm limit. Sample sizes can vary from millimeter to centimeter scale, and analysis times are relatively short. Furthermore, the technique is non-destructive, allows for a lot of peripheral equipment for the study of dynamic processes and is becoming widely accessible at hundreds of research institutes across the world. Results are three-dimensional, and data analysis algorithms and software have reached a point where quantitative results can be obtained. However, spatial resolution typically remains restricted to a few hundreds of nanometers, quantitative chemical data remains an issue, and results are often user-dependent. Especially for materials with a widespread pore size distribution (PSD), a combination of multiple techniques will probably remain essential for many years to come.

Recent advances in computing power and in modeling algorithms have made it possible to simulate transport properties directly on images of a rock's pore space. If good experimental images on a rock's microstructure and composition can be obtained (e.g. with micro-CT, FIB-nt or ptychographic imaging), many of its transport properties can be calculated by solving the transport equations in question with boundary conditions provided by the pore walls in the obtained pore space representation. This is helping researchers to gain a better understanding on the fundamentals of transport processes in geological porous media, on the sensitivities of transport processes to various parameters (e.g. wettability) and on the link between different material properties (e.g. pore space connectivity versus amount of trapped non-wetting phase in a reservoir rock). These findings are critically important to several global challenges (e.g. improved oil and gas recovery, environmental remediation of polluted soils and aquifers, subsurface storage of CO₂). Furthermore, transport simulations are becoming more and more predictive, causing them to become a valuable complementary tool to experimental measurements, as they are in some cases faster to perform and require less sample material.

Solving transport properties on the complex boundary conditions posed by the pore space of natural porous media is however computationally challenging. Several methods exist, each with advantages and limitations when it comes to computational efficiency and stability,

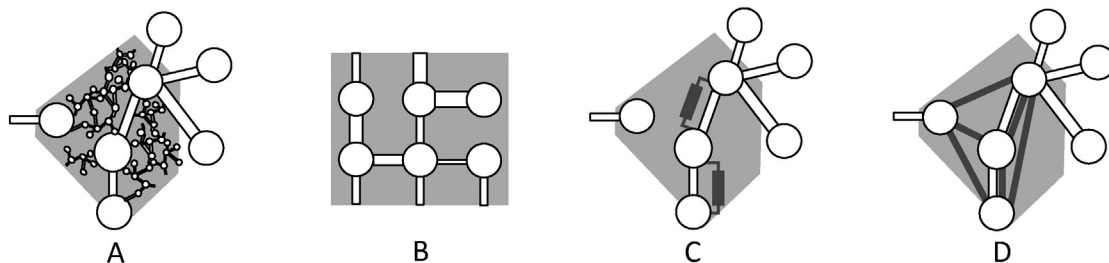


Fig. 28. Model A takes individual micropores into account, e.g. Jiang et al. (2013). In model B a cubic-lattice based network is embedded in a microporous matrix (Bekri et al., 2005), model C is image-based but only takes into account microporosity in parallel to throats in the macro-pore PNM (Bauer et al., 2012), and model D takes microporosity both serial as parallel microporosity into account in an upscaled fashion (Bultreys et al., 2015c). Microporous regions are depicted in dark gray.

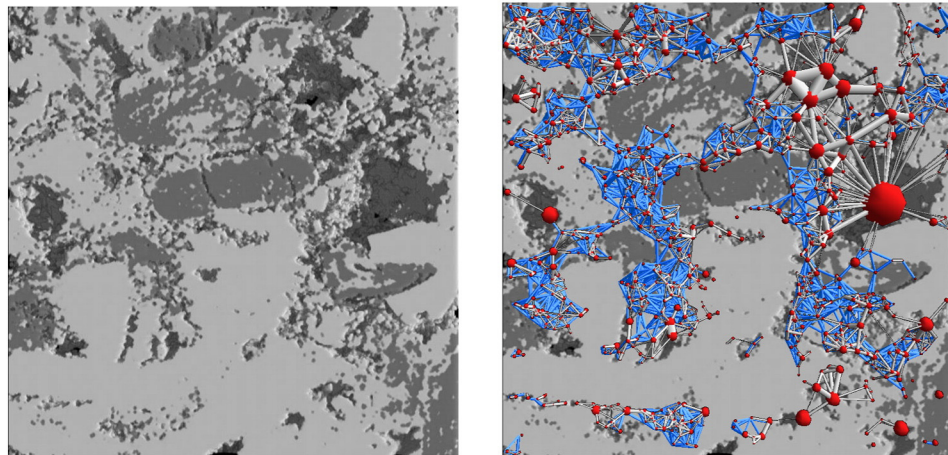


Fig. 29. Left: a micro-CT image of Estaiades carbonate, with microporous regions rendered in dark gray. A dual PNM (Bultreys et al., 2015c) is overlaid in the image on the right, with micro-links in blue, pores in red and throats in white.

difficulty of implementation and parallelization, accuracy, amount of parameters and versatility in the range of transport problems they are applicable to. The ideal method would solve the transport equations from first principles on images which are large enough to capture the rock's centimeter-scale heterogeneity (as this is the largest scale we can hope to sample and measure the pore structure of), with a minimum of user input. Currently, lattice Boltzmann and classical CFD methods come close to these requirements when it comes to solving single-phase flow on relatively homogeneous rocks.

However, most transport processes in geological materials involve the presence of multiple immiscible fluids. Solving multi-phase transport is much more challenging than single-phase flow, chiefly because of the need to track fluid interfaces and contact lines in a complicated geometry. We discern two approaches: direct methods, which run on a gridded or meshed pore space image, and pore network models, which approximate the pore space as a network of separate pores and throats with idealized geometries. Direct methods generally impose much less simplifications on the pore space geometry and on the sub-pore-scale physics which are taken into account than pore network models. However, they are much more computationally intensive, and are therefore currently limited to simulations on small pore space images of relatively simple rock types (or, very often, digitally generated sphere packings and other similar artificial porous media). Therefore, pore network models have been the most broadly applicable and successful modeling tool for multi-phase flow problems as of yet.

Among the direct methods, we discussed the lattice Boltzmann method, the more traditional CFD methods (most notably finite volume approaches), smoothed particle/semi-implicit-particle/dissipative hydrodynamics, and direct hydrodynamics. Among these, lattice Boltzmann is currently the most mature approach to solve multi-phase flow problems in rocks, thanks to its natural suitability to deal with complex boundary conditions and to large-scale parallelization. Furthermore, it does not require explicit interface tracking. Since this model is based on molecular concepts, it is applicable to many different transport problems (including diffusion, reactive transport and mineral precipitation or dissolution (Kang, 2004; Kang et al., 2006)).

Pore network models can be extracted directly from pore space images, in order to capture the real medium's topology and geometry as well as possible. Many algorithms to perform this task exist, and it is not straightforward to decide which algorithm will result in the best modeling results. In general, for most proven methods the non-uniqueness of splitting up the pore space into separate pores and pore throats during the extraction workflow is somewhat alleviated by a trade-off in competing pore properties (e.g. more short pores versus fewer longer throats). Network models are therefore more sensitive to how geometrical pore and pore throat properties are determined than to how the pore space is initially split up. Another concern is the large amount of parameters which often go into generating a network model.

A pore network model can be used to simulate two-phase and three-phase flow, as well as e.g. diffusion, reactive flow (including pore space

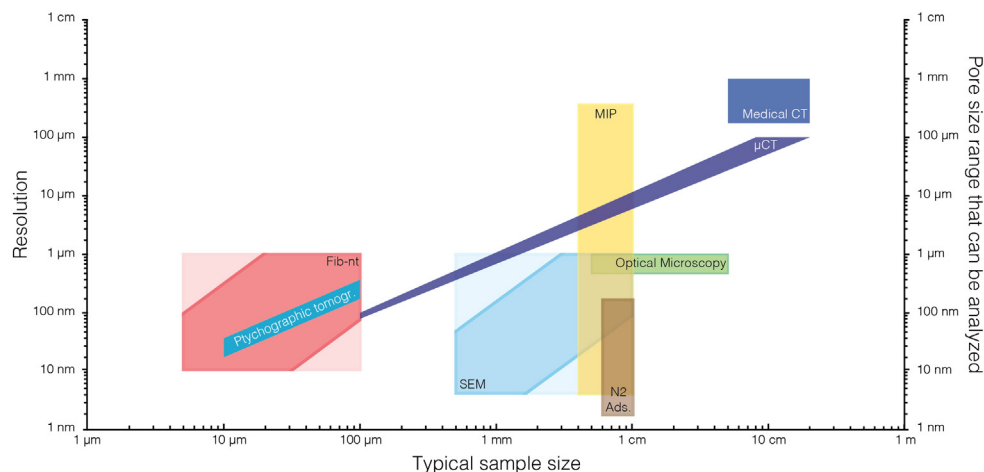


Fig. 30. Typical sample sizes vs. obtainable resolution for the discussed techniques. Transparent corners for the FIB-nt and SEM rectangles indicate that some resolution/size combinations are not common, but possible. MIP and N2 analyze a porosity range, and are therefore scaled to the axis on the right.

modifications due to these reactions) and electrical properties. It should be noted that they need to be supplied with a contact angle model, meaning that they can be used to investigate the influence of contact angles, but cannot provide insight into the physics which determine contact angle behavior. The native length scale for pore network models is a scale comprising many pores, yet which is smaller than the continuum scale, whereas direct methods necessarily work on the sub-pore-length scale. Network models are then very useful to investigate the collective behavior of a pore space with all its complex correlated heterogeneity, if one assumes single pores behave a certain way. Direct models are currently mostly useful to learn about the behavior on this smaller scale, by running models which comprise only few pores. It is therefore obvious that direct methods and network methods can be used as complementary approaches.

6. Outlook

Due to the increased accessibility and ease of use of digital imaging techniques and image analysis software, these technologies are becoming a standard method to study the properties of porous geological materials. However, the user-dependency of image based methods means that one should be careful in the interpretation of these data as absolute values. Therefore, the scientific community needs a standardized workflow that can be carried out by researchers of all facilities worldwide. Although this necessity is widely accepted, its execution is hampered by the fact that the quality of acquired images (and therefore the analysis method) depends on many different factors, e.g. the hardware setup (illumination source, energy, etc.) and the sample (sample preparation, composition, shape, etc.). For many applications, image analysis results will remain dependent on the interpretation and experience of the researchers who generated the images.

When dealing with materials with a wide PSD, which are common in geosciences, the choice of a certain technique or combination of techniques will often be difficult. Few techniques are particularly suited for this kind of materials, and as a general rule counts: the smaller the pores to be investigated, the smaller the analyzed volume. This is less of a problem in 2D analysis methods (e.g. SEM, optical microscopy), since mosaic or panoramic images can easily be created. On the other hand, larger surfaces generate much longer analysis time, and researchers have to decide how far they want to stretch this time vs. surface relation. In 3D analysis techniques, image correlation between different scales is much more complicated, as there usually is a direct and binding sample size/resolution trade-off. The most common way to overcome this problem is a 'refinement' approach, where one starts with the largest samples at the worst resolution, and consecutively performs an intelligent subsampling to 'zoom in' on relevant parts of the material. All of these issues call for new developments in terms of hardware and software.

When it comes to pore-scale modeling of multi-phase transport, we expect that the further development of computing power and efficient algorithms will cause direct modeling methods to gain in importance for many applications in the future, compared to pore network modeling. A notable exception may be the simulation of transport properties in materials with a very broad range of pore sizes present, like many carbonates and clay-bearing sandstones, for which we see specialized pore network models as the key development in the next few years. To improve the understanding of the transport properties of these materials, network models need to capture the real interconnectivity of the different pore scales present, as well as the relevant physics at each of those scales. Both requirements underline the need for sound experimental work as well.

An important problem to be solved in direct models, next to increasing the computational efficiency, is the difficulty many methods have when there are large viscosity and density contrasts between the fluids. Further developments are needed in the modeling of flow in fractured

porous materials and on multi-physics models which couple chemical, mechanical and hydraulic behavior of porous media.

Pore scale modeling methods would benefit from the existence of standardized pore space geometries to use as test cases for the comparison of new algorithms, and standard implementations of algorithms to compare new methods with. Next to comparison between algorithms, many methods are also in need of direct experimental validation. This is hampered by the difficulty and the cost of obtaining experimental measurements of many continuum properties (e.g. relative permeability measurements), and by the even bigger challenge to obtain experimental information on the physics of transport processes in (groups of) individual pores, especially in realistic three-dimensional pore geometries. This includes local wettability characterization (e.g. Schmatz et al., 2015) and investigations on the influence of dynamic effects and local geometries on fluid flow properties. For the former, we expect that the combination of micro-CT with chemical analysis methods may become important, while to solve the latter problem, we see an important role for fast, time-resolved micro-CT.

Acknowledgments

The entire UGCT team is gratefully thanked for helpful discussions and contributions. The Agency for Promotion of Innovation by Science and Technology in Flanders, Belgium (IWT) (121042) is acknowledged for the PhD scholarship of Tom Bultreys. The Special Research Fund of Ghent University (BOF11/STA/002) is acknowledged for providing the scholarship of Wesley De Boever.

References

- Acharya, R.C., Van der Zee, S.E.A.T.M., Leijnse, A., 2005. Transport modeling of nonlinearly adsorbing solutes in physically heterogeneous pore networks. *Water Resour. Res.* 41. <http://dx.doi.org/10.1029/2004WR003500> (n/a-n/a).
- Aghaei, A., Piri, M., 2015. Direct pore-to-core up-scaling of displacement processes: dynamic pore network modeling and experimentation. *J. Hydrol.* 522, 488–509. <http://dx.doi.org/10.1016/j.jhydrol.2015.01.004>.
- Aligve, L., Békri, S., Nader, F.H., Lerat, O., Vizika, O., 2012. Impact of diagenetic alterations on the petrophysical and multiphase flow properties of carbonate rocks using a reactive pore network modeling approach. *Oil Gas Sci. Technol. – Rev. d'IFP Energies Nouv.* 67, 147–160. <http://dx.doi.org/10.2516/ogst/2011171>.
- Alhashmi, Z., Blunt, M.J., Bijeljic, B., 2015. Predictions of dynamic changes in reaction rates as a consequence of incomplete mixing using pore scale reactive transport modeling on images of porous media. *J. Contam. Hydrol.* 179, 171–181. <http://dx.doi.org/10.1016/j.jconhyd.2015.06.004>.
- Al-Kharusi, A.S., Blunt, M.J., 2007. Network extraction from sandstone and carbonate pore space images. *J. Pet. Sci. Eng.* 56, 219–231. <http://dx.doi.org/10.1016/j.petrol.2006.09.003>.
- Al-Raoush, R.I., Willson, C.S., 2005. Extraction of physically realistic pore network properties from three-dimensional synchrotron X-ray microtomography images of unconsolidated porous media systems. *J. Hydrol.* 300, 44–64. <http://dx.doi.org/10.1016/j.jhydrol.2004.05.005>.
- Al-Raoush, R., Thompson, K., Willson, C.S., 2003. Comparison of network generation techniques for unconsolidated porous media. *Soil Sci. Soc. Am. J.* 67, 1687. <http://dx.doi.org/10.2136/sssaj2003.1687>.
- Ammouche, A., Riss, J., Breysse, D., Marchand, J., 2001. Image analysis for the automated study of microcracks in concrete. *Cem. Concr. Compos.* 23, 267–278. [http://dx.doi.org/10.1016/S0958-9465\(00\)00054-8](http://dx.doi.org/10.1016/S0958-9465(00)00054-8).
- Andrä, H., Combaret, N., Dvorkin, J., Glatt, E., Han, J., Kabel, M., Keehm, Y., Krzikalla, F., Lee, M., Madonna, C., Marsh, M., Mukerji, T., Saenger, E.H., Sain, R., Saxena, N., Ricker, S., Wiegmann, A., Zhan, X., 2013. Digital rock physics benchmarks—part II: computing effective properties. *Comput. Geosci.* 50, 33–43. <http://dx.doi.org/10.1016/j.cageo.2012.09.008>.
- Andrew, M., Bijeljic, B., Blunt, M.J., 2013. Pore-scale imaging of geological carbon dioxide storage under in situ conditions. *Geophys. Res. Lett.* 40, 3915–3918. <http://dx.doi.org/10.1002/grl.50771>.
- Andrew, M., Bijeljic, B., Blunt, M.J., 2014. Pore-scale imaging of trapped supercritical carbon dioxide in sandstones and carbonates. *Int. J. Greenhouse Gas Control* 22, 1–14. <http://dx.doi.org/10.1016/j.ijggc.2013.12.018>.
- Andrew, M., Menke, H., Blunt, M.J., Bijeljic, B., 2015. The imaging of dynamic multiphase fluid flow using synchrotron-based X-ray microtomography at reservoir conditions. *Transp. Porous Media* 110, 1–24. <http://dx.doi.org/10.1007/s11242-015-0553-2>.
- Andriani, G.F., Walsh, N., 2002. Physical properties and textural parameters of calcarenous rocks: qualitative and quantitative evaluations. *Eng. Geol.* 67, 5–15. [http://dx.doi.org/10.1016/S0013-7952\(02\)00106-0](http://dx.doi.org/10.1016/S0013-7952(02)00106-0).
- Anselmetti, F.S., Lüthi, S., Eberli, G.P., 1998. Quantitative characterization of carbonate pore systems by digital image analysis. *Am. Assoc. Pet. Geol. Bull.* 82, 1815–1836.

- Arbogast, T., Gomez, M.S.M., 2009. A discretization and multigrid solver for a Darcy-Stokes system of three dimensional vuggy porous media. *Comput. Geosci.* 13, 331–348. <http://dx.doi.org/10.1007/s10596-008-9121-y>.
- Armstrong, R.T., Georgiadis, A., Ott, H., Klemm, D., Berg, S., 2014a. Critical capillary number: desaturation studied with fast X-ray computed microtomography. *Geophys. Res. Lett.* 41, 55–60. <http://dx.doi.org/10.1002/2013GL058075>.
- Armstrong, R.T., Ott, H., Georgiadis, A., Rücker, M., Schwing, A., Berg, S., 2014b. Subsecond pore-scale displacement processes and relaxation dynamics in multiphase flow. *Water Resour. Res.* 50, 9162–9176. <http://dx.doi.org/10.1002/2014WR015858>. Received.
- Arns, C., Knackstedt, M., Pinczewski, W., Mecke, K., 2001. Euler-Poincaré characteristics of classes of disordered media. *Phys. Rev. E* 63, 031112. <http://dx.doi.org/10.1103/PhysRevE.63.031112>.
- Arns, J.-Y., Robins, V., Sheppard, A.P., Sok, R.M., Pinczewski, W.V., Knackstedt, M.A., 2004. Effect of network topology on relative permeability. *Transp. Porous Media* 55, 21–46. <http://dx.doi.org/10.1023/B:TIPM.0000007252.68488.43>.
- Arns, C.H., Mecke, J., Mecke, K., Stoyan, D., 2005. Second-order analysis by variograms for curvature measures of two-phase structures. *Eur. Phys. J. B* 47, 397–409. <http://dx.doi.org/10.1140/epjb/e2005-00338-5>.
- Arns, J.Y., Sheppard, A.P., Arns, C.H., Knackstedt, M.A., Yelkhovsky, A., 2007. Pore level validation of representative pore networks obtained from micro-CT images. *Int. Symp. Soc. Core Analysts. Society of Core Analysts, Calgary, Canada*, pp. 1–12.
- Arrufat, T., Bondino, I., Zaleski, S., LAGREE, B., Keskes, N., 2014. Developments on relative permeability computation in 3D rock images. Abu Dhabi International Petroleum Exhibition and Conference. Society of Petroleum Engineers <http://dx.doi.org/10.2118/172025-MS>.
- Bakke, S., Øren, P.-E., 1997. 3-D pore-scale modelling of sandstones and flow simulations in the pore networks. *SPE J.* 2, 136–149. <http://dx.doi.org/10.2118/35479-PA>.
- Baldwin, C.A., Sederman, A.J., Mantle, M.D., Alexander, P., Gladden, L.F., 1996. Determination and characterization of the structure of a pore space from 3D volume images. *J. Colloid Interface Sci.* 181, 79–92. <http://dx.doi.org/10.1006/jcis.1996.0358>.
- Bandara, U.C., Tartakovsky, A.M., Oostrom, M., Palmer, B.J., Grate, J., Zhang, C., 2013. Smoothed particle hydrodynamics pore-scale simulations of unstable immiscible flow in porous media. *Adv. Water Resour.* 62, 356–369. <http://dx.doi.org/10.1016/j.advwatres.2013.09.014>.
- Batenburg, K.J., Sijbers, J., 2011. DART: a practical reconstruction algorithm for discrete tomography. *IEEE Trans. Image Process.* 20, 2542–2553. <http://dx.doi.org/10.1109/TIP.2011.2131661>.
- Bauer, D., Youssef, S., Han, M., Bekri, S., Rosenberg, E., Fleurty, M., Vizika, O., 2011. From computed microtomography images to resistivity index calculations of heterogeneous carbonates using a dual-porosity pore-network approach: influence of percolation on the electrical transport properties. *Phys. Rev. E* 84, 11133. <http://dx.doi.org/10.1103/PhysRevE.84.011133>.
- Bauer, D., Youssef, S., Fleurty, M., Bekri, S., Rosenberg, E., Vizika, O., 2012. Improving the estimations of petrophysical transport behavior of carbonate rocks using a dual pore network approach combined with computed microtomography. *Transp. Porous Media* 94, 505–524. <http://dx.doi.org/10.1007/s11242-012-9941-z>.
- Bear, J., 1975. *Dynamics of fluids in porous media*. *Sci. Technol.* 120.
- Beckmann, F., Bonse, U., Busch, F., Günnewig, O., 1997. X-ray microtomography (μ CT) using phase contrast for the investigation of organic matter. *J. Comput. Assist. Tomogr.* 21, 539–553.
- Beckmann, F., Heise, K., Kölsch, B., Bonse, U., Rajewsky, M.F., Bartscher, M., Biermann, T., 1999. Three-dimensional imaging of nerve tissue by X-ray phase-contrast microtomography. *Biophys. J.* 76, 98–102. [http://dx.doi.org/10.1016/S0006-3495\(99\)77181-X](http://dx.doi.org/10.1016/S0006-3495(99)77181-X).
- Bekri, S., Laroche, C., Vizika, O., 2005. Pore network models to calculate transport and electrical properties of single or dual-porosity rocks. *Int. Symp. Soc. Core Analysts.*
- Bera, B., Mitra, S.K., Vick, D., 2011. Understanding the micro structure of Berea sandstone by the simultaneous use of micro-computed tomography (micro-CT) and focused ion beam-scanning electron microscopy (FIB-SEM). *Micron* 42, 412–418. <http://dx.doi.org/10.1016/j.micron.2010.12.002>.
- Berg, S., Ott, H., Klapp, S. a., Schwing, A., Neiteler, R., Brussee, N., Makurat, A., Leu, L., Enzmann, F., Schwarz, J.-O., Kersten, M., Irvine, S., Stampaioni, M., 2013. Real-time 3D imaging of Haines jumps in porous media flow. *Proc. Natl. Acad. Sci. U. S. A.* 110, 3755–3759. <http://dx.doi.org/10.1073/pnas.1221373110>.
- Berry, R.a, Martineau, R.C., Wood, T.R., 2004. Particle-based direct numerical simulation of contaminant transport and deposition in porous flow. *Vadose Zone J.* 3, 164–169. <http://dx.doi.org/10.2113/3.1.164>.
- Bhat, S.K., Kovsek, A.R., 2013. Permeability modification of diatomite during hot fluid injection. SPE Western Regional Meeting. Society of Petroleum Engineers <http://dx.doi.org/10.2118/46210-MS>.
- Bhattad, P., Willson, C.S., Thompson, K.E., 2011. Effect of network structure on characterization and flow modeling using X-ray micro-tomography images of granular and fibrous porous media. *Transp. Porous Media* 90, 363–391. <http://dx.doi.org/10.1007/s11242-011-9789-7>.
- Bijeljic, B., Mostaghimi, P., Blunt, M.J., 2013a. Insights into non-Fickian solute transport in carbonates. *Water Resour. Res.* 49, 2714–2728. <http://dx.doi.org/10.1002/wrcr.20238>.
- Bijeljic, B., Raeini, A., Mostaghimi, P., Blunt, M., 2013b. Predictions of non-fickian solute transport in different classes of porous media using direct simulation on pore-scale images. *Phys. Rev. E* 87, 013011. <http://dx.doi.org/10.1103/PhysRevE.87.013011>.
- Bisschop, J., van Mier, J.G., 2002. How to study drying shrinkage microcracking in cement-based materials using optical and scanning electron microscopy? *Cem. Concr. Res.* 32, 279–287. [http://dx.doi.org/10.1016/S0008-8846\(01\)00671-8](http://dx.doi.org/10.1016/S0008-8846(01)00671-8).
- Blair, S.C., Berge, P.A., Berryman, J.G., 1996. Using two-point correlation functions to characterize microgeometry and estimate permeabilities of sandstones and porous glass. *J. Geophys. Res.* 101, 20359. <http://dx.doi.org/10.1029/96JB00879>.
- Blunt, M.J., 2001. Flow in porous media – pore-network models and multiphase flow. *Curr. Opin. Colloid Interface Sci.* 6, 197–207. [http://dx.doi.org/10.1016/S1359-0294\(01\)00084-X](http://dx.doi.org/10.1016/S1359-0294(01)00084-X).
- Blunt, M.J., Jackson, M.D., Piri, M., Valvatne, P.H., 2002. Detailed physics, predictive capabilities and macroscopic consequences for pore-network models of multiphase flow. *Adv. Water Resour.* 25, 1069–1089. [http://dx.doi.org/10.1016/S0309-1708\(02\)00049-0](http://dx.doi.org/10.1016/S0309-1708(02)00049-0).
- Blunt, M.J., Bijeljic, B., Dong, H., Gharbi, O., Iglauder, S., Mostaghimi, P., Paluszny, A., Pentland, C., 2013. Pore-scale imaging and modelling. *Adv. Water Resour.* 51, 197–216. <http://dx.doi.org/10.1016/j.advwatres.2012.03.003>.
- Boek, E.S., Venturoli, M., 2010. Lattice-Boltzmann studies of fluid flow in porous media with realistic rock geometries. *Comput. Math. Appl.* 59, 2305–2314. <http://dx.doi.org/10.1016/j.camwa.2009.08.063>.
- Boek, E.S., Zacharoudiou, I., Gray, F., Shah, S.M.K., Crawshaw, J., Yang, J., 2014. Multiphase flow and reactive transport at the pore scale using lattice-Boltzmann computer simulations. SPE Annual Technical Conference and Exhibition. Society of Petroleum Engineers <http://dx.doi.org/10.2118/170941-MS>.
- Bondino, I., Hamon, G., Kallel, W., Kachuma, D., 2012. Relative permeabilities from simulation in 3D rock models and equivalent pore networks: critical review and way forward. *Int. Symp. Soc. Core Analysts. Society of Core Analysts, Aberdeen, Scotland.*
- Bookstein, F.L., 1986. Size and shape spaces for landmark data in two dimensions. *Stat. Sci.* 1, 238–242. <http://dx.doi.org/10.1214/ss/1177013702>.
- Boone, M.A., Quaghebeur, M., Nielsen, P., Cnudde, V., 2013. In situ monitoring of mineral waste carbonation under high CO₂ pressure. 4th International Conference on Accelerated Carbonatation for Environmental and Materials Engineering, 2013, Leuven, Belgium.
- Boone, M.A., Nielsen, P., De Kock, T., Boone, M.N., Quaghebeur, M., Cnudde, V., 2014. Monitoring of stainless-steel slag carbonation using X-ray computed microtomography. *Environ. Sci. Technol.* 48, 674–680. <http://dx.doi.org/10.1021/es402767q>.
- Boone, M., Bultreys, T., Masschaele, B., Cnudde, V., De Schryver, T., Van Loo, D., Van Hoorebeke, L., 2015. Fast time resolved micro-CT imaging: visualizing dynamic pore scale processes at high resolution. *Acta Stereol. Proc. ICSIA, 14th ICSIA Abstr.*
- Bovik, A.C., Aggarwal, S.J., Merchant, F., Kim, N.H., Diller, K.R., 2001. Automatic area and volume measurements from digital biomedical images. In: Häder, D.-P. (Ed.), *Image Analysis. Methods and Applications*. CRC Press, Boca Raton, FL, pp. 23–64.
- Brabant, L., Vlassenbroeck, J., De Witte, Y., Cnudde, V., Boone, M.N., Dewanckele, J., Van Hoorebeke, L., 2011. Three-dimensional analysis of high-resolution X-ray computed tomography data with Morpho+. *Microsc. Microanal.* 17, 252–263. <http://dx.doi.org/10.1017/S1431927610094389>.
- Brabant, L., Dierick, M., Pauwels, E., Boone, M.N., Hoorebeke, L., Van, 2014. EDART, a discrete algebraic reconstructing technique for experimental data obtained with high resolution computed tomography. *J. Xray Sci. Technol.* 22, 47–61. <http://dx.doi.org/10.3233/XST-130408>.
- Bronnikov, A.V., 2002. Theory of quantitative phase-contrast computed tomography. *J. Opt. Soc. Am. A* 19, 472. <http://dx.doi.org/10.1364/JOSAA.19.000472>.
- Brun, F., Mancini, L., Kasaei, P., Favretto, S., Dreossi, D., Tromba, G., 2010. Pore3D: a software library for quantitative analysis of porous media. *Nucl. Instrum. Methods Phys. Res., Sect. A* 615, 326–332. <http://dx.doi.org/10.1016/j.nima.2010.02.063>.
- Buffiere, J.-Y., Maire, E., Adrien, J., Masse, J.-P., Boller, E., 2010. In situ experiments with X-ray tomography: an attractive tool for experimental mechanics. *Exp. Mech.* 50, 289–305. <http://dx.doi.org/10.1007/s11340-010-9333-7>.
- Bultreys, T., Boone, M.A., Boone, M.N., De Schryver, T., Masschaele, B., Van Hoorebeke, L., Cnudde, V., 2015a. Fast laboratory-based micro-computed tomography for pore-scale research: illustrative experiments and perspectives on the future. *Adv. Water Resour.* 1, 1–11. <http://dx.doi.org/10.1016/j.advwatres.2015.05.012>.
- Bultreys, T., Boone, M.A., Boone, M.N., De Schryver, T., Masschaele, B., Van Loo, D., Van Hoorebeke, L., Cnudde, V., 2015b. Real-time visualization of Haines jumps in sandstone with laboratory-based microcomputed tomography. *Water Resour. Res.* 51, <http://dx.doi.org/10.1002/2015WR017502> (n/a-n/a).
- Bultreys, T., Van Hoorebeke, L., Cnudde, V., 2015c. Multi-scale, micro-computed tomography-based pore network models to simulate drainage in heterogeneous rocks. *Adv. Water Resour.* 78, 36–49. <http://dx.doi.org/10.1016/j.advwatres.2015.02.003>.
- Cardenas, M.B., 2008. Three-dimensional vortices in single pores and their effects on transport. *Geophys. Res. Lett.* 35, 1–6. <http://dx.doi.org/10.1029/2008GL035343>.
- Caubit, C., Hamon, G., Sheppard, A.P., Øren, P.E., 2008. Evaluation of the reliability of prediction of petrophysical data through imagery. *Int. Symp. Soc. Core Analysts.*
- Chareyre, B., Cortis, A., Catalano, E., Barthélémy, E., 2012. Pore-scale modeling of viscous flow and induced forces in dense sphere packings. *Transp. Porous Media* 94, 595–615. <http://dx.doi.org/10.1007/s11242-012-0057-2>.
- Chen, B., Guizar-Sicairos, M., Xiong, G., Shemilt, L., Diaz, A., Nutter, J., Burdet, N., Huo, S., Mancuso, J., Monteith, A., Vergeer, F., Burgess, A., Robinson, I., 2013. Three-dimensional structure analysis and percolation properties of a barrier marine coating. *Sci. Rep.* 3, 1177. <http://dx.doi.org/10.1038/srep01177>.
- Chen, L., Fang, W., Kang, Q., De'Haven Hyman, J., Viswanathan, H.S., Tao, W.-Q., 2015. Generalized lattice Boltzmann model for flow through tight porous media with Klinkenberg's effect. *Phys. Rev. E* 91, 033004. <http://dx.doi.org/10.1103/PhysRevE.91.033004>.
- Cheng, Z., 1998. Development of ion and electron dual focused beam apparatus for high spatial resolution three-dimensional microanalysis of solid materials. *J. Vac. Sci. Technol., B: Microelectron. Nanometer Struct.* 16, 2473. <http://dx.doi.org/10.1116/1.590193>.
- Chukwudzie, C.P., Tyagi, M., Sears, S.O., White, C.D., 2012. Prediction of non-Darcy coefficients for inertial flows through the castlegate sandstone using image-

- based modeling. *Transp. Porous Media* 95, 563–580. <http://dx.doi.org/10.1007/s11242-012-0062-5>.
- Cloetens, P., Ludwig, W., Baruchel, J., Van Dyck, D., Van Landuyt, J., Guigay, J.P., Schlenker, M., 1999. Holotomography: quantitative phase tomography with micrometer resolution using hard synchrotron radiation X rays. *Appl. Phys. Lett.* 75, 2912. <http://dx.doi.org/10.1063/1.125225>.
- Cnudde, V., Boone, M.N., 2013. High-resolution X-ray computed tomography in geosciences: a review of the current technology and applications. *Earth-Sci. Rev.* 123, 1–17. <http://dx.doi.org/10.1016/j.earscirev.2013.04.003>.
- Cnudde, V., Dierick, M., Vlassenbroeck, J., Masschaele, B., Lehmann, E., Jacobs, P., Van Hoorebeke, L., 2008. High-speed neutron radiography for monitoring the water absorption by capillarity in porous materials. *Nucl. Instrum. Methods Phys. Res., Sect. B* 266, 155–163. <http://dx.doi.org/10.1016/j.nimb.2007.10.030>.
- Cnudde, V., De Boever, W., Dewanckele, J., De Kock, T., Boone, M., Boone, M.N., Silversmit, G., Vincze, L., Van Ranst, E., Derluyn, H., Peetersmans, S., Hovind, J., Modregger, P., Stampanoni, M., De Buyster, K., De Schutter, G., 2013. Multi-disciplinary characterization and monitoring of sandstone (Kandla Grey) under different external conditions. *Q. J. Eng. Geol. Hydrogeol.* 46, 95–106. <http://dx.doi.org/10.1144/qjegh2012-005>.
- Coles, M.E., Hazlett, R.D., Spanne, P., Soll, W.E., Muegge, E.L., Jones, K.W., 1998. Pore level imaging of fluid transport using synchrotron X-ray microtomography. *J. Pet. Sci. Eng.* 19, 55–63. [http://dx.doi.org/10.1016/S0920-4105\(97\)00035-1](http://dx.doi.org/10.1016/S0920-4105(97)00035-1).
- Coon, E.T., Porter, M.L., Kang, Q., 2013. Taxila LBM: a parallel, modular lattice Boltzmann framework for simulating pore-scale flow in porous media. *Comput. Geosci.* 18, 17–27. <http://dx.doi.org/10.1007/s10596-013-9379-6>.
- Corne, N.D., Silver, D., Min, P., 2007. Curve-skeleton properties, applications, and algorithms. *IEEE Trans. Vis. Comput. Graphs.* 13, 530–548. <http://dx.doi.org/10.1109/TCVG.2007.1002>.
- Crandall, D., Ahmadi, G., Smith, D.H., 2010. Computational modeling of fluid flow through a fracture in permeable rock. *Transp. Porous Media* 84, 493–510. <http://dx.doi.org/10.1007/s11242-009-9516-9>.
- Curtis, M.E., Cardott, B.J., Sondergeld, C.H., Rai, C.S., 2012. Development of organic porosity in the Woodford Shale with increasing thermal maturity. *Int. J. Coal Geol.* 103, 26–31. <http://dx.doi.org/10.1016/j.coal.2012.08.004>.
- Dam, H.F., Andersen, T.R., Pedersen, E.B.L., Thydén, K.T.S., Helgesen, M., Carlé, J.E., Jørgensen, P.S., Reinhardt, J., Søndergaard, R.R., Jørgensen, M., Bundgaard, E., Krebs, F.C., Andreassen, J.W., 2015. Enabling flexible polymer tandem solar cells by 3D ptychographic imaging. *Adv. Energy Mater.* 5. [\(n/a–n/a\)](http://dx.doi.org/10.1002/aenm.201400736).
- De Boever, W., Diaz, A., Derluyn, H., De Kock, T., Van Stappen, J., Dewanckele, J., Bultreys, T., Boone, M., De Schryver, T., Skjønsfjell, E.T.B., Holler, M., Breiby, D.W., Cnudde, V., 2015a. Characterization of composition and structure of clay minerals in sandstone with ptychographic X-ray nanotomography. *Appl. Clay Sci.* 118, 258–264. <http://dx.doi.org/10.1016/j.clay.2015.09.020>.
- De Boever, W., Derluyn, H., Van Loo, D., Van Hoorebeke, L., Cnudde, V., 2015b. Data-fusion of high resolution X-ray CT, SEM and EDS for 3D and pseudo-3D chemical and structural characterization of sandstone. *Micron* 74, 15–21. <http://dx.doi.org/10.1016/j.micron.2015.04.003>.
- De Kock, T., Boone, M., Dewanckele, J., Boever, W., De, Boone, M., Schutter, G., De, Lehmann, E., 2013. Monitoring frost susceptibility of limestone faces. 12th International Congress on the Deterioration and Conservation of Stone.
- De Kock, T., Boone, M.A., De Schryver, T., Van Stappen, J., Derluyn, H., Masschaele, B., De Schutter, G., Cnudde, V., 2015. A pore-scale study of fracture dynamics in rock using X-ray micro-CT under ambient freeze-thaw cycling. *Environ. Sci. Technol.* <http://dx.doi.org/10.1021/es055738d> 150204202251005.
- De Prisco, G., Toelke, J., Dernika, M.R., 2012. Computation of relative permeability functions in 3D digital rocks by a fractional flow approach using the lattice Boltzmann method. *Int. Symp. Soc. Core Analysts. Society of Core Analysts*, pp. 1–12.
- Demianov, A., Dinariev, O., Esvsev, N., 2011. Density functional modelling in multiphase compositional hydrodynamics. *Can. J. Chem. Eng.* 89, 206–226. <http://dx.doi.org/10.1002/cjce.20457>.
- Derluyn, H., Griffa, M., Mannes, D., Jerjen, I., Dewanckele, J., Vontobel, P., Sheppard, A., Derome, D., Cnudde, V., Lehmann, E., Carmeliet, J., 2013. Characterizing saline uptake and salt distributions in porous limestone with neutron radiography and X-ray micro-tomography. *J. Build. Phys.* 36, 353–374. <http://dx.doi.org/10.1177/1744259112473947>.
- Derluyn, H., Dewanckele, J., Boone, M.N., Cnudde, V., Derome, D., Carmeliet, J., 2014. Crystallization of hydrated and anhydrous salts in porous limestone resolved by synchrotron X-ray microtomography. *Nucl. Instrum. Methods Phys. Res., Sect. B* 324, 102–112. <http://dx.doi.org/10.1016/j.nimb.2013.08.065>.
- Desbois, G., Urai, J.L., Kukla, P.A., 2009. Morphology of the pore space in claystones – evidence from BIB/FIB ion beam sectioning and cryo-SEM observations. *eEarth Discuss.* 4, 1–19. <http://dx.doi.org/10.5194/eed-4-1-2009>.
- Dewanckele, J., De Kock, T., Boone, M.A., Cnudde, V., Brabant, L., Boone, M.N., Fronteau, G., Van Hoorebeke, L., Jacobs, P., 2012. 4D imaging and quantification of pore structure modifications inside natural building stones by means of high resolution X-ray CT. *Sci. Total Environ.* 416, 436–448. <http://dx.doi.org/10.1016/j.scitotenv.2011.11.018>.
- Dewanckele, J., Boone, M.A., De Kock, T., De Boever, W., Brabant, L., Boone, M.N., Fronteau, G., Dils, J., Van Hoorebeke, L., Jacobs, P., Cnudde, V., 2013. Holistic approach of pre-existing flaws on the decay of two limestones. *Sci. Total Environ.* 447, 403–414. <http://dx.doi.org/10.1016/j.scitotenv.2012.12.094>.
- Dewanckele, J., De Kock, T., Fronteau, G., Derluyn, H., Vontobel, P., Dierick, M., Van Hoorebeke, L., Jacobs, P., Cnudde, V., 2014. Neutron radiography and X-ray computed tomography for quantifying weathering and water uptake processes inside porous limestone used as building material. *Mater. Charact.* 88, 86–99. <http://dx.doi.org/10.1016/j.matchar.2013.12.007>.
- Diaz, A., Trtik, P., Guizar-Sicairos, M., Menzel, A., Thibault, P., Bunk, O., 2012. Quantitative X-ray phase nanotomography. *Phys. Rev. B* 85, 020104. <http://dx.doi.org/10.1103/PhysRevB.85.020104>.
- Diaz, a., Guizar-Sicairos, M., Poepel, a., Menzel, a., Bunk, O., 2014. Characterization of carbon fibers using X-ray phase nanotomography. *Carbon* 67, 98–103. <http://dx.doi.org/10.1016/j.carbon.2013.09.066>.
- Dierick, M., Van Loo, D., Masschaele, B., Van den Bulcke, J., Van Acker, J., Cnudde, V., Van Hoorebeke, L., 2014. Recent micro-CT scanner developments at UGCT. *Nucl. Instrum. Methods Phys. Res., Sect. B* 324, 35–40. <http://dx.doi.org/10.1016/j.nimb.2013.10.051>.
- Dierolf, M., Menzel, A., Thibault, P., Schneider, P., Kewish, C.M., Wepf, R., Bunk, O., Pfeiffer, F., 2010. Ptychographic X-ray computed tomography at the nanoscale. *Nature* 467, 436–439. <http://dx.doi.org/10.1038/nature09419>.
- Dong, H., Blunt, M., 2009. Pore-network extraction from micro-computerized-tomography images. *Phys. Rev. E* 80, 036307. <http://dx.doi.org/10.1103/PhysRevE.80.036307>.
- Dong, H., Fjeldstad, S., Alberts, L., Roth, S., Bakke, S., Øren, P.-E., 2008. Pore network modelling on carbonate: a comparative study of different micro-CT network extraction methods. *Int. Symp. Soc. Core Analysts. Society of Core Analysts*.
- Dullien, F.A.L., 1992. *Porous Media – Fluid Transport and Pore Structure*. Academic Press, Inc.
- Dunn, D.N., Hull, R., 1999. Reconstruction of three-dimensional chemistry and geometry using focused ion beam microscopy. *Appl. Phys. Lett.* 75, 3414. <http://dx.doi.org/10.1016/1.125311>.
- Dupin, H.J., Kitanidis, P.K., McCarty, P.L., 2001. Pore-scale modeling of biological clogging due to aggregate expansion: a material mechanics approach. *Water Resour. Res.* 37, 2965–2979. <http://dx.doi.org/10.1029/2001WR000306>.
- Earl, J.S., Leary, R.K., Perrin, J.S., Brydson, R., Harrington, J.P., Markowitz, K., Milne, S.J., 2010. Characterization of dentine structure in three dimensions using FIB-SEM. *J. Microsc.* 240, 1–5. <http://dx.doi.org/10.1111/j.1365-2818.2010.03396.x>.
- Esmaeili, M., Fløystad, J.B., Diaz, A., Høydalsvik, K., Guizar-Sicairos, M., Andreassen, J.W., Breiby, D.W., 2013. Ptychographic X-ray tomography of silk fiber hydration. *Macromolecules* 46, 434–439. <http://dx.doi.org/10.1021/ma3021163>.
- Español, P., Warren, P., 2007. Statistical mechanics of dissipative particle dynamics. *Europhys. Lett.* <http://dx.doi.org/10.1209/0295-5075/30/4/001>.
- Eymard, R., Gallouët, T., Herbin, R., 2000. Finite volume methods. In: Glowinski, R., Xu, J. (Eds.), *Handbook of Numerical Analysis*, pp. 713–1018.
- Fanis, A., De Pešić, Z.D., Wagner, U., Rau, C., 2013. Fast X-ray imaging at beamline I13L at Diamond Light Source. *J. Phys. Conf. Ser.* 425, 192014. <http://dx.doi.org/10.1088/1742-6596/425/19/192014>.
- Farmer, C.L., 2002. Upscaling: a review. *Int. J. Numer. Methods Fluids* 40, 63–78. <http://dx.doi.org/10.1002/fld.267>.
- Fatt, I., 1956. The network model of porous media. *Pet. Trans. AIME* 207, 144–181.
- Ferrari, A., Lunati, I., 2013. Direct numerical simulations of interface dynamics to link capillary pressure and total surface energy. *Adv. Water Resour.* 57, 19–31. <http://dx.doi.org/10.1016/j.advwatres.2013.03.005>.
- Ferréol, B., Rothman, D.H., 1995. Lattice-Boltzmann simulations of flow through Fontainebleau sandstone. *Transp. Porous Media* 20, 3–20. <http://dx.doi.org/10.1007/BF00616923>.
- Feser, M., Gelb, J., Chang, H., Cui, H., Duewer, F., Lau, S.H., Tkachuk, A., Yun, W., 2008. Sub-micron resolution CT for failure analysis and process development. *Meas. Sci. Technol.* 19, 094001. <http://dx.doi.org/10.1088/0957-0233/19/9/094001>.
- Fredrich, J.T., DiGiovanni, A.A., Noble, D.R., 2006. Predicting macroscopic transport properties using microscopic image data. *J. Geophys. Res.* 111, B03201. <http://dx.doi.org/10.1029/2005JB003774>.
- Freitas, D.S., Prat, M., 2000. Pore network simulation of evaporation of a binary liquid from a capillary porous medium. *Transp. Porous Media* 40, 1–25. <http://dx.doi.org/10.1023/A:1006651524722>.
- Gao, J., Xing, H., Rudolph, V., Li, Q., Golding, S.D., 2015. Parallel lattice Boltzmann computing and applications in core sample feature evaluation. *Transp. Porous Media* 107, 65–77. <http://dx.doi.org/10.1007/s11242-014-0425-1>.
- Geiger, S., Schmid, K.S., Zaretskiy, Y., 2012. Mathematical analysis and numerical simulation of multi-phase multi-component flow in heterogeneous porous media. *Curr. Opin. Colloid Interface Sci.* 17, 147–155. <http://dx.doi.org/10.1016/j.cocis.2012.01.003>.
- Gelb, J., Feser, M., Tkachuk, a., Hsu, G., Chen, S., Chang, H., Fong, T., Hunter, L., Goldberger, I., Lau, S.-H., Yun, W., 2009. Sub-micron X-ray computed tomography for non-destructive 3D visualization and analysis. *Microsc. Microanal.* 15, 618–619. <http://dx.doi.org/10.1017/S1431927609093623>.
- Georgiadis, A., Berg, S., Makurat, A., Maitland, G., Ott, H., 2013. Pore-scale micro-computed-tomography imaging: non-wetting-phase cluster-size distribution during drainage and imbibition. *Phys. Rev. E* 88, 33002. <http://dx.doi.org/10.1103/PhysRevE.88.033002>.
- Gharaso, M., Centler, F., Regnier, P., Harms, H., Thullner, M., 2012. A reactive transport modeling approach to simulate biogeochemical processes in pore structures with pore-scale heterogeneities. *Environ. Model. Softw.* 30, 102–114. <http://dx.doi.org/10.1016/j.envsoft.2011.10.010>.
- Gharbi, O., Blunt, M.J., 2012. The impact of wettability and connectivity on relative permeability in carbonates: a pore network modeling analysis. *Water Resour. Res.* 48, [\(n/a–n/a\)](http://dx.doi.org/10.1029/2012WR011877).
- Giannuzzi, L.A., Phifer, D., Giannuzzi, N.J., Capuano, M.J., 2007. Two-dimensional and 3-dimensional analysis of bone/dental implant interfaces with the use of focused ion beam and electron microscopy. *J. Oral Maxillofac. Surg.* 65, 737–747. <http://dx.doi.org/10.1016/j.joms.2006.10.025>.
- Ginzburg, I., 2014. Comment on “An improved gray lattice Boltzmann model for simulating fluid flow in multi-scale porous media”: intrinsic links between LBE

- Brinkman schemes. *Adv. Water Resour.* <http://dx.doi.org/10.1016/j.advwatres.2014.05.007>.
- Gostovic, D., Vito, N.J., O'Hara, K.A., Jones, K.S., Wachsman, E.D., 2011. Microstructure and connectivity quantification of complex composite solid oxide fuel cell electrode three-dimensional networks. *J. Am. Ceram. Soc.* 94, 620–627. <http://dx.doi.org/10.1111/j.1551-2916.2010.04111.x>.
- Gran, H.C., 1995. Fluorescent liquid replacement technique. A means of crack detection and water: binder ratio determination in high strength concretes. *Cem. Concr. Res.* 25, 1063–1074. [http://dx.doi.org/10.1016/0008-8846\(95\)00101-H](http://dx.doi.org/10.1016/0008-8846(95)00101-H).
- Gunstensen, A.K., Rothman, D.H., Zaleski, S., Zanetti, G., 1991. Lattice Boltzmann model of immiscible fluids. *Phys. Rev. A* 43, 4320–4327. <http://dx.doi.org/10.1103/PhysRevA.43.4320>.
- Gustafsson, M.G.L., 2000. Surpassing the lateral resolution limit by a factor of two using structured illumination microscopy. *J. Microsc.* 198, 82–87. <http://dx.doi.org/10.1046/j.1365-2818.2000.00710.x>.
- Hammond, P.S., Unsal, E., 2012. A dynamic pore network model for oil displacement by wettability-altering surfactant solution. *Transp. Porous Media* 92, 789–817. <http://dx.doi.org/10.1007/s11242-011-9933-4>.
- Harting, J., Chin, J., Venturoli, M., Coveney, P.V., 2005. Large-scale lattice Boltzmann simulations of complex fluids: advances through the advent of computational grids. *Philos. Transact. A Math. Phys. Eng. Sci.* 363, 1895–1915. <http://dx.doi.org/10.1098/rsta.2005.1618>.
- Hazlett, R.D., Chen, S.Y., Soll, W.E., 1998. Wettability and rate effects on immiscible displacement: lattice Boltzmann simulation in microtomographic images of reservoir rocks. *J. Pet. Sci. Eng.* 20, 167–175. [http://dx.doi.org/10.1016/S0920-4105\(98\)00017-5](http://dx.doi.org/10.1016/S0920-4105(98)00017-5).
- Heath, J.E., Dewers, T.a., McPherson, B.J.O.L., Petrusak, R., Chidsey, T.C., Rinehart, A.J., Mozley, P.S., 2011. Pore networks in continental and marine mudstones: characteristics and controls on sealing behavior. *Geosphere* 7, 429–454. <http://dx.doi.org/10.1130/GES00619.1>.
- Heethof, M., Cloetens, P., 2008. A comparison of synchrotron X-ray phase contrast tomography and holotomography for non-invasive investigations of the internal anatomy of mites. *Soil Org. Soil* 82, 301–316.
- Heintzmann, R., Ficz, G., 2006. Breaking the resolution limit in light microscopy. *Brief. Funct. Genomic. Proteomic.* 5, 289–301. <http://dx.doi.org/10.1093/bfgp/ell036>.
- Held, R.J., Celia, M.A., 2001. Pore-scale modeling and upscaling of nonaqueous phase liquid mass transfer. *Water Resour. Res.* 37, 539–549. <http://dx.doi.org/10.1029/2000WR900274>.
- Hemes, S., Desbois, G., Urai, J.L., Schröppel, B., Schwarz, J.-O., 2015. Multi-scale characterization of porosity in boom clay (HADES-level, Mol, Belgium) using a combination of X-ray μ -CT, 2D BIB-SEM and FIB-SEM tomography. *Microporous Mesoporous Mater.* 208, 1–20. <http://dx.doi.org/10.1016/j.micromeso.2015.01.022>.
- Henderickx, H., Cnudde, V., Masschaele, B., Dierick, M., Vlassenbroeck, J., Van Hoorebeke, L., 2006. Description of a new fossil *Pseudogarypus* (*Pseudoscorpiones : Pseudogarypidae*) with the use of X-ray micro-CT to penetrate opaque amber. *Zootaxa* 41–50.
- Henderickx, H., Tafforeau, P., Soriano, C., 2012. Phase-contrast synchrotron microtomography reveals the morphology of a partially visible new *Pseudogarypus* in Baltic amber (*Pseudoscorpiones : Pseudogarypidae*). *Palaeontol. Electron.* 15.
- Herring, A.L., Andersson, L., Newell, D.L., Carey, J.W., Wildenschild, D., 2014. Pore-scale observations of supercritical CO₂ drainage in Bentheimer sandstone by synchrotron X-ray imaging. *Int. J. Greenhouse Gas Control* 25, 93–101. <http://dx.doi.org/10.1016/j.ijggc.2014.04.003>.
- Herring, A.L., Andersson, L., Schlüter, S., Sheppard, A., Wildenschild, D., 2015. Efficiently engineering pore-scale processes: the role of force dominance and topology during nonwetting phase trapping in porous media. *Adv. Water Resour.* 79, 91–102. <http://dx.doi.org/10.1016/j.advwatres.2015.02.005>.
- Higuera, F.J., Succi, S., Benzi, R., 1989. Lattice gas dynamics with enhanced collisions. *Europhys. Lett.* 9, 345–349. <http://dx.doi.org/10.1209/0295-5075/9/4/008>.
- Hillier, S., 1994. Pore-lining chlorites in siliciclastic reservoir sandstones: electron microprobe, SEM and XRD data, and implications for their origin. *Clay Miner.* 29, 665–679. <http://dx.doi.org/10.1180/claymin.1994.029.4.20>.
- Hoal, K.O., Stammer, J.G., Appleby, S.K., Botha, J., Ross, J.K., Botha, P.W., 2009. Research in quantitative mineralogy: examples from diverse applications. *Miner. Eng.* 22, 402–408. <http://dx.doi.org/10.1016/j.mineeng.2008.11.003>.
- Holler, M., Diaz, A., Guizar-Sicairos, M., Karvinen, P., Färm, E., Häkkinen, E., Ritala, M., Menzel, a, Raabe, J., Bunk, O., 2014. X-ray tomographic computed tomography at 16 nm isotropic 3D resolution. *Sci. Rep.* 4, 3857. <http://dx.doi.org/10.1038/srep03857>.
- Holzer, L., Indutnyi, F., Gasser, P.H., Münnich, B., Wegmann, M., 2004. Three-dimensional analysis of porous BaTiO₃ ceramics using FIB nanotomography. *J. Microsc.* 216, 84–95. <http://dx.doi.org/10.1111/j.0022-2720.2004.01397.x>.
- Huang, L.-K., Wang, M.-J.J., 1995. Image thresholding by minimizing the measures of fuzziness. *Pattern Recogn.* 28, 41–51. [http://dx.doi.org/10.1016/0031-3203\(94\)E0043-K](http://dx.doi.org/10.1016/0031-3203(94)E0043-K).
- Huang, H., Meakin, P., Liu, M., 2005. Computer simulation of two-phase immiscible fluid motion in unsaturated complex fractures using a volume of fluid method. *Water Resour. Res.* 41. <http://dx.doi.org/10.1029/2005WR004204> (n/a-n/a).
- Huang, Z., Chen, J., Xue, H., Wang, Y., Wang, M., Deng, C., 2013. Microstructural characteristics of the Cretaceous Qingshankou Formation shale, Songliao Basin. *Pet. Explor. Dev.* 40, 61–68. [http://dx.doi.org/10.1016/S1876-3804\(13\)60006-3](http://dx.doi.org/10.1016/S1876-3804(13)60006-3).
- Huber, F., Enzmann, F., Wenka, A., Bouby, M., Dentz, M., Schäfer, T., 2012. Natural micro-scale heterogeneity induced solute and nanoparticle retardation in fractured crystalline rock. *J. Contam. Hydrol.* 133, 40–52. <http://dx.doi.org/10.1016/j.jconhyd.2012.03.004>.
- Huber, C., Shafei, B., Parmigiani, A., 2014. A new pore-scale model for linear and non-linear heterogeneous dissolution and precipitation. *Geochim. Cosmochim. Acta* 124, 109–130. <http://dx.doi.org/10.1016/j.gca.2013.09.003>.
- Hunt, A., Ewing, R., Ghanbarian, B., 2014. *Percolation Theory for Flow in Porous Media*. third ed. Springer.
- Hutzenlaub, T., Thiele, S., Zengerle, R., Ziegler, C., 2012. Three-dimensional reconstruction of a LiCoO₂ Li-ion battery cathode. *Electrochem. Solid-State Lett.* 15, A33. <http://dx.doi.org/10.1149/2.002203esl>.
- Hyman, J.D., Smolarkiewicz, P.K., Winter, C.L., 2012. Heterogeneities of flow in stochastically generated porous media. *Phys. Rev. E* 86, 056701. <http://dx.doi.org/10.1103/PhysRevE.86.056701>.
- Iassonov, P., Gebranegus, T., Tuller, M., 2009. Segmentation of X-ray computed tomography images of porous materials: a crucial step for characterization and quantitative analysis of pore structures. *Water Resour. Res.* 45. <http://dx.doi.org/10.1029/2009WR008087> (n/a-n/a).
- Icardi, M., Boccardo, G., Marchisio, D.L., Tosco, T., Sethi, R., 2014. Pore-scale simulation of fluid flow and solute dispersion in three-dimensional porous media. *Phys. Rev. E* 90, 013032. <http://dx.doi.org/10.1103/PhysRevE.90.013032>.
- Idowu, N.A., Blunt, M.J., 2010. Pore-scale modelling of rate effects in waterflooding. *Transp. Porous Media* 83, 151–169. <http://dx.doi.org/10.1007/s11242-009-9468-0>.
- Idowu, N., Nardi, C., Long, H., Øren, P., 2012. Pore-scale modeling: effects of network properties on predictive capabilities. *Int. Symp. Soc. Core Analysts. Society of Core Analysts, Aberdeen, Scotland*, pp. 1–12.
- Idowu, N., Nardi, C., Long, H., Bondino, I., 2013. Improving digital rock physics predictive potential for relative permeabilities from equivalent pore networks. *Int. Symp. Soc. Core Analysts. Society of Core Analysts, Napa Valley, USA*, pp. 1–12.
- Idowu, N.A., Nardi, C., Long, H., Varslot, T., Øren, P.-E., 2014. Effects of segmentation and skeletonization algorithms on pore networks and predicted multiphase-transport properties of reservoir-rock samples. *SPE Reserv. Eval. Eng.* 1–13 <http://dx.doi.org/10.2118/166030-PA>.
- Iglauer, S., Fernø, M. a, Shearing, P., Blunt, M.J., 2012. Comparison of residual oil cluster size distribution, morphology and saturation in oil-wet and water-wet sandstone. *J. Colloid Interface Sci.* 375, 187–192. <http://dx.doi.org/10.1016/j.jcis.2012.02.025>.
- Ingham, J., 2013. *Geomaterials Under the Microscope*. Academic Press.
- Jacobsen, S., Gran, H.C., Sellevold, E.J., Bakke, J.A., 1995. High strength concrete – freeze/thaw testing and cracking. *Cem. Concr. Res.* 25, 1775–1780. [http://dx.doi.org/10.1016/0008-8846\(95\)00173-5](http://dx.doi.org/10.1016/0008-8846(95)00173-5).
- Jerauld, G.R., Salter, S.J., 1990. The effect of pore-structure on hysteresis in relative permeability and capillary pressure: pore-level modeling. *Transp. Porous Media* 5, 103–151. <http://dx.doi.org/10.1007/BF00144600>.
- Jiang, F., Tsuji, T., 2015. Impact of interfacial tension on residual CO₂ clusters in porous sandstone. *Water Resour. Res.* 51, 1710–1722. <http://dx.doi.org/10.1002/2014WR016070>.
- Jiang, Z., Wu, K., Couples, G., van Dijke, M.I.J., Sorbie, K.S., Ma, J., 2007. Efficient extraction of networks from three-dimensional porous media. *Water Resour. Res.* 43. <http://dx.doi.org/10.1029/2006WR005780> (n/a-n/a).
- Jiang, Z., van Dijke, M.I.J., Wu, K., Couples, G.D., Sorbie, K.S., Ma, J., 2011. Stochastic pore network generation from 3D rock images. *Transp. Porous Media* 94, 571–593. <http://dx.doi.org/10.1007/s11242-011-9792-z>.
- Jiang, Z., van Dijke, M.I.J., Sorbie, K.S., Couples, G.D., 2013. Representation of multiscale heterogeneity via multiscale pore networks. *Water Resour. Res.* 49, 5437–5449. <http://dx.doi.org/10.1002/wrcr.20304>.
- Jiang, F., Tsuji, T., Hu, C., 2014. Elucidating the role of interfacial tension for hydrological properties of two-phase flow in natural sandstone by an improved lattice Boltzmann method. *Transp. Porous Media* <http://dx.doi.org/10.1007/s11242-014-0329-0>.
- Jiao, K., Yao, S., Liu, C., Gao, Y., Wu, H., Li, M., Tang, Z., 2014. The characterization and quantitative analysis of nanopores in unconventional gas reservoirs utilizing FESEM-FIB and image processing: an example from the lower Silurian Longmaxi Shale, upper Yangtze region, China. *Int. J. Coal Geol.* 128–129, 1–11. <http://dx.doi.org/10.1016/j.coal.2014.03.004>.
- Jiménez-Hornero, F.J., Giráldez, J.V., Laguna, A., 2005. Simulation of tracer dispersion in porous media using lattice Boltzmann and random walk models. *Vadose Zone J.* 4, 310. <http://dx.doi.org/10.2136/vzj2004.0090>.
- Jin, G., Patzek, T.W., Sulin, D.B., 2004. Direct prediction of the absolute permeability of unconsolidated and consolidated reservoir rock. *SPE Annual Technical Conference and Exhibition. Society of Petroleum Engineers*. <http://dx.doi.org/10.2118/90084-MS>.
- Joekar-Niasar, V., Hassanizadeh, S.M., 2012. Analysis of fundamentals of two-phase flow in porous media using dynamic pore-network models: a review. *Crit. Rev. Environ. Sci. Technol.* 42, 1895–1976. <http://dx.doi.org/10.1080/10643389.2011.574101>.
- Joekar-Niasar, V., Prodanović, M., Wildenschild, D., Hassanizadeh, S.M., 2010a. Network model investigation of interfacial area, capillary pressure and saturation relationships in granular porous media. *Water Resour. Res.* 46. <http://dx.doi.org/10.1029/2009WR008585> (n/a-n/a).
- Joekar-Niasar, V., Hassanizadeh, S.M., Dahle, H.K., 2010b. Non-equilibrium effects in capillarity and interfacial area in two-phase flow: dynamic pore-network modelling. *J. Fluid Mech.* 655, 38–71. <http://dx.doi.org/10.1017/S0022112010000704>.
- Joekar-Niasar, V., Doster, F., Armstrong, R.T., Wildenschild, D., Celia, M.A., 2013. Trapping and hysteresis in two-phase flow in porous media: a pore-network study. *Water Resour. Res.* 49, 4244–4256. <http://dx.doi.org/10.1002/wrcr.20313>.
- Joos, J., Carraro, T., Weber, A., Ivers-Tiffée, E., 2011. Reconstruction of porous electrodes by FIB/SEM for detailed microstructure modeling. *J. Power Sources* 196, 7302–7307. <http://dx.doi.org/10.1016/j.jpowsour.2010.10.006>.
- Kang, Q., 2004. Lattice Boltzmann model for crystal growth from supersaturated solution. *Geophys. Res. Lett.* 31, L21604. <http://dx.doi.org/10.1029/2004GL021107>.
- Kang, Q., Zhang, D., Chen, S., 2002. Unified lattice Boltzmann method for flow in multiscale porous media. *Phys. Rev. E* 66, 056307. <http://dx.doi.org/10.1103/PhysRevE.66.056307>.
- Kang, Q., Lichtner, P.C., Zhang, D., 2006. Lattice Boltzmann pore-scale model for multicomponent reactive transport in porous media. *J. Geophys. Res.* 111, B05203. <http://dx.doi.org/10.1029/2005JB003951>.

- Kang, Q., Lichtner, P.C., Viswanathan, H.S., Abdel-Fattah, A.I., 2009. Pore scale modeling of reactive transport involved in geologic CO₂ sequestration. *Transp. Porous Media* 82, 197–213. <http://dx.doi.org/10.1007/s11242-009-9443-9>.
- Kang, Q., Wang, M., Mukherjee, P.P., Lichtner, P.C., 2010. Mesoscopic modeling of multiphysicochemical transport phenomena in porous media. *Adv. Mech. Eng.* 2. <http://dx.doi.org/10.1155/2010/142879>.
- Katsube, T.J., Williamson, M.A., 1994. Effects of diagenesis on shale nano-pore structure and implications for sealing capacity. *Clay Miner.* 29, 451–461. <http://dx.doi.org/10.1180/claymin.1994.029.4.05>.
- Kazantsev, D., Thompson, W.M., Lionheart, W.R.B., Eyndhoven, G. Van, Kaestner, A.P., Dobson, K.J., Withers, P.J., Lee, P.D., 2015. 4D-CT reconstruction with unified spatial-temporal patch-based regularization. *Inverse Prob. Imaging* 9, 447–467. <http://dx.doi.org/10.3934/ipi.2015.9.447>.
- Kehm, Y., 2004. Permeability prediction from thin sections: 3D reconstruction and lattice-Boltzmann flow simulation. *Geophys. Res. Lett.* 31, L04606. <http://dx.doi.org/10.1029/2003GL018761>.
- Keller, W.D., 1978. Kaolinization of feldspar as displayed in scanning electron micrographs. *Geology* 6, 184–188. [http://dx.doi.org/10.1130/0091-7613\(1978\)6<184](http://dx.doi.org/10.1130/0091-7613(1978)6<184).
- Keller, L.M., Holzer, L., Wepf, R., Gasser, P., Münch, B., Marschall, P., 2011. On the application of focused ion beam nanotomography in characterizing the 3D pore space geometry of Opalinus clay. *Phys. Chem. Earth Parts A/B/C* 36, 1539–1544. <http://dx.doi.org/10.1016/j.pce.2011.07.010>.
- Kelly, S., El-Sobky, H., Torres-Verdín, C., Balhoff, M.T., 2015. Assessing the utility of FIB-SEM images for shale digital rock physics. *Adv. Water Resour.* <http://dx.doi.org/10.1016/j.advwatres.2015.06.010>.
- Ketcham, R.A., Carlson, W.D., 2001. Acquisition, optimization and interpretation of X-ray computed tomographic imagery: applications to the geosciences. *Comput. Geosci.* 27, 381–400. [http://dx.doi.org/10.1016/S0098-3004\(00\)00116-3](http://dx.doi.org/10.1016/S0098-3004(00)00116-3).
- Khan, F., Enzmann, F., Kersten, M., Wiegmann, A., Steiner, K., 2012. 3D simulation of the permeability tensor in a soil aggregate on basis of nanotomographic imaging and LBE solver. *J. Soils Sediments* 12, 86–96. <http://dx.doi.org/10.1007/s11368-011-0435-3>.
- Kim, D.-S., Fogler, H.S., 2000. Biomass evolution in porous media and its effects on permeability under starvation conditions. *Biotechnol. Bioeng.* 69, 47–56. [http://dx.doi.org/10.1002/\(SICI\)1097-0290\(20000705\)69:1<47::AID-BIT6>3.0.CO;2-N](http://dx.doi.org/10.1002/(SICI)1097-0290(20000705)69:1<47::AID-BIT6>3.0.CO;2-N).
- Kim, D., Peters, C.A., Lindquist, W.B., 2011. Upscaling geochemical reaction rates accompanying acidic CO₂-saturated brine flow in sandstone aquifers. *Water Resour. Res.* 47. [\(n/a-n/a\)](http://dx.doi.org/10.1029/2010WR009472).
- Klaever, J., Desbois, G., Urai, J.L., Little, R., 2012. BIB-SEM study of the pore space morphology in early mature Posidonia Shale from the Hils area, Germany. *Int. J. Coal Geol.* 103, 12–25. <http://dx.doi.org/10.1016/j.coal.2012.06.012>.
- Knight, S.P., Salgaras, M., Wythe, A.M., De Carlo, F., Davenport, A.J., Trueman, A.R., 2010. In situ X-ray tomography of intergranular corrosion of 2024 and 7050 aluminium alloys. *Corros. Sci.* 52, 3855–3860. <http://dx.doi.org/10.1016/j.corsci.2010.08.026>.
- Koestel, J., Larsbo, M., 2014. Imaging and quantification of preferential solute transport in soil macropores. *Water Resour. Res.* 50, 4357–4378. <http://dx.doi.org/10.1002/2014WR015351>.
- Köhne, J.M., Schlüter, S., Vogel, H.-J., 2011. Predicting solute transport in structured soil using pore network models. *Vadose Zone J.* 10, 1082. <http://dx.doi.org/10.2136/vzj2010.0158>.
- Koroteev, D., Dinariev, O., Evseev, N., Klemin, D., Safonov, S., Berg, S., Van Kreijdsdijk, C., Armstrong, R., Myers, M.T., Hathorn, L., De Jong, H., Reservoir, S., Group, C., Global, S., International, S., 2013. *Direct hydrodynamic simulation of multiphase flow in porous rock. Int. Symp. Soc. Core Analysts. Society of Core Analysts, Napa Valley, USA*.
- Krohn, C.E., Thompson, A.H., 1986. Fractal sandstone pores: automated measurements using scanning-electron-microscope images. *Phys. Rev. B* 33, 6366–6374. <http://dx.doi.org/10.1103/PhysRevB.33.6366>.
- Krotkiewski, M., Ligaarden, I.S., Lie, K.-A., Schmid, D.W., 2011. On the importance of the Stokes-Brinkman equations for computing effective permeability in karst reservoirs. *Commun. Comput. Phys.* <http://dx.doi.org/10.4208/cicp.290610.020211a>.
- Kuzmin, a., Mohamad, a.a., 2010. Multirange multi-relaxation time Shan-Chen model with extended equilibrium. *Comput. Math. Appl.* 59, 2260–2270. <http://dx.doi.org/10.1016/j.camwa.2009.08.042>.
- Lak, M., Neraudeau, D., Nel, A., Cloetens, P., Perrichot, V., Tafforeau, P., 2008. Phase contrast X-ray synchrotron imaging: opening access to fossil inclusions in opaque amber. *Microsc. Microanal.* 14, 251–259. <http://dx.doi.org/10.1017/s1431927608080264>.
- Lakshmanan, S., Holmes, W.M., Sloan, W.T., Phoenix, V.R., 2015. Characterization of nanoparticle transport through quartz and dolomite gravels by magnetic resonance imaging. *Int. J. Environ. Sci. Technol.* 12, 3373–3384. <http://dx.doi.org/10.1007/s13762-015-0767-4>.
- Landrot, G., Ajo-Franklin, J.B., Yang, L., Cabrini, S., Steefel, C.I., 2012. Measurement of accessible reactive surface area in a sandstone, with application to CO₂ mineralization. *Chem. Geol.* 318–319, 113–125. <http://dx.doi.org/10.1016/j.chemgeo.2012.05.010>.
- Landry, C.J., Karpyn, Z.T., Ayala, O., 2014a. Pore-scale lattice Boltzmann modeling and 4D X-ray computed microtomography imaging of fracture-matrix fluid transfer. *Transp. Porous Media* 103, 449–468. <http://dx.doi.org/10.1007/s11242-014-0311-x>.
- Landry, C.J., Karpyn, Z.T., Ayala, O., 2014b. Relative permeability of homogenous-wet and mixed-wet porous media as determined by pore-scale lattice Boltzmann modeling. *Water Resour. Res.* 50, 3672–3689. <http://dx.doi.org/10.1002/2013WR015148>.
- Latham, S., Varslot, T., Sheppard, A., 2008. Image registration : enhancing and calibrating X-ray micro-Ct imaging. *Int. Symp. Soc. Core Analysts. Society of Core Analysts, Abu Dhabi, UAE*, pp. 1–12.
- Leith, S.D., Reddy, M.M., Ramirez, W.F.F., Heymans, M.J., 1996. Limestone characterization to model damage from acidic precipitation: effect of pore structure on mass transfer. *Environ. Sci. Technol.* 30, 2202–2210. <http://dx.doi.org/10.1021/es950583q>.
- Lenormand, R., Zarcone, C., Sarr, A., 1983. Mechanisms of the displacement of one fluid by another in a network of capillary ducts. *J. Fluid Mech.* 135, 337. <http://dx.doi.org/10.1017/S0022112083003110>.
- Lewis, R. a., 2004. Medical phase contrast X-ray imaging: current status and future prospects. *Phys. Med. Biol.* 49, 3573–3583. <http://dx.doi.org/10.1088/0031-9155/49/16/005>.
- Li, L., Peters, C.A., Celia, M.A., 2006. Upscaling geochemical reaction rates using pore-scale network modeling. *Adv. Water Resour.* 29, 1351–1370. <http://dx.doi.org/10.1016/j.advwatres.2005.10.011>.
- Li, R., Yang, Y.S., Pan, J., Pereira, G.G., Taylor, J.a., Cennell, B., Zou, C., 2014a. Lattice Boltzmann modeling of permeability in porous materials with partially percolating voxels. *Phys. Rev. E* 90, 033301. <http://dx.doi.org/10.1103/PhysRevE.90.033301>.
- Li, S., Chen, G., Ji, G., Lu, Y., 2014b. Quantitative damage evaluation of concrete suffered freezing-thawing by DIP technique. *Constr. Build. Mater.* 69, 177–185. <http://dx.doi.org/10.1016/j.conbuildmat.2014.07.072>.
- Liang, Z., Ioannidis, M., Chatzis, I., 2000. Geometric and topological analysis of three-dimensional porous media: pore space partitioning based on morphological skeletonization. *J. Colloid Interface Sci.* 221, 13–24. <http://dx.doi.org/10.1006/jcis.1999.6559>.
- Ligaarden, I., Krotkiewski, M., Lie, K.A., Pal, M., Schmid, D., 2010. On the Stokes-Brinkman equations for modeling flow in carbonate reservoirs. *Proceedings of the 12th European Conference on the Mathematics of Oil Recovery* <http://dx.doi.org/10.3997/2214-4609.20144924>.
- Lindquist, W.B., 2002. Quantitative analysis of three-dimensional X-ray tomographic images. In: Bonse, U. (Ed.), *Developments in X-ray Tomography III* Proceedings of SPIE 4503. SPIE, pp. 103–115. <http://dx.doi.org/10.1117/12.452833>.
- Lindquist, W.B., Venkataraman, A., 1999. Investigating 3D geometry of porous media from high resolution images. *Phys. Chem. Earth Solid Earth Geod.* 24, 593–599. [http://dx.doi.org/10.1016/S1464-1895\(99\)00085-X](http://dx.doi.org/10.1016/S1464-1895(99)00085-X).
- Lindquist, W.B., Lee, S., Coker, D.A., Jones, K.W., Spanne, P., 1996. Medial axis analysis of void structure in three-dimensional tomographic images of porous media. *J. Geophys. Res.* 101, 8297. <http://dx.doi.org/10.1029/95JB03039>.
- Liu, H., Valocchi, A.J., Kang, Q., Werth, C., 2013. Pore-scale simulations of gas displacing liquid in a homogeneous pore network using the lattice Boltzmann method. *Transp. Porous Media* 99, 555–580. <http://dx.doi.org/10.1007/s11242-013-0200-8>.
- Liu, H., Valocchi, A.J., Werth, C., Kang, Q., Oostrom, M., 2014. Pore-scale simulation of liquid CO₂ displacement of water using a two-phase lattice Boltzmann model. *Adv. Water Resour.* 73, 144–158. <http://dx.doi.org/10.1016/j.advwatres.2014.07.010>.
- Llewellyn, E.W., 2010. LB flow: an extensible lattice Boltzmann framework for the simulation of geophysical flows. Part I: theory and implementation. *Comput. Geosci.* 36, 115–122. <http://dx.doi.org/10.1016/j.cageo.2009.08.004>.
- Lloyd, G.E., 1987. Atomic number and crystallographic contrast images with the SEM: a review of backscattered electron techniques. *Mineral. Mag.* 51, 3–19. <http://dx.doi.org/10.1108/minmag.1987.051.359.02>.
- Lombardo, J.J., Ristau, R., Harris, W.M., Chiu, W.K.S., 2012. Focused ion beam preparation of samples for X-ray nanotomography. *J. Synchrotron Radiat.* 19, 789–796. <http://dx.doi.org/10.1107/S0909049512027252>.
- Longman, M.W., Mench, P.A., 1978. Diagenesis of Cretaceous limestones in the Edwards aquifer system of south-central Texas: a scanning electron microscope study. *Sediment. Geol.* 21, 241–276. [http://dx.doi.org/10.1016/0037-0738\(78\)90022-2](http://dx.doi.org/10.1016/0037-0738(78)90022-2).
- Loucks, R.G., Reed, R.M., Ruppel, S.C., Jarvie, D.M., 2009. Morphology, genesis, and distribution of nanometer-scale pores in siliceous mudstones of the Mississippian Barnett shale. *J. Sediment. Res.* 79, 848–861. <http://dx.doi.org/10.2110/jsr.2009.092>.
- Lubelli, B., de Winter, D.a.M., Post, J.a., van Hees, R.P.J., Drury, M.R., 2013. Cryo-FIB-SEM and MIP study of porosity and pore size distribution of bentonite and kaolin at different moisture contents. *Appl. Clay Sci.* 80–81, 358–365. <http://dx.doi.org/10.1016/j.clay.2013.06.032>.
- Ma, S., Mason, G., Morrow, N.R., 1996. Effect of contact angle on drainage and imbibition in regular polygonal tubes. *Colloids Surf. A Physicochem. Eng. Asp.* 117, 273–291. [http://dx.doi.org/10.1016/0927-7757\(96\)03702-8](http://dx.doi.org/10.1016/0927-7757(96)03702-8).
- Ma, J., Wu, K., Jiang, Z., Couples, G.D., 2010. SHIFT: an implementation for lattice Boltzmann simulation in low-porosity porous media. *Phys. Rev. E* 81, 056702. <http://dx.doi.org/10.1103/PhysRevE.81.056702>.
- Madonna, C., Quintal, B., Frehner, M., Almqvist, B.S.G., Tisato, N., Pistone, M., Marone, F., Saenger, E.H., 2013. Synchrotron-based X-ray tomographic microscopy for rock physics investigations. *Geophysics* 78, D53–D64. <http://dx.doi.org/10.1190/geo2012-0113.1>.
- Mahmud, W.M., Arms, J.Y., Sheppard, A., Knackstedt, M.A., Pinczewski, W.V., 2007. Effect of network topology on two-phase imbibition relative permeability. *Transp. Porous Media* 66, 481–493. <http://dx.doi.org/10.1007/s11242-006-0026-8>.
- Maire, E., Withers, P.J., 2014. Quantitative X-ray tomography. *Int. Mater. Rev.* 59, 1–43. <http://dx.doi.org/10.1117/143280413Y.0000000023>.
- Malaga-Starzec, K., Akesson, U., Lindqvist, J.E., Schouenberg, B., 2006. Microscopic and macroscopic characterization of the porosity of marble as a function of temperature and impregnation. *Constr. Build. Mater.* 20, 939–947. <http://dx.doi.org/10.1016/j.conbuildmat.2005.06.016>.
- Manwart, C., Aaltosalmi, U., Koponen, A., Hilfer, R., Timonen, J., 2002. Lattice-Boltzmann and finite-difference simulations for the permeability for three-dimensional porous media. *Phys. Rev. E* 66, 016702. <http://dx.doi.org/10.1103/PhysRevE.66.016702>.
- Marcelino, V., Cnudde, V., Vansteelandt, S., Carò, F., 2007. An evaluation of 2D-image analysis techniques for measuring soil microporosity. *Eur. J. Soil Sci.* 58, 133–140. <http://dx.doi.org/10.1111/j.1365-2389.2006.00819.x>.
- Margolis, S., Rex, R.W., 1971. Endolithic algae and micrite envelope formation in Bahamian ooids as revealed by scanning electron microscopy. *Geol. Soc. Am. Bull.* 82, 843–852. [http://dx.doi.org/10.1130/0016-7606\(1971\)82<843:EAO>2.0.CO;2](http://dx.doi.org/10.1130/0016-7606(1971)82<843:EAO>2.0.CO;2).
- Marszałek, M., Alexandrowicz, Z., Rzepa, G., 2014. Composition of weathering crusts on sandstones from natural outcrops and architectonic elements in an urban

- environment. *Environ. Sci. Pollut. Res. Int.* <http://dx.doi.org/10.1007/s11356-014-3312-y>.
- Mason, G., Morrow, N.R., 1991. Capillary behavior of a perfectly wetting liquid in irregular triangular tubes. *J. Colloid Interface Sci.* 141, 262–274. [http://dx.doi.org/10.1016/0021-9777\(91\)90321-X](http://dx.doi.org/10.1016/0021-9777(91)90321-X).
- Matějíček, J., Kolman, B., Dubský, J., Neufuss, K., Hopkins, N., Zwick, J., 2006. Alternative methods for determination of composition and porosity in abradable materials. *Miner. Charact.* 57, 17–29. <http://dx.doi.org/10.1016/j.matchar.2005.12.004>.
- Mavris, C., Götz, J., Plötz, M., Egli, M., 2012. Weathering and mineralogical evolution in a high Alpine soil chronosequence: a combined approach using SEM-EDX, cathodoluminescence and Nomarski DIC microscopy. *Sediment. Geol.* 280, 108–118. <http://dx.doi.org/10.1016/j.sedgeo.2012.04.008>.
- McClure, J.E., Prins, J.F., Miller, C.T., 2014. A novel heterogeneous algorithm to simulate multiphase flow in porous media on multicore CPU-GPU systems. *Comput. Phys. Commun.* 185, 1865–1874. <http://dx.doi.org/10.1016/j.cpc.2014.03.012>.
- Meakin, P., Tartakovsky, A.M., 2009. Modeling and simulation of pore-scale multiphase fluid flow and reactive transport in fractured and porous media. *Rev. Geophys.* <http://dx.doi.org/10.1029/2008RG000263>.
- Mehmani, Y., Balhoff, M.T., 2015. Mesoscale and hybrid models of fluid flow and solute transport. *Rev. Mineral. Geochem.* 80, 433–459. <http://dx.doi.org/10.2138/rmg.2015.80.13>.
- Mehmani, A., Prodanović, M., 2014. The effect of microporosity on transport properties in porous media. *Adv. Water Resour.* 63, 104–119. <http://dx.doi.org/10.1016/j.advwatres.2013.10.009>.
- Mendrik, A., Vonken, E.-J., Witkamp, T., Prokop, M., van Ginneken, B., Viergever, M., 2015. Using the Fourth Dimension to Distinguish Between Structures for Anisotropic Diffusion Filtering in 4D CT Perfusion Scans, Spatio-temporal Image Analysis for Longitudinal and Time-Series Image Data. Springer International Publishing, Boston, MA, USA <http://dx.doi.org/10.1007/978-3-319-14905-9>.
- Menke, H., Bijeljic, B., Andrew, M.G., Blunt, M.J., 2014. Dynamic pore-scale imaging of reactive transport in heterogeneous carbonates at reservoir conditions. *Energy Procedia* 63, 5503–5511. <http://dx.doi.org/10.1016/j.egypro.2014.11.583>.
- Menk, H.P., Bijeljic, B., Andrew, M.G., Blunt, M.J., 2015. Dynamic three-dimensional pore-scale imaging of reaction in a carbonate at reservoir conditions. *Environ. Sci. Technol.* 49, 4407–4414. <http://dx.doi.org/10.1021/es505789f>.
- Meyer, M.C., Austin, P., Tropper, P., 2013. Quantitative evaluation of mineral grains using automated SEM-EDS analysis and its application potential in optically stimulated luminescence dating. *Radiat. Meas.* 58, 1–11. <http://dx.doi.org/10.1016/j.radmeas.2013.07.004>.
- Möbus, G., Inkson, B.J., 2007. Nanoscale tomography in materials science. *Mater. Today* 10, 18–25. [http://dx.doi.org/10.1016/S1369-7021\(07\)70304-8](http://dx.doi.org/10.1016/S1369-7021(07)70304-8).
- Moctezuma, A., Békri, S., Larache, C., Vizika, O., 2003. A dual network model for relative permeability of bimodal rocks application in a vuggy carbonate. *Int. Symp. Soc. Core Analysts, Society of Core Analysts*.
- Mohnke, O., Stiebler, M., Klitzsch, N., 2014. Joint numerical microscale simulations of multiphase flow and NMR relaxation behavior in porous media using lattice Boltzmann methods. *Water Resour. Res.* 50, 7378–7393. <http://dx.doi.org/10.1002/2013WR014684>.
- Molins, S., Trebotich, D., Yang, L., Ajo-Franklin, J.B., Ligocki, T.J., Shen, C., Steefel, C.I., 2014. Pore-scale controls on calcite dissolution rates from flow-through laboratory and numerical experiments. *Environ. Sci. Technol.* 48, 7453–7460. <http://dx.doi.org/10.1021/es5013438>.
- Morrow, N.R., 1975. The effects of surface roughness on contact: angle with special reference to petroleum recovery. *J. Can. Pet. Technol.* 14, 42–53. <http://dx.doi.org/10.2118/75-04-04>.
- Mostaghimi, P., Bijeljic, B., Blunt, M., 2012. Simulation of flow and dispersion on pore-space images. *SPE J.* 17, 1131–1141. <http://dx.doi.org/10.2118/135261-PA>.
- Mostaghimi, P., Blunt, M.J., Bijeljic, B., 2013. Computations of absolute permeability on micro-CT images. *Math. Geosci.* 45, 103–125. <http://dx.doi.org/10.1007/s11004-012-9431-4>.
- Muljadi, B.P., Blunt, M.J., Raeini, A.Q., Bijeljic, B., 2015. The impact of porous media heterogeneity on non-Darcy flow behaviour from pore-scale simulation. *Adv. Water Resour.* <http://dx.doi.org/10.1016/j.advwatres.2015.05.019>.
- Munch, B., Gasser, P., Holzer, L., Flatt, R., 2006. FIB-nanotomography of particulate systems—part II: particle recognition and effect of boundary truncation. *J. Am. Ceram. Soc.* 89, 2586–2595. <http://dx.doi.org/10.1111/j.1551-2916.2006.01121.x>.
- Myers, G.R., Kingston, A.M., Varslot, T.K., Turner, M.L., Sheppard, A.P., 2011a. Dynamic tomography with a priori information. *Appl. Opt.* 50, 3685–3690. <http://dx.doi.org/10.1364/AO.50.003685>.
- Myers, G.R., Kingston, A.M., Varslot, T.K., Turner, M.L., Sheppard, A.P., 2011b. Dynamic X-ray micro-tomography for real time imaging of drainage and imbibition processes at the pore scale. *Int. Symp. Soc. Core Analysts, Society of Core Analysts*.
- Myers, G.R., Geleta, M., Kingston, A.M., Recur, B., Sheppard, A.P., 2014. In: Stock, S.R. (Ed.), Improving dynamic tomography, through maximum a posteriori estimation, p. 921211 <http://dx.doi.org/10.1111/12.2061604>.
- Nejad Ebrahimi, A., Jamshidi, S., Iglaue, S., Boozarjomehry, R.B., 2013. Genetic algorithm-based pore network extraction from micro-computed tomography images. *Chem. Eng. Sci.* 92, 157–166. <http://dx.doi.org/10.1016/j.ces.2013.01.045>.
- Neville, A., 2003. How closely can we determine the water-cement ratio of hardened concrete? *Mater. Struct.* 36, 311–318.
- Ngom, N.F., Garnier, P., Monga, O., Peth, S., 2011. Extraction of three-dimensional soil pore space from microtomography images using a geometrical approach. *Geoderma* 163, 127–134. <http://dx.doi.org/10.1016/j.geoderma.2011.04.013>.
- Nguyen, V.H., Sheppard, A.P., Knackstedt, M.A., Val Pinczewski, W., 2006. The effect of displacement rate on imbibition relative permeability and residual saturation. *J. Pet. Sci. Eng.* 52, 54–70. <http://dx.doi.org/10.1016/j.petrol.2006.03.020>.
- Nishiyama, T., Kusuda, H., 1994. Identification of pore spaces and microcracks using fluorescent resins. *Int. J. Rock Mech. Min. Sci. Geomech. Abstr.* 31, 369–375. [http://dx.doi.org/10.1016/0148-9062\(94\)90904-0](http://dx.doi.org/10.1016/0148-9062(94)90904-0).
- Noiriel, C., 2015. Resolving time-dependent evolution of pore-scale structure, permeability and reactivity using X-ray microtomography. *Rev. Mineral. Geochem.* 80, 247–285. <http://dx.doi.org/10.2138/rmg.2015.80.08>.
- Nugent, K.A., 2010. Coherent methods in the X-ray sciences. *Adv. Phys.* 59, 1–99. <http://dx.doi.org/10.1080/00018730903270926>.
- Ochi, J., Vernoux, J.-F., 1999. A two-dimensional network model to simulate permeability decrease under hydrodynamic effect of particle release and capture. *Transp. Porous Media* 37, 303–325. <http://dx.doi.org/10.1023/A:1006690700000>.
- Ören, P.-E., Bakke, S., 2002. Process based reconstruction of sandstones and prediction of transport properties. *Transp. Porous Media* 46, 311–343. <http://dx.doi.org/10.1023/A:1015031122338>.
- Ören, P.-E., Bakke, S., Arntzen, O.J., 1998. Extending predictive capabilities to network models. *SPE J.* 3, 324–336. <http://dx.doi.org/10.2118/52052-PA>.
- Otsu, N., 1979. A threshold selection method from gray-level histograms. *IEEE Trans. Syst. Man Cybern.* 9, 62–66. <http://dx.doi.org/10.1109/TSMC.1979.4310076>.
- Ott, H., Andrew, M., Snippe, J., Blunt, M.J., 2014. Micro-scale solute transport and precipitation in complex rock during drying. *Geophys. Res. Lett.* <http://dx.doi.org/10.1002/2014GL062266> (n/a-n/a).
- Övaysi, S., Piri, M., 2011. Pore-scale modeling of dispersion in disordered porous media. *J. Contam. Hydrol.* 124, 68–81. <http://dx.doi.org/10.1016/j.jconhyd.2011.02.004>.
- Övaysi, S., Wheeler, M.F., Balhoff, M., 2014. Quantifying the representative size in porous media. *Transp. Porous Media* 104, 349–362. <http://dx.doi.org/10.1007/s11242-014-0338-z>.
- Pak, T., Butler, I.B., Geiger, S., van Dijke, M.I.J., Sorbie, K.S., 2015. Droplet fragmentation: 3D imaging of a previously unidentified pore-scale process during multiphase flow in porous media. *Proc. Natl. Acad. Sci.* 201420202. <http://dx.doi.org/10.1073/pnas.1420202112>.
- Pan, W., Tartakovsky, A.M., 2013. Dissipative particle dynamics model for colloid transport in porous media. *Adv. Water Resour.* 58, 41–48. <http://dx.doi.org/10.1016/j.advwatres.2013.04.004>.
- Pan, C., Hilpert, M., Miller, C.T., 2004. Lattice-Boltzmann simulation of two-phase flow in porous media. *Water Resour. Res.* 40. <http://dx.doi.org/10.1029/2003WR002120> (n/a-n/a).
- Panahi, H., Meakin, P., Renard, F., Kobchenko, M., Scheibert, J., Mazzini, A., Jamtveit, B., Malthe-Sørensen, A., Dysthe, D.K., 2013. A 4D synchrotron X-ray tomography study of the formation of hydrocarbon-migration pathways in heated organic-rich shale. *SPE J.* 18, 366–377. <http://dx.doi.org/10.2118/162939-PA>.
- Parmigiani, A., Huber, C., Bachmann, O., Chopard, B., 2011. Pore-scale mass and reactant transport in multiphase porous media flows. *J. Fluid Mech.* 686, 40–76. <http://dx.doi.org/10.1017/jfm.2011.268>.
- Patel, R.A., Perko, J., Jacques, D., De Schutter, G., Van Breugel, K., Ye, G., 2014a. A versatile pore-scale multicomponent reactive transport approach based on lattice Boltzmann method: application to portlandite dissolution. *Phys. Chem. Earth Parts A/B/C* 70–71, 127–137. <http://dx.doi.org/10.1016/j.pce.2014.03.001>.
- Patel, R.A., Perko, J., Jacques, D., De Schutter, G., Ye, G., van Breugel, K., 2014b. Application of a pore-scale reactive transport model to study the influence of pore network characteristics on calcium leaching in cementitious systems. CONMOD. RILEM Publications, Beijing, China.
- Patzek, T.W., 2001. Verification of a complete pore network simulator of drainage and imbibition. *SPE J.* 6, 144–156. <http://dx.doi.org/10.2118/71310-PA>.
- Patzek, T.W., Silin, D.B., 2001. Shape factor and hydraulic conductance in noncircular capillaries. *J. Colloid Interface Sci.* 236, 295–304. <http://dx.doi.org/10.1006/jcis.2000.7413>.
- Peng, S., Marone, F., Dultz, S., 2014. Resolution effect in X-ray microcomputed tomography imaging and small pore's contribution to permeability for Berea sandstone. *J. Hydrol.* 510, 403–411. <http://dx.doi.org/10.1016/j.jhydrol.2013.12.028>.
- Pereira Nunes, J.P., Bijeljic, B., Blunt, M.J., 2015. Time-of-flight distributions and breakthrough curves in heterogeneous porous media using a pore-scale streamline tracing algorithm. *Transp. Porous Media* 109, 317–336. <http://dx.doi.org/10.1007/s11242-015-0520-y>.
- Peters, C.A., 2009. Accessibilities of reactive minerals in consolidated sedimentary rock: An imaging study of three sandstones. *Chem. Geol.* 265, 198–208. <http://dx.doi.org/10.1016/j.chemgeo.2008.11.014>.
- Peth, S., Nelelsen, J., Fischer, G., Horn, R., 2010. Non-invasive 3D analysis of local soil deformation under mechanical and hydraulic stresses by mu CT and digital image correlation. *Soil Tillage Res.* 111, 3–18. <http://dx.doi.org/10.1016/j.sti.2010.02.007>.
- Piller, M., Casagrande, D., Schena, G., Santini, M., 2014. Pore-scale simulation of laminar flow through porous media. *J. Phys. Conf. Ser.* 501, 012010. <http://dx.doi.org/10.1088/1742-6596/501/1/012010>.
- Piri, M., Blunt, M., 2005. Three-dimensional mixed-wet random pore-scale network modeling of two- and three-phase flow in porous media. II. Results. *Phys. Rev. E* 71, 026302. <http://dx.doi.org/10.1103/PhysRevE.71.026302>.
- Pistone, M., Arzilli, F., Dobson, K.J., Cordonnier, B., Reusser, E., Ulmer, P., Marone, F., Whittington, A.G., Mancini, L., Fife, J.L., Blundy, J.D., 2015. Gas-driven filter pressing in magmas: insights into in-situ melt segregation from crystal mushes. *Geology* 43, G36766.1. <http://dx.doi.org/10.1130/G36766.1>.
- Plougonven, E., Bernard, D., 2011. Optimal removal of topological artefacts in microtomographic images of porous materials. *Adv. Water Resour.* 34, 731–736. <http://dx.doi.org/10.1016/j.advwatres.2011.03.004>.
- Popov, P., Efendiev, Y., Qin, G., 2009. Multiscale modeling and simulations of flows in naturally fractured karst reservoirs. *Commun. Comput. Phys.* 6, 162–184. <http://dx.doi.org/10.4208/cicp.2009.v6.p162>.

- Porter, M.L., Schaap, M.G., Wildenschild, D., 2009. Lattice-Boltzmann simulations of the capillary pressure–saturation–interfacial area relationship for porous media. *Adv. Water Resour.* 32, 1632–1640. <http://dx.doi.org/10.1016/j.advwatres.2009.08.009>.
- Poulakacos, I.D., Partl, M.N., 2010. Investigation of porous asphalt microstructure using optical and electron microscopy. *J. Microsc.* 240, 145–154. <http://dx.doi.org/10.1111/j.1365-2818.2010.03388.x>.
- Pradel, A., Langer, M., Maisey, J.G., Geffard-Kuriyama, D., Cloetens, P., Janvier, P., Tafforeau, P., 2009. Skull and brain of a 300-million-year-old chimaeroid fish revealed by synchrotron holotomography. *Proc. Natl. Acad. Sci. U. S. A.* 106, 5224–5228. <http://dx.doi.org/10.1073/pnas.0807047106>.
- Prakongkep, N., Sudhiprakarn, A., Kheoruenromne, I., Gilkes, R.J., 2010. SEM image analysis for characterization of sand grains in Thai paddy soils. *Geoderma* 156, 20–31. <http://dx.doi.org/10.1016/j.geoderma.2010.01.003>.
- Prodanović, M., 2008. A level set method for fluid displacement in realistic porous media [WWW Document]. URL http://users.ices.utexas.edu/~masha/presentations/ImperialCollegeTalk_2008.pdf (accessed 11.1.15).
- Prodanović, M., Bryant, S.L., 2006. A level set method for determining critical curvatures for drainage and imbibition. *J. Colloid Interface Sci.* 304, 442–458. <http://dx.doi.org/10.1016/j.jcis.2006.08.048>.
- Prodanović, M., Mehmani, A., Sheppard, A.P., 2014. Imaged-based multiscale network modelling of microporosity in carbonates. *Geol. Soc. Lond., Spec. Publ.* 406, SP406–SP409. <http://dx.doi.org/10.1144/SP406.9>.
- Prodanović, M., Esteve, M., Hanlon, M., Nanda, G., Agarwal, P., 2015. Digital Rocks Portal: A Repository for Porous Media Images [WWW Document]. <http://dx.doi.org/10.17612/P7CC7K>.
- Pudney, C., 1998. Distance-ordered homotopic thinning: a skeletonization algorithm for 3D digital images. *Comput. Vis. Image Underst.* 72, 404–413. <http://dx.doi.org/10.1006/cviu.1998.0680>.
- Rabbani, A., Jamshidi, S., Salehi, S., 2014. An automated simple algorithm for realistic pore network extraction from micro-tomography images. *J. Pet. Sci. Eng.* 123, 164–171. <http://dx.doi.org/10.1016/j.petrol.2014.08.020>.
- Rad, M.N., Shokri, N., Keshmiri, A., Withers, P.J., 2015. Effects of grain and pore size on salt precipitation during evaporation from porous media. *Transp. Porous Media* 110, 281–294. <http://dx.doi.org/10.1007/s11242-015-0515-8>.
- Raeini, A.Q., 2013. Modelling Multiphase Flow through Micro-CT Images of the Pore Space. Imperial College.
- Raeini, A.Q., Bijeljic, B., Blunt, M.J., 2013. Numerical modelling of sub-pore scale events in two-phase flow through porous media. *Transp. Porous Media* 101, 191–213. <http://dx.doi.org/10.1007/s11242-013-0239-6>.
- Raeini, A.Q., Blunt, M.J., Bijeljic, B., 2014. Direct simulations of two-phase flow on micro-CT images of porous media and upscaling of pore-scale forces. *Adv. Water Resour.* 74, 116–126. <http://dx.doi.org/10.1016/j.advwatres.2014.08.012>.
- Raeini, A.Q., Bijeljic, B., Blunt, M.J., 2015. Modelling capillary trapping using finite-volume simulation of two-phase flow directly on micro-CT images. *Adv. Water Resour.* 83, 102–110. <http://dx.doi.org/10.1016/j.advwatres.2015.05.008>.
- Ramandi, H.L., Mostaghimi, P., Armstrong, R.T., Saadatfar, M., Val Pinczewski, W., 2015. Porosity and permeability characterization of coal – a micro-computed tomography study. *Int. J. Coal Geol.* <http://dx.doi.org/10.1016/j.coal.2015.10.001>.
- Ramstad, T., Øren, P.-E., Bakke, S., 2010. Simulation of two-phase flow in reservoir rocks using a lattice Boltzmann method. *SPE J.* 15, 917–927. <http://dx.doi.org/10.2118/124617-PA>.
- Ramstad, T., Idowu, N., Nardi, C., Øren, P.E., 2012. Relative permeability calculations from two-phase flow simulations directly on digital images of porous rocks. *Transp. Porous Media* 94, 487–504. <http://dx.doi.org/10.1007/s11242-011-9877-8>.
- Raoof, A., Hassanzadeh, S.M., 2010. A new method for generating pore-network models of porous media. *Transp. Porous Media* 81, 391–407. <http://dx.doi.org/10.1007/s11242-009-9412-3>.
- Raoof, A., Hassanzadeh, S.M., Leijnse, A., 2010. Upscaling transport of adsorbing solutes in porous media: pore-network modeling. *Vadose Zone J.* 9, 624. <http://dx.doi.org/10.1111/j.1536-vzj2010.00026>.
- Raoof, A., Nick, H.M., Wolterbeek, T.K.T., Spiers, C.J., 2012. Pore-scale modeling of reactive transport in wellbore cement under CO₂ storage conditions. *Int. J. Greenhouse Gas Control* 11, S67–S77. <http://dx.doi.org/10.1016/j.ijggc.2012.09.012>.
- Raoof, A., Nick, H.M., Hassanzadeh, S.M., Spiers, C.J., 2013. PoreFlow: a complex pore-network model for simulation of reactive transport in variably saturated porous media. *Comput. Geosci.* 61, 160–174. <http://dx.doi.org/10.1016/j.cageo.2013.08.005>.
- Ravlo, V., Arland, K.S., 2014. Calibration of digital pore scale models. *Int. Symp. Soc. Core Analysts. Society of Core Analysts, Avignon, France*.
- Reed, S.J.B., 2005. Electron Microprobe Analysis and Scanning Electron Microscopy in Geology. Cambridge University Press, Cambridge <http://dx.doi.org/10.1017/CBO9780511610561>.
- Rego, E.H., Shao, L., Macklin, J.J., Winoto, L., Johansson, G. a., Kamps-Hughes, N., Davidson, M.W., Gustafsson, M.G.L., 2012. Nonlinear structured-illumination microscopy with a photoswitchable protein reveals cellular structures at 50-nm resolution. *Proc. Natl. Acad. Sci. U. S. A.* 109, E135–E143. <http://dx.doi.org/10.1073/pnas.1107547108>.
- Renardy, Y., Renardy, M., 2002. PROST: a parabolic reconstruction of surface tension for the volume-of-fluid method. *J. Comput. Phys.* 183, 400–421. <http://dx.doi.org/10.1006/jcph.2002.7190>.
- Ridder, T.W., Calvard, S., 1978. Picture thresholding using an iterative selection method. *IEEE Trans. Syst. Man Cybern.* 8, 630–632. <http://dx.doi.org/10.1109/TSMC.1978.4310039>.
- Rivas, T., Prieto, B., Silva, B., Virginie, J.M., 2003. Weathering of granitic rocks by chlorides: effect of the nature of the solution on weathering morphology. *Earth Surf. Process. Landf.* 28, 425–436. <http://dx.doi.org/10.1002/esp.492>.
- Robinson, B.W., Nickel, E.H., 1979. A useful new technique for mineralogy: the backscattered-electron/low vacuum mode of SEM operation. *Am. Mineral.* 64, 1322–1328.
- Rosenzweig, R., Furman, A., Shavit, U., 2013. A channel network model as a framework for characterizing variably saturated flow in biofilm-affected soils. *Vadose Zone J.* 12 <http://dx.doi.org/10.2136/vzj2012.0079>.
- Rothman, D.H., Zaleski, S., 1994. Lattice-gas models of phase separation: interfaces, phase transitions, and multiphase flow. *Rev. Mod. Phys.* 66, 1417–1479. <http://dx.doi.org/10.1103/RevModPhys.66.1417>.
- Rücker, M., Berg, S., Armstrong, R.T., Georgiadis, A., Ott, H., Schwing, A., Neiteler, R., Brussee, N., Makurat, A., Leu, L., Wolf, M., Khan, F., Enzmann, F., Kersten, M., 2015. From connected pathway flow to ganglion dynamics. *Geophys. Res. Lett.* 42, 3888–3894. <http://dx.doi.org/10.1002/2015GL064007>.
- Russ, J.C., 1999. *The Image Processing Handbook*. fourth ed. CRC Press, Boca Raton, FL.
- Ryazanov, A.V., van Dijke, M.I.J., Sorbie, K.S., 2009. Two-phase pore-network modelling: existence of oil layers during water invasion. *Transp. Porous Media* 80, 79–99. <http://dx.doi.org/10.1007/s11242-009-9345-x>.
- Sahimi, M., 2011. *Flow and Transport in Porous Media and Fractured Rock*. Wiley-VCH.
- Sahimi, M., Mehrabi, A.R., Mirzaei, N., Rassamdana, H., 2000. The effect of asphalt precipitation on flow behavior and production of a fractured carbonate oil reservoir during gas injection. *Transp. Porous Media* 41, 325–347. <http://dx.doi.org/10.1023/A:1006759524127>.
- Schaap, M.G., Porter, M.L., Christensen, B.S.B., Wildenschild, D., 2007. Comparison of pressure-saturation characteristics derived from computed tomography and lattice Boltzmann simulations. *Water Resour. Res.* 43, <http://dx.doi.org/10.1029/2006WR005730> (n/a–n/a).
- Scheibe, T.D., Perkins, W.A., Richmond, M.C., McKinley, M.I., Romero-Gomez, P.D.J., Oostrom, M., Wietsma, T.W., Serkowski, J. a., Zachara, J.M., 2015. Pore-scale and multiscale numerical simulation of flow and transport in a laboratory-scale column. *Water Resour. Res.* 51, 1023–1035. <http://dx.doi.org/10.1002/2014WR015959>.
- Schindelin, J., Arganda-Carreras, I., Frise, E., Kaynig, V., Longair, M., Pietzsch, T., Preibisch, S., Rueden, C., Saalfeld, S., Schmid, B., Tinevez, J.-Y., White, D.J., Hartenstein, V., Elceirí, K., Tomancák, P., Cardona, A., 2012. Fiji: an open-source platform for biological-image analysis. *Nat. Methods* 9, 676–682. <http://dx.doi.org/10.1038/nmeth.2019>.
- Schladitz, K., 2011. Quantitative micro-CT. *J. Microsc.* 243, 111–117. <http://dx.doi.org/10.1111/j.1365-2818.2011.03513.x>.
- Schmatz, J., Urail, J.L., Berg, S., Ott, H., 2015. Nano-scale imaging of pore-scale fluid–fluid–solid contacts in sandstone. *Geophys. Res. Lett.* <http://dx.doi.org/10.1002/2015GL063354> (n/a–n/a).
- Schropp, A., Hoppe, R., Patommel, J., Samberg, D., Seibold, F., Stephan, S., Wellenreuther, G., Falkenberg, G., Schroer, C.G., 2012. Hard X-ray scanning microscopy with coherent radiation: beyond the resolution of conventional X-ray microscopes. *Appl. Phys. Lett.* 100, 10–13. <http://dx.doi.org/10.1063/1.4729942>.
- Sezgin, M., Sankur, B., 2004. Survey over image thresholding techniques and quantitative performance evaluation. *J. Electron. Imaging* 13, 146. <http://dx.doi.org/10.1117/1.1631315>.
- Shah, S.M., Gray, F., Crawshaw, J.P., Boek, E.S., 2015. Micro-computed tomography pore-scale study of flow in porous media: effect of voxel resolution. *Adv. Water Resour.* 80, 1–12. <http://dx.doi.org/10.1016/j.advwatres.2015.07.012>.
- Shan, X., Chen, H., 1993. Lattice Boltzmann model for simulating flows with multiple phases and components. *Phys. Rev. E* 47, 1815–1819. <http://dx.doi.org/10.1103/PhysRevE.47.1815>.
- Sharkey Jr., A.G., McCartney, J.T., 1981. Physical properties of coal and its products. In: Elliot, M.A. (Ed.) *Chemistry of Coal Utilization Vol.II Supplementary*. Wiley Interscience, New York, N.Y., pp. 159–284.
- Sheppard, A.P., Sok, R.M., Averdunk, H., 2005. Improved pore network extraction methods. *Int. Symp. Soc. Core Analysts. Society of Core Analysts*.
- Sheppard, A.P., Sok, R.M., Averdunk, H., Robins, V.B., Ghous, A., 2006. Analysis of rock microstructure using high-resolution X-ray tomography. *Int. Symp. Soc. Core Analysts. Society of Core Analysts*, pp. 1–12.
- Sheppard, A., Latham, S., Middleton, J., Kingston, A., Myers, G., Varslot, T., Fogden, A., Sawkins, T., Cruikshank, R., Saadatfar, M., Francois, N., Arns, C., Senden, T., 2014. Techniques in helical scanning, dynamic imaging and image segmentation for improved quantitative analysis with X-ray micro-CT. *Nucl. Instrum. Methods Phys. Res., Sect. B* 324, 49–56. <http://dx.doi.org/10.1016/j.nimb.2013.08.072>.
- Sholokhova, Y., Kim, D., Brent Lindquist, W., 2009. Network flow modeling via lattice-Boltzmann based channel conductance. *Adv. Water Resour.* 32, 205–212. <http://dx.doi.org/10.1016/j.advwatres.2008.10.016>.
- Siena, M., Riva, M., Hyman, J.D., Winter, C.L., Guadagnini, A., 2014. Relationship between pore size and velocity probability distributions in stochastically generated porous media. *Phys. Rev. E* 89, 013018. <http://dx.doi.org/10.1103/PhysRevE.89.013018>.
- Siena, M., Hyman, J.D., Riva, M., Guadagnini, A., Winter, C.L., Smolarkiewicz, P.K., Gouze, P., Sadhukhan, S., Inzoli, F., Guédon, G., Colombo, E., 2015. Direct numerical simulation of fully saturated flow in natural porous media at the pore scale: a comparison of three computational systems. *Comput. Geosci.* 19, 423–437. <http://dx.doi.org/10.1007/s10596-015-9486-7>.
- Silin, D., Patzek, T., 2006. Pore space morphology analysis using maximal inscribed spheres. *Phys. A Stat. Mech. Appl.* 371, 336–360. <http://dx.doi.org/10.1016/j.physa.2006.04.048>.
- Sivanesapillai, R., Falkner, N., Hartmaier, A., Steeb, H., 2015. A CSF-SPH method for simulating drainage and imbibition at pore-scale resolution while tracking interfacial areas. *Adv. Water Resour.* <http://dx.doi.org/10.1016/j.advwatres.2015.08.012>.
- Smith, T.M., Tafforeau, P., Reid, D.J., Pouech, J., Lazzari, V., Zermeno, J.P., Guatelli-Steinberg, D., Olejniczak, A.J., Hoffman, A., Radovic, J., Makarem, M., Toussaint, M., Stringer, C., Hublin, J.-J., 2010. Dental evidence for ontogenetic differences between modern

- humans and Neanderthals. Proc. Natl. Acad. Sci. U. S. A. 107, 20923–20928. <http://dx.doi.org/10.1073/pnas.1010906107>.
- Soille, P., 1999. *Morphological Image Analysis*. Springer-Verlag, Berlin.
- Sok, R.M., Knackstedt, M.A., Sheppard, A.P., Pinczewski, W.V., Lindquist, W.B., Venkatarangan, A., Paterson, L., 2002. Direct and stochastic generation of network models from tomographic images; effect of topology on residual saturations. *Transp. Porous Media* 46, 345–371. <http://dx.doi.org/10.1023/A:1015034924371>.
- Sok, R.M., Varslot, T., Ghosh, A., Latham, S., Sheppard, A.P., Knackstedt, M.A., 2010. *Pore scale characterization of carbonates at multiple Scales: integration of micro-CT, BSEM, and FIBSEM*. *Petrophysics* 51, 379–387.
- Sorbie, K.S., Skauge, A., 2011. Can network modelling predict two-phase flow functions?, *Int. Symp. Soc. Core Analysts. Society of Core Analysts, Austin, USA*.
- Soroushian, P., Elzafraney, M., Nossoni, A., 2003. Specimen preparation and image processing and analysis techniques for automated quantification of concrete microcracks and voids. *Cem. Concr. Res.* 33, 1949–1962. [http://dx.doi.org/10.1016/S0008-8846\(03\)00219-9](http://dx.doi.org/10.1016/S0008-8846(03)00219-9).
- Sousa, L.M.O., Suárez del Río, L.M., Calleja, L., Ruiz de Argandoña, V.G., Rey, A.R., 2005. Influence of microfractures and porosity on the physico-mechanical properties and weathering of ornamental granites. *Eng. Geol.* 77, 153–168. <http://dx.doi.org/10.1016/j.jenggeo.2004.10.001>.
- Stockman, H.W., 2006. Lattice Boltzmann method for calculating fluid flow and dispersion in porous and fractured media. *Gas Transport in Porous Media*. Springer, Netherlands, pp. 221–242. http://dx.doi.org/10.1007/1-4020-3962-X_13.
- Suchomel, B.J., Chen, B.M., Allen III, M.B., 1998. Network model of flow, transport and biofilm effects in porous media. *Transp. Porous Media* 30, 1–23. <http://dx.doi.org/10.1023/A:1006560705680>.
- Sukop, M.C., Thorne, D.T., 2006. *Lattice Boltzmann Modeling: An Introduction for Geoscientists and Engineers*. Springer Berlin Heidelberg, Berlin, Heidelberg. <http://dx.doi.org/10.1007/978-3-540-27982-2>.
- Sukop, M.C., Huang, H., Lin, C.L., Deo, M.D., Oh, K., Miller, J.D., 2008. Distribution of multi-phase fluids in porous media: comparison between lattice Boltzmann modeling and micro-X-ray tomography. *Phys. Rev. E* 77, 026710. <http://dx.doi.org/10.1103/PhysRevE.77.026710>.
- Sullivan, S.P., Sani, F.M., Johns, M.L., Gladden, L.F., 2005. Simulation of packed bed reactors using lattice Boltzmann methods. *Chem. Eng. Sci.* 60, 3405–3418. <http://dx.doi.org/10.1016/j.ces.2005.01.038>.
- Sutherland, D., 2007. Estimation of mineral grain size using automated mineralogy. *Miner. Eng.* 20, 452–460. <http://dx.doi.org/10.1016/j.mineeng.2006.12.011>.
- Swift, M.R., Orlandini, E., Osborn, W.R., Yeomans, J.M., 1996. Lattice Boltzmann simulations of liquid–gas and binary fluid systems. *Phys. Rev. E* 54, 5041–5052. <http://dx.doi.org/10.1103/PhysRevE.54.5041>.
- Tafforeau, P., Boistel, R., Boller, E., Bravin, a., Brunet, M., Chaimanee, Y., Cloetens, P., Feist, M., Hoszowska, J., Jaeger, J.-J., Kay, R.F., Lazzari, V., Marivaux, L., Nel, a., Nemoz, C., Thibault, X., Vignaud, P., Zabler, S., 2006. Applications of X-ray synchrotron micromotography for non-destructive 3D studies of paleontological specimens. *Appl. Phys. A Mater. Sci. Process.* 83, 195–202. <http://dx.doi.org/10.1007/s00339-006-3507-2>.
- Takeda, T., Momose, A., Itai, Y., Jin, W., Hirano, K., 1995. Phase-contrast imaging with synchrotron X-rays for detecting cancer lesions. *Acad. Radiol.* 2, 799–803. [http://dx.doi.org/10.1016/S1076-6332\(05\)80490-8](http://dx.doi.org/10.1016/S1076-6332(05)80490-8).
- Takeda, T., Momose, a., Hirano, K., Haraoka, S., Watanabe, T., Itai, Y., 2000. Human carcinoma: early experience with phase-contrast X-ray CT with synchrotron radiation—comparative specimen study with optical microscopy. *Radiology* 214, 298–301. <http://dx.doi.org/10.1148/radiology.214.1.r00ja08298>.
- Talon, L., Bauer, D., Gland, N., Youssef, S., Auradou, H., Ginzburg, I., 2012. Assessment of the two relaxation time lattice-Boltzmann scheme to simulate Stokes flow in porous media. *Water Resour. Res.* 48. <http://dx.doi.org/10.1029/2011WR011385> (n/a-n/a).
- Tanino, Y., Blunt, M.J., 2012. Capillary trapping in sandstones and carbonates: dependence on pore structure. *Water Resour. Res.* 48. <http://dx.doi.org/10.1029/2011WR011712> (n/a-n/a).
- Tartakovsky, A.M., Meakin, P., 2006. Pore scale modeling of immiscible and miscible fluid flows using smoothed particle hydrodynamics. *Adv. Water Resour.* 29, 1464–1478. <http://dx.doi.org/10.1016/j.advwatres.2005.11.014>.
- Tartakovsky, A.M., Panchenko, A., 2015. Pairwise force smoothed particle hydrodynamics model for multiphase flow: surface tension and contact line dynamics. *J. Comput. Phys.* <http://dx.doi.org/10.1016/j.jcp.2015.08.037>.
- Tartakovsky, A.M., Ferris, K.F., Meakin, P., 2009. Lagrangian particle model for multiphase flows. *Comput. Phys. Commun.* 180, 1874–1881. <http://dx.doi.org/10.1016/j.cpc.2009.06.002>.
- Terzi, S., Salvo, L., Suéry, M., Limodin, N., Adrien, J., Maire, E., Pannier, Y., Bornert, M., Bernard, D., Felberbaum, M., 2009. In situ X-ray tomography observation of inhomogeneous deformation in semi-solid aluminium alloys. *Scr. Mater.* 61, 449–452. <http://dx.doi.org/10.1016/j.scriptamat.2009.04.041>.
- Thibault, P., Dierolf, M., Menzel, A., Bunk, O., David, C., Pfeiffer, F., 2008. High-resolution scanning X-ray diffraction microscopy. *Science* 321, 379–382. <http://dx.doi.org/10.1126/science.1158573>.
- Thijssen, J., 2007. *Computational Physics*. Cambridge University Press, Cambridge.
- Thompson, K.E., Willson, C.S., White, C.D., Nyman, S., Bhattacharya, J., Reed, A.H., 2005. Application of a new grain-based reconstruction algorithm to microtomography images for quantitative characterization and flow modeling. *SPE Annual Technical Conference and Exhibition. Society of Petroleum Engineers* <http://dx.doi.org/10.2118/95887-MS>.
- Timur, A., Hemphicks, W.B., Weinbrandt, R.M., 1971. Scanning electron microscope study of pore systems in rocks. *J. Geophys. Res.* 76, 4932–4984. <http://dx.doi.org/10.1029/JB071020p04932>.
- Torquato, S., 2002. Statistical description of microstructures. *Annu. Rev. Mater. Res.* 32, 77–111. <http://dx.doi.org/10.1146/annurev.matsci.32.110101.155324>.
- Trebichot, D., Adams, M.F., Molins, S., Steefel, C.I., Shen, C., 2014. High-resolution simulation of pore-scale reactive transport processes associated with carbon sequestration. *Comput. Sci. Eng.* 16, 22–31. <http://dx.doi.org/10.1109/MCSE.2014.77>.
- Trtik, P., Münch, B., Gasser, P., Leemann, a., Loser, R., Wepf, R., Lura, P., 2011. Focussed ion beam nanotomography reveals the 3D morphology of different solid phases in hardened cement pastes. *J. Microsc.* 241, 234–242. <http://dx.doi.org/10.1111/j.1365-2818.2010.03433.x>.
- Trtik, P., Diaz, A., Guizar-Sicairos, M., Menzel, A., Bunk, O., 2013. Density mapping of hardened cement paste using ptychographic X-ray computed tomography. *Cem. Concr. Compos.* 36, 71–77. <http://dx.doi.org/10.1016/j.cemconcomp.2012.06.001>.
- Valvatne, P.H., Blunt, M.J., 2004. Predictive pore-scale modeling of two-phase flow in mixed wet media. *Water Resour. Res.* 40. <http://dx.doi.org/10.1029/2003WR002627> (n/a-n/a).
- Varloteaux, C., Békri, S., Adler, P.M., 2013. Pore network modelling to determine the transport properties in presence of a reactive fluid: from pore to reservoir scale. *Adv. Water Resour.* 53, 87–100. <http://dx.doi.org/10.1016/j.advwatres.2012.10.004>.
- Vasilyev, L., Raoof, A., Nordbotten, J.M., 2012. Effect of mean network coordination number on dispersivity characteristics. *Transp. Porous Media* 95, 447–463. <http://dx.doi.org/10.1007/s11242-012-0054-5>.
- Vázquez, M.A., Galán, E., Ortiz, P., Ortiz, R., 2013. Digital image analysis and EDX SEM as combined techniques to evaluate salt damp on walls. *Constr. Build. Mater.* 45, 95–105. <http://dx.doi.org/10.1016/j.conbuildmat.2013.03.067>.
- Vazquez-Calvo, C., De Buergo, M.A., Fort, R., Varas, M.J., 2007. Characterization of patinas by means of microscopic techniques. *Mater. Charact.* 58, 1119–1132. <http://dx.doi.org/10.1016/j.matchar.2007.04.024>.
- Veselý, M., Bultreys, T., Peksa, M., Lang, J., Cnudde, V., Van Hoorebeke, L., Kočířík, M., Hejmánek, V., Šolcová, O., Soukup, K., Gerke, K., Stallmach, F., Čapek, P., 2015. Prediction and evaluation of time-dependent effective self-diffusivity of water and other effective transport properties associated with reconstructed porous solids. *Transp. Porous Media* <http://dx.doi.org/10.1007/s11242-015-0557-y>.
- Vincent, L., Soille, P., 1991. Watersheds in digital spaces: an efficient algorithm based on immersion simulations. *IEEE Trans. Pattern Anal. Mach. Intell.* 13, 583–598. <http://dx.doi.org/10.1109/34.87344>.
- Vlassenbroeck, J., Dierick, M., Masschaele, B., Cnudde, V., Hoorebeke, L., Jacobs, P., 2007. Software tools for quantification of X-ray microtomography. *Nucl. Instrum. Methods Phys. Res., Sect. A* 580, 442–445. <http://dx.doi.org/10.1016/j.nima.2007.05.073>.
- Vogel, H.-J., Roth, K., 2001. Quantitative morphology and network representation of soil pore structure. *Adv. Water Resour.* 24, 233–242. [http://dx.doi.org/10.1016/S0309-1708\(00\)00055-5](http://dx.doi.org/10.1016/S0309-1708(00)00055-5).
- Voide, R., Schneider, P., Stauber, M., Wyss, P., Stampanoni, M., Sennhauser, U., van Lenthe, G.H., Müller, R., 2009. Time-lapsed assessment of microcrack initiation and propagation in murine cortical bone at submicrometer resolution. *Bone* 45, 164–173. <http://dx.doi.org/10.1016/j.bone.2009.04.248>.
- Wajima, T., Okura, S., Chen, Y., Bessho, M., Nishiyama, T., 2000. Observation of pore spaces and microcracks using a fluorescent technique in some reservoir rocks of oil, gas and geothermal fields in the Green Tuff region, Japan. *Resour. Geol.* 50, 191–200. <http://dx.doi.org/10.1111/j.1751-3928.2000.tb00069.x>.
- Walker, S.M., Schwyn, D.a, Mokso, R., Wicklein, M., Müller, T., Doube, M., Stampanoni, M., Krapp, H.G., Taylor, G.K., 2014. In vivo time-resolved microtomography reveals the mechanics of the blowfly flight motor. *PLoS Biol.* 12 <http://dx.doi.org/10.1371/journal.pbio.1001823>.
- Welch, N.J., Crawshaw, J.P., Boek, E.S., 2015. Computerized X-ray microtomography observations and fluid flow measurements of the effect of effective stress on fractured low permeability porous media. *Int. Symp. Soc. Core Analysts. Society of Core Analysts, St. John's, CA*, pp. 1–12.
- Welton, J.E., 1984. *SEM Petrology Atlas*. The American Association of Petroleum Geologists, Tulsa.
- Wildenschild, D., Sheppard, A.P., 2013. X-ray imaging and analysis techniques for quantifying pore-scale structure and processes in subsurface porous medium systems. *Adv. Water Resour.* 51, 217–246. <http://dx.doi.org/10.1016/j.advwatres.2012.07.018>.
- Wilkinson, D., Willemsen, J.F., 1983. Invasion percolation: a new form of percolation theory. *J. Phys. A Math. Gen.* 16, 3365–3376. <http://dx.doi.org/10.1088/0305-4470/16/14/028>.
- Wirth, R., 2009. Focused Ion Beam (FIB) combined with SEM and TEM: advanced analytical tools for studies of chemical composition, microstructure and crystal structure in geomaterials on a nanometre scale. *Chem. Geol.* 261, 217–229. <http://dx.doi.org/10.1016/j.chemgeo.2008.05.019>.
- Wirth, R., Morales, L.F., 2012. Combined FIB-SEM techniques: advanced tools to resolve microstructures and mineral phases in sedimentary rocks. In: Sylvester, P. (Ed.), *Quantitative Mineralogy and Microanalysis of Sediments and Sedimentary Rocks*. Mineralogical Association of Canada, pp. 17–34.
- Wu, H.Z., Roberts, S.G., Möbus, G., Inkson, B.J., 2003. Subsurface damage analysis by TEM and 3D FIB crack mapping in alumina and alumina/5 vol.% SiC nanocomposites. *Acta Mater.* 51, 149–163. [http://dx.doi.org/10.1016/S1359-6454\(02\)00387-7](http://dx.doi.org/10.1016/S1359-6454(02)00387-7).
- Wu, K., Dijke, M.I.J., Couples, G.D., Jiang, Z., Ma, J., Sorbie, K.S., Crawford, J., Young, I., Zhang, X., 2006. 3D stochastic modelling of heterogeneous porous media – applications to reservoir rocks. *Transp. Porous Media* 65, 443–467. <http://dx.doi.org/10.1007/s11242-006-0006-z>.
- Yang, J., Boek, E.S., 2013. A comparison study of multi-component lattice Boltzmann models for flow in porous media applications. *Comput. Math. Appl.* 65, 882–890. <http://dx.doi.org/10.1016/j.camwa.2012.11.022>.
- Yang, X., Scheibe, T.D., Richmond, M.C., Perkins, W.a., Vogt, S.J., Codd, S.L., Seymour, J.D., McKinley, M.I., 2013a. Direct numerical simulation of pore-scale flow in a bead pack: comparison with magnetic resonance imaging observations. *Adv. Water Resour.* 54, 228–241. <http://dx.doi.org/10.1016/j.advwatres.2013.01.009>.
- Yang, J., Crawshaw, J., Boek, E.S., 2013b. Quantitative determination of molecular propagator distributions for solute transport in homogeneous and heterogeneous porous

- media using lattice Boltzmann simulations. *Water Resour. Res.* 49, 8531–8538. <http://dx.doi.org/10.1002/2013WR013877>.
- Yang, X., Liu, C., Shang, J., Fang, Y., Bailey, V.L., 2014. A unified multiscale model for pore-scale flow simulations in soils. *Soil Sci. Soc. Am. J.* 78, 108. <http://dx.doi.org/10.2136/sssaj2013.05.0190>.
- Yang, X., Mehmani, Y., Perkins, W.a., Pasquali, A., Schönherr, M., Kim, K., Perego, M., Parks, M.L., Trask, N., Balhoff, M.T., Richmond, M.C., Geier, M., Kraftczyk, M., Luo, L.-S., Tartakovsky, A.M., Scheibe, T.D., 2015. Intercomparison of 3D pore-scale flow and solute transport simulation methods. *Adv. Water Resour.* 000, 1–14. <http://dx.doi.org/10.1016/j.advwatres.2015.09.015>.
- Yehya, a., Naji, H., Sukop, M.C., 2015. Simulating flows in multi-layered and spatially-variable permeability media via a new gray lattice Boltzmann model. *Comput. Geotech.* 70, 150–158. <http://dx.doi.org/10.1016/j.compgeo.2015.07.017>.
- Yiotis, A.G., Tsimpanogiannis, I.N., Stubos, A.K., Yortsos, Y.C., 2006. Pore-network study of the characteristic periods in the drying of porous materials. *J. Colloid Interface Sci.* 297, 738–748. <http://dx.doi.org/10.1016/j.jcis.2005.11.043>.
- Yoon, H., Dewers, T.A., 2013. Nanopore structures, statistically representative elementary volumes, and transport properties of chalk. *Geophys. Res. Lett.* 40, 4294–4298. <http://dx.doi.org/10.1002/grl.50803>.
- Yoon, H., Kang, Q., Valocchi, A.J., 2015. Lattice Boltzmann-based approaches for pore-scale reactive transport. *Rev. Mineral. Geochem.* 80, 393–431. <http://dx.doi.org/10.2138/rmg.2015.80.12>.
- Youssef, S., Rosenberg, E., Gland, N., Bekri, S., Vizika, O., 2007. Quantitative 3D characterisation of the pore space of real rocks: improved μ CT resolution and pore extraction methodology. *Int. Symp. Soc. Core Analysts. Society of Core Analysts.*
- Youssef, S., Han, M., Bauer, D., Rosenberg, E., Bekri, S., Fleury, M., Vizika, O., 2008. High resolution μ -CT combined to numerical models to assess electrical properties of bimodal carbonates. *Int. Symp. Soc. Core Analysts. Society of Core Analysts, Abu Dhabi, UAE*, pp. 1–12.
- Youssef, S., Deschamps, H., Dautriat, J., Rosenberg, E., Oughanem, R., Maire, E., Mokso, R., 2013. 4D imaging of fluid flow dynamics in natural porous media with ultra-fast X-ray microtomography. *Int. Symp. Soc. Core Analysts. Society of Core Analysts, Napa Valley, USA.*
- Zaretskii, Y., Geiger, S., Sorbie, K., Förster, M., 2010. Efficient flow and transport simulations in reconstructed 3D pore geometries. *Adv. Water Resour.* 33, 1508–1516. <http://dx.doi.org/10.1016/j.advwatres.2010.08.008>.
- Zhang, L., Bai, G., Luo, X., Ma, X., Chen, M., Wu, M., Yang, W., 2009. Diagenetic history of tight sandstones and gas entrapment in the Yulin Gas Field in the central area of the Ordos Basin, China. *Mar. Pet. Geol.* 26, 974–989. <http://dx.doi.org/10.1016/j.marpetgeo.2008.05.003>.
- Zhang, S., Klimentidis, R.E., Barthelemy, P., 2012. Micron to millimeter upscaling of shale rock properties based on 3D imaging and modeling. *Int. Symp. Soc. Core Analysts. Society of Core Analysts.*
- Zhang, X., Pease, V., Omma, J., Benedictus, A., 2015. Provenance of Late Carboniferous to Jurassic sandstones for southern Taimyr, Arctic Russia: a comparison of heavy mineral analysis by optical and QEMSCAN methods. *Sediment. Geol.* 329, 166–176. <http://dx.doi.org/10.1016/j.sedgeo.2015.09.008>.
- Zhao, H.Q., Macdonald, I.F., Kwiecien, M.J., 1994. Multi-orientation scanning: a necessity in the identification of pore necks in porous media by 3-D computer reconstruction from serial section data. *J. Colloid Interface Sci.* 162, 390–401. <http://dx.doi.org/10.1006/jcis.1994.1053>.
- Zhou, D., Dillard, L.A., Blunt, M.J., 2000. A physically based model of dissolution of non-aqueous phase liquids in the saturated zone. *Transp. Porous Media* 39, 227–255. <http://dx.doi.org/10.1023/A:1006693126316>.
- Zhu, J., Ma, J., 2013. An improved gray lattice Boltzmann model for simulating fluid flow in multi-scale porous media. *Adv. Water Resour.* 56, 61–76. <http://dx.doi.org/10.1016/j.advwatres.2013.03.001>.